Scuola Internazionale Superiore di Studi Avanzati
International School for Advanced Studies

Sensory transduction and firing in vomeronasal sensory neurons: the role of the signal transduction protein TMEM16A

Thesis submitted for the degree of "*Doctor Philosophiae*"
Academic Year 2016/2017

CANDIDATE
Andres Alberto Hernandez-Clavijo

SUPERVISOR
Prof. Anna Menini

CO-SUPERVISOR
Dr. Simone Pifferi

SISSA – Via Bonomea 265 – 34136 TRIESTE - ITALY

Scuola Internazionale Superiore di Studi Avanzati-SISSA
International School for Advanced Studies
Trieste – Italy

Sensory transduction and firing in vomeronasal sensory neurons: the role of the signal transduction protein TMEM16A

Thesis submitted for the degree of "*Doctor Philosophiae*"
Academic Year 2016/2017

CANDIDATE
Andres Alberto Hernandez-Clavijo

SUPERVISOR
Prof. Anna Menini

CO-SUPERVISOR
Dr. Simone Pifferi

DECLARATION

The work described in this thesis was carried out at the International School for Advanced Studies (SISSA), between November-2013 and October-2017.

Experiments performed during these four years are included in:

Amjad, A.*, **Hernandez-Clavijo, A**.*, Pifferi, S.*, Maurya, D. K., Boccaccio, A., Franzot, J., Rock, J., and Menini, A. (2015).
Conditional knockout of TMEM16A/anoctamin1 abolishes the calcium-activated chloride current in mouse vomeronasal sensory neurons.
J Gen Physiol, 145.
*A.A., **H-C.A** and P.S. contributed equally to this work.

Hernandez-Clavijo, A., Pifferi, S., J., Rock, J., and Menini
Sensory information representation in mouse vomeronasal sensory neurons is modified by the Ca^{2+}-activated Cl^- channel TMEM16A
(Manuscript in preparation)

"Todos nosotros sabemos algo. Todos nosotros ignoramos algo. Por eso, aprendemos siempre"
Paulo Freire

"An ordinary passerby would think my rose looked just like you. But my rose, all on her own, is more important than all of you together, since she's the one I've watered. Since she's the one I put under glass, since she's the one I sheltered behind the screen. Since she's the one for whom I killed the caterpillars (except the two or three butterflies). Since she's the one I listened to when she complained, or when she boasted, or even sometimes when she said nothing at all. Since she's my rose"

Antoine de Saint-Exupéry, The Little Prince

ABSTRACT

The vomeronasal organ (VNO) is a peripheral sensory organ present in many mammals that is involved in the detection of pheromones, substances released by animals affecting behavior or physiology of other individuals of the same species. The VNO contains specialized neurons, called vomeronasal sensory neurons (VSNs), expressing individual types of vomeronasal receptors from large families and capable to detect chemical stimuli by transducing their binding into electrical signals that are transferred to the central nervous system to be processed. Ligand binding to vomeronasal receptors on microvilli of the dendritic knobs of VSNs activates a PLC-dependent second messenger transduction cascade that produces an increase in intracellular calcium concentration. The increase in cytosolic calcium concentration plays several roles in signal transduction, involving the activation of other ion channels and enzymes. Previous studies showed that calcium-activated chloride currents are activated by cytosolic calcium increase in mouse VSNs, and that both TMEM16A and TMEM16B, two proteins forming calcium-activated chloride channels, are expressed in microvilli of VSNs.

Here, we used whole-cell and inside-out patch-clamp recordings to provide a functional characterization of currents activated by calcium in isolated mouse VSNs. We found that intracellular calcium activated anionic currents in whole-cell and inside-out patches from the dendritic knob/microvilli. These currents were activated at sub-micromolar calcium concentration, were voltage-dependent and were blocked by commonly used chloride channel blockers. We compared the electrophysiological properties of the native currents with those mediated by heterologously expressed TMEM16A or TMEM16B calcium-activated chloride channels, which are co-expressed in microvilli of mouse VSNs, and found a closer resemblance to those of TMEM16A. We used the Cre–loxP system to selectively knock out TMEM16A in mature VSNs. We showed that calcium-activated currents were abolished in VSNs of TMEM16A conditional knockout mice (TMEM16A cKO), demonstrating that TMEM16A is an essential component of calcium-activated chloride currents in mouse VSNs.

As TMEM16A cKO VSNs do not present calcium-activated chloride currents, this mouse line is a good model to study the role of calcium-activated chloride currents in vomeronasal physiology. We performed electrophysiological recordings to compare the properties of the membrane and the spontaneous and evoked activity in WT and TMEM16A cKO VSNs. In whole-cell experiments in the voltage-clamp configuration, we found that deleting TMEM16A channel in VSNs did not affect the membrane input resistance, resting membrane potential or current-voltage relations of voltage-activated inward and outward currents. Extracellular recordings in loose-patch configuration showed that firing pattern of spontaneous activity was affected in VSNs from TMEM16A cKO mice, showing less activity coded in burst with respect to WT neurons, while the mean frequency was not affected. We recorded the capability of VSNs to respond to urine at 1:50 dilution presented for a 10 s period. We found urine responses both in WT and TMEM16A cKO VSNs, indicating that neurons lacking calcium-activated chloride currents

were still able to activate signal transduction after stimulus presentation and to increase firing activity. When we compared the firing activity of evoked activity, we found that mean frequency was not altered, while the firing pattern was strongly affected. Inter-spike interval distribution of evoked activity showed that VSNs from TMEM16A cKO fired with shorter intervals than WT neurons. We conclude that the calcium-activated chloride current in VSNs depends on TMEM16A expression and that it regulates the spike firing pattern both during spontaneous and evoked activity.

TABLE OF CONTENTS

1. INTRODUCTION

1.1 Chemoreception and chemoreceptor organs in mouse

Chemoreception is the ability of animals to detect chemical stimuli in the environment and to respond by regulating their behaviors. This task is essential for survival of the individual and of the species, indeed it enables localization of nutritious food and suitable mating partners, and to avoid being eaten by predators or eating toxic substances. In animals chemoreception depends primarily on the senses of taste and smell. In mouse, different organs are responsible for the detection of chemical substances in the nasal cavity; the main olfactory epithelium (MOE), the vomeronasal organ (VNO), the Grüneberg ganglion (GG) and the septal organ of Masera (SO) (Fig 1).

1.1.1 Main Olfactory Epithelium (MOE)

The main olfactory epithelium (MOE) is a pseudostratified columnar epithelium located inside the nasal cavity and its main function is to detect odorants. The MOE is mainly composed by three different types of cells: olfactory sensory neurons (OSNs), supporting or sustentacular cells and basal cells (Fig 2A). The MOE from all vertebrates contains secretory glands, called Bowman's glands, responsible for secreting the fluid, or mucus, that cover the surface of the epithelium. The Bowman's glands have a tubulo/alveolar shape with the alveoli positioned in the basal region of the MOE and a duct or tubule that reach the surface of the epithelium.

The OSNs are the cells responsible to detect the odorants and make connection with the central nervous system to transfer the information from the external world. OSNs are bipolar neurons with a long dendrite that finished in a knob with several cilia that protrude inside the mucus layer that covers the epithelium. The signaling transduction machinery responsible to transduce chemical stimuli into an electrical signal is located in the cilia. From the opposite side of the soma, every OSN presents a single axon that projects to the main olfactory bulb (MOB) of the brain and transmits the electrical signal to be further processed (Firestein, 2001).

The OSNs are responsible for detecting odor molecules and transforming the chemical energy into electrical signals. The first step in signal transduction in OSNs is the binding of the odor molecule with their specific receptor in the ciliary membrane. In 1991 Linda Buck and Richard Axel identified a multigene family that appeared to encode candidate receptors for odorants in rats (Buck and Axel, 1991). The encoded proteins were named olfactory receptors or odorant receptors (ORs): olfactory receptor because the proteins are expressed in olfactory sensory neurons (OSNs), and odorant receptor because the proteins were thought to recognize odorant molecules, neither turned out to be strictly the case, because ORs are now known to be expressed in tissues other than the olfactory epithelium and some ORs have been found to detect chemicals other than odorants

(Touhara et al., 2016). The first demonstration that an OR is responsible of the initiation of the transduction cascade was obtained 7 years after Buck and Axel (1991) described the candidate ORs family; Zhao and co-workers (1998) showed that over-expression of a particular OR protein, in rat olfactory sensory neurons, gives a higher sensitivity for a subset of odorants molecules (Zhao et al., 1998). The OR proteins belong to the class A rhodopsin-like GPCR family that includes rhodopsin and the β2-adrenergic receptor. The ORs possess structural features in common with class A GPCRs: seven transmembrane (TM) domains, a conserved glycosylation site in the N-terminal region, and a disulfide bond between the conserved cysteines in the extracellular loops (Touhara et al., 2016). OR gene repertoires are highly variable among mammals and reflect their ecological diversity. The largest number of intact OR was found in African elephants with around 2000, twice than those found in mice and dogs (~1000), and five times more than humans (~400) (Niimura et al., 2014).

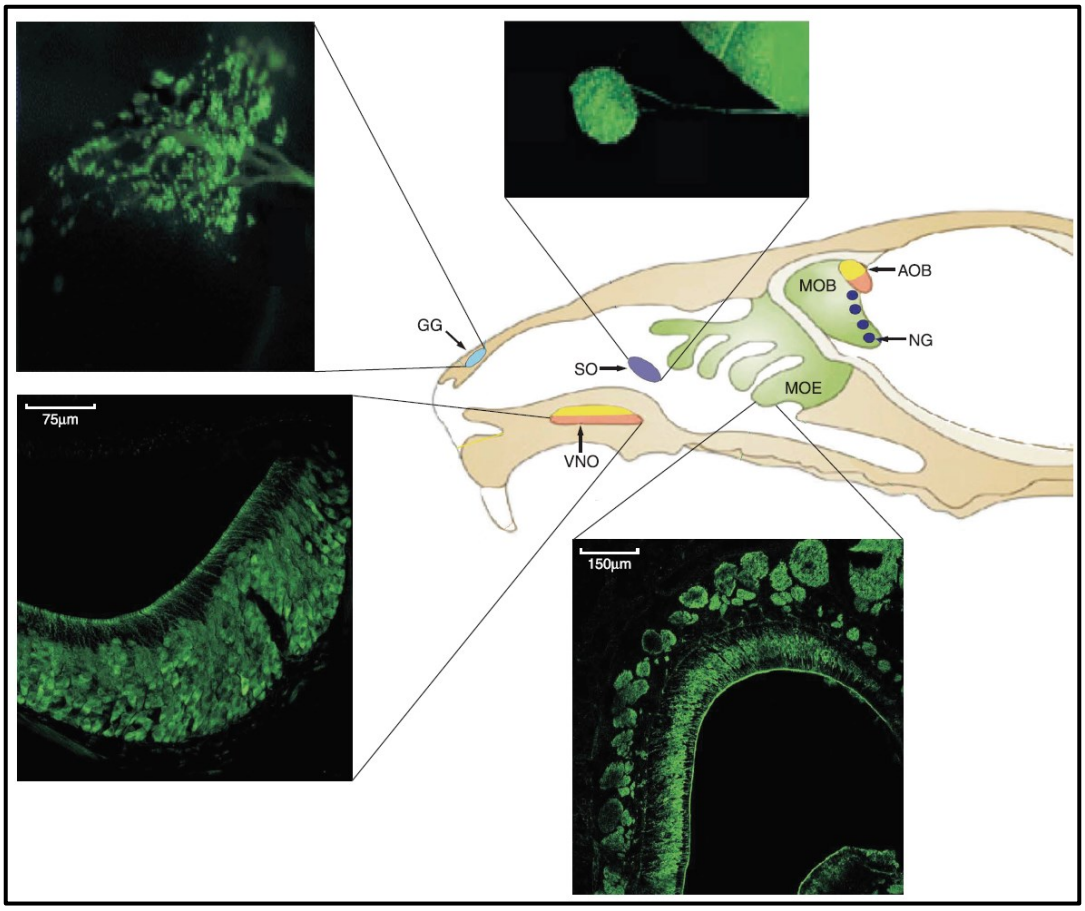

Figure 1. Chemosensory organs in mouse nasal cavity. *Schematic representation of four different chemosensory organs present in the mouse nasal cavity. The main olfactory epithelium (MOE) located in the upper-posterior region of the nasal cavity. Vomeronasal organ (VNO) an encapsulated tubular tissue located in basal region of the nasal cavity. The septal organ of Masera (SO) located anterior to the MOE in the septal bone. The Grüneberg ganglion (GG) in the most anterior part of the nasal cavity Main olfactory bulb (MOB) with necklace glomeruli (NG) and the accessory olfactory bulb (AOB). Color code indicates the projections from chemosensory organs to the MOB and AOB. Insets show images obtained from tissue from a mouse expressing green fluorescent protein (GFP) under the control of olfactory marker protein (OMP). Top left: the Grüneberg ganglion has an arrow-like shape with neurons clustered in small groups. Top right: the septal organ of Masera is an island of sensory epithelium. Bottom left: mature vomeronasal sensory neurons in a coronal section of the vomeronasal organ. Bottom right: mature olfactory sensory neurons in a coronal section of the main olfactory epithelium. [Taken from (Tirindelli et al., 2009)].*

Binding of odor molecules to odorant receptors (ORs) activates a series of events, which eventually lead to generation of action potentials sending the information to the olfactory bulb. The ligand-bound OR activates an olfactory-specific G protein (Golf), which in turn activates adenylyl cyclase type III (ACIII). The cyclase catalyzes the production of cAMP, a second messenger that directly opens a cyclic nucleotide-gated (CNG) channel. This non-selective cation channel allows the influx of sodium and calcium into the cell, which depolarizes the cell membrane (Ma, 2007). Increase of cytosolic calcium concentration activates a calcium-activated chloride channel, TMEM16B, generating an unusual outward current, which non-linearly amplifies the transduction current carried by the CNG channel. The OSNs maintain a relatively high intracellular chloride concentration via Na-K-Cl cotransporters (NKCC1) located in the cilia and the cell body (Hengl et al., 2010; Kaneko et al., 2004; Reisert et al., 2005)

The receptor potential generated by the transduction current passively propagates through the dendrite and soma. If the stimulation is above the threshold potential, action potential firing is evoked and it is transmitted through the axon to the olfactory bulb. In the main olfactory bulb, the OSN terminals make synaptic contacts in specialized structures called glomeruli, conglomerates of neuropil some 50–100 µm in diameter that consist of the incoming axons of OSNs and the dendrites of the main projection cells in the bulb, the mitral cells. Axons of all the OSNs expressing a particular OR converge to only two glomeruli in the main olfactory bulb. In mice there are about 2,000 glomeruli and their localization is roughly conserved among individuals (Mombaerts et al., 1996; Zapiec and Mombaerts, 2015). Therefore the olfactory bulb is topographically organized, with each glomerulus representing a single type of odorant receptor (Mombaerts et al., 1996; Ressler et al., 1993; Vassar et al., 1993). In the main olfactory bulb a single mitral cell with its dendritic arborization makes synapses at the level of only one glomerulus. The axons of mitral and tufted cells project through the lateral olfactory tract to the primary olfactory cortex, including the anterior olfactory nucleus (AON), the olfactory tubercle (OT), the piriform cortex (Pir), and the entorhinal cortex (Ent). Olfactory information is subsequently relayed to the higher cortex for cognitive processing, which underlies the perception of odors (Ma, 2007).

1.1.2 Septal organ of Masera (SO)

The septal organ (SO), also called organ of Masera or septal organ of Masera, was first described by Rodolfo Masera in 1943. The SO is a small group of sensory neurons present in the basal region of the septal bone in the anterior part of the main olfactory epithelium (Fig 1). The sensory neurons in the SO maintain the basic morphology present in the MOE with some small differences; the SO contains just three layers of cells, while the MOE is much thicker with at least 6 layers of neurons. The neurons from the SO project their axon to a subset of glomeruli in the posterior ventromedial main olfactory bulb (MOB). Because of its anterior position it is thought that the SO could be involved in the early detection of biologically relevant molecules (Tirindelli et al., 2009). The first approach to describe the olfactory transduction in sensory neurons of the SO was made looking for molecules responsible for signaling transduction in OSNs, such as Golf protein, adenylyl cyclase type III (ACIII), and cyclic nucleotide-gated channels (CNG). Immunohistochemical and electrophysiological experiments showed that sensory neurons in the SO use a cAMP-second messenger cascade for signal transduction, similar to OSNs in the MOE (Ma et al.,

2003). Sensory neurons in the SO express ORs following the rule of one cell-one receptor (Tian and Ma, 2004). It has been proposed than the SO can work as an "alert" system, because of its anterior position, allowing access to odorant molecules before they reach the MOE. However, surgical removal of the SO in rats did not show any clear behavioral effect (Giannetti et al., 1992). Interestingly, it has been suggested that the SO may detect low volatile molecules that cannot reach the MOE but do access the SO and the vomeronasal organ (Wysocki et al., 1980).

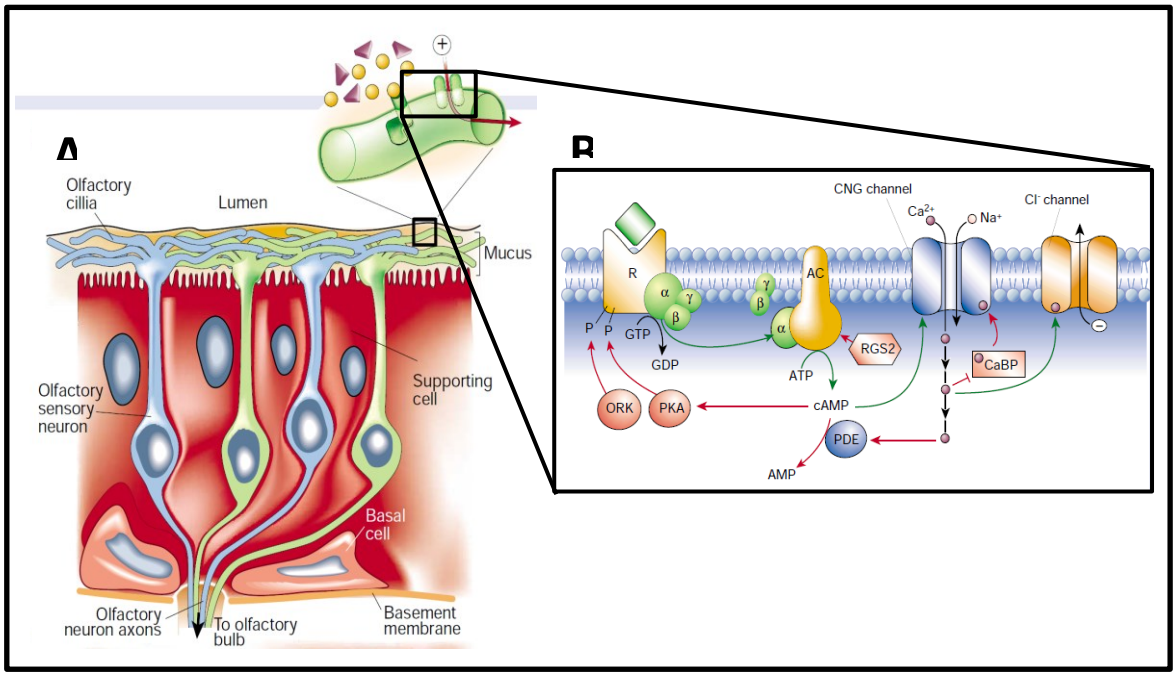

Figure 2. Structure and signal transduction in the MOE. *Left. Schematic representation of the main olfactory epithelium composed by three types of cells: olfactory sensory neurons (OSNs; the only neuronal cell type), supporting or sustentacular cells (a kind of glial cell, which possesses microvilli on their apical surface), and a stem-cell population, known as basal cells, from which new OSNs are generated. OSNs are bipolar cells that project one dendrite to the luminal surface of the epithelium, the dendrite finishes in a specialized structure called knob from where cilia are projected. The machinery for chemosignaling transduction is present in the cilia in direct contact with the nasal mucus. From the opposite region of the soma OSN project a single axon to the main olfactory bulb (MOB). Inset represent the transduction signaling after olfactory receptor (OR) activation by the binding of a ligand. This is a classic cyclic nucleotide transduction pathway in which all of the proteins involved have been identified, cloned, expressed and characterized. Additionally, many of them have been genetically deleted from strains of mice, making this one of the most investigated and best understood second-messenger pathways in the nervous system. AC, adenylyl cyclase; CNG channel, cyclic nucleotide-gated channel; PDE, phosphodiesterase; PKA, protein kinase A; ORK, olfactory receptor kinase; RGS, regulator of G proteins (but here acts on the AC); CaBP, calmodulin-binding protein. Green arrows indicate stimulatory pathways; red indicates inhibitory (feedback).[Modified from (Firestein, 2001)]*

1.1.3 Grüneberg ganglion (GG)

The Grüneberg ganglion (GG) is a cluster of neurons present in the vestibule of the anterior nasal cavity (Fig 1). Such a cluster of neurons lining both sides of the most rostral septum has been found in different mammalian species (Brechbühl et al., 2014; Grüneberg, 1973; Tachibana et al., 1990). Several GG neurons express vomeronasal receptors and co-express the G proteins Gαo and Gαi, both of which are also present in sensory neurons of the vomeronasal organ (see later). Some GG neurons express adenylyl

cyclase type III and Golf/s, characteristic signaling elements of the main olfactory system. Thus, the GG has two kinds of cells, VNO-like or MOE-like (Fleischer et al., 2006). Each GG has about 500 cells arranged in several densely packed cell clusters. Individual cells give rise to single axons, which fasciculate to form a nerve bundle that projects caudally. The axons terminate in glomeruli of the olfactory bulb, one or two large glomeruli associated with a semicircle of up to 10 smaller, somewhat diffusely organized glomeruli that surround the most anterior part of the accessory olfactory bulb (Bumbalo et al., 2017; Fuss et al., 2005; Koos and Fraser, 2005).

It has been shown that the GG, in the mouse, is an olfactory subsystem implicated both in chemo and thermal sensing (Brechbühl et al., 2008, 2013, 2014; Bumbalo et al., 2017; Fleischer et al., 2006; Mamasuew et al., 2008). It is specifically involved in the recognition of volatile danger cues such as alarm pheromones (APs) and structurally-related predator scents. APs evoked calcium responses in GG neurons in vitro and induced freezing behavior in vivo, which completely disappeared when the GG degenerated after axotomy (Brechbühl et al., 2008, 2013). The role of GG in thermal sensation was tested through expression of the activity-dependent gene c-Fos in the GG of neonatal mouse pups. Cool ambient temperatures were found to induce strong c-Fos expression in GG neurons whereas warmer temperatures did not. GG responsiveness to coolness was remarkably reduced in older stages (Mamasuew et al., 2008).

1.2 Vomeronasal Organ – VNO

1.2.1 Discovery.

The vomeronasal organ (Fig 3) was discovered by the Danish anatomist Ludvig Jacobson and described in detail in a publication in 1813 (see translation in English in Trotier & Døving, 1998). He described brilliantly and in great detail many anatomical aspects that were not seen even by later anatomists. Jacobson studied a large number of animals in order to determine if the 'new' organ was present also in species other than various domesticated animals. In principle the organ was called “organ of Jacobson”, but at the ninth meeting of the scientific society ‘Der Anatomische Gesellschaft'’ in Basel in 1895, the society proposed that the organ of Jacobson should be called: 'organon vomeronasale (Jacobsoni)' (Trotier and Døving, 1998).

1.2.2 Morphology of the VNO

In most mammals the VNO is located in the foremost part of the nasal cavity, in close contact with the nasal cartilage (septum) (Fig 3A), on the palatal elongations of the intermaxillary bone. The organ is surrounded by a cartilaginous capsule that is open in the anterior part from where the encapsulated VNO makes contact with the nasal cavity (Trotier and Døving, 1998). The vomeronasal organ is a tubular structure composed by two epithelia, the non-sensory epithelium and the sensory epithelium, and a central lumen full of fluid in direct contact with the nasal cavity fluids (Fig 3B). The non-sensory epithelium is a cavernous tissue well vascularized with one or two large veins running along the organ in the tissue forming the mushroom body. Filling of the cavernous tissue of the vomeronasal organ with blood will cause an efflux of fluid from the organ; instead a vasoconstriction of the walls of the large vein of the organ will increase the volume of

the lumen and create suction. This “pumping” mechanism is the responsible for sucking into the lumen of the organ the fluids carrying the stimuli (Trotier and Døving, 1998).

The sensory epithelium is a pseudostratified epithelium composed of three types of cells: sensory neurons, supporting cells, and basal cells. Vomeronasal sensory neurons are divided in two classes, basal and apical, according to their location in the vomeronasal epithelium and to the expression of receptors (Fig 3C) (Tirindelli et al., 2009). They are going to be described in detail later in this thesis. Supporting cells are located in the superficial layer of the sensory epithelium, while basal cells are located both along the basal membrane of the sensory epithelium and at the boundary with the non-sensory epithelium.

1.2.3 Pheromones

Chemicals from outside an organism that provide information about another organism are called semiochemicals. Semiochemicals that carry information between two different species are termed allelochemicals, while semiochemical that carry information between members of the same species are termed pheromones (Mucignat-Caretta, 2014). The term pheromone was introduced in 1959 by the entomologists Peter Karlson and Martin Luscher (Karlson and Luscher, 1959) to identify specific biologically active substances “which are secreted to the outside by an individual and received by a second individual of the same species, in which they release a specific reaction, for example, a definite behavior or a developmental process”. The word pheromone comes from the Greek *pherrein,* to carry or transfer, and *hormone,* to excite or stimulate (Karlson and Luscher, 1959).

Pheromones are found in the animal kingdom, from crustacean to fishes to terrestrial mammals. In mammals, even if pheromones are hard to study, they have been reported to be involved in a variety of behavioral effects (Wyatt, 2003). To study pheromones in mammals, as for many other research projects, the mouse has been used as animal model for a long time. In the last years, many new data have emerged from several groups helping to understand the pheromone transduction process in mammals. Nowdays we know something about the organs responsible for sensing pheromones, the putative receptors which bind pheromones, the signaling cascades inside the cells, the axonal projections from the periphery to the central system, etc. but many aspects are still unknown and waiting to be described.

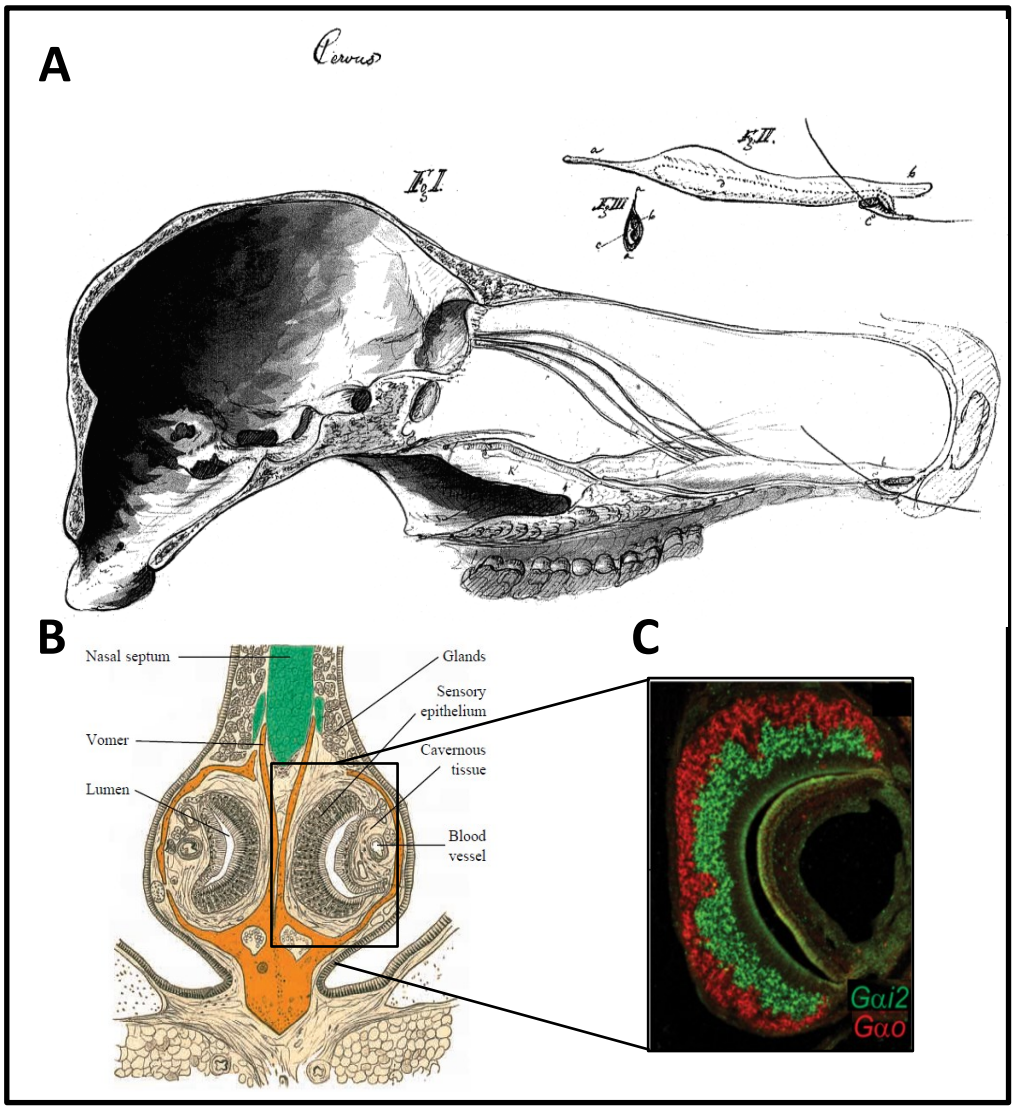

Figure 3. Morphology of the VNO. A. *Jacobson's unpublished drawing of the VNO at the Agricultural University in Copenhagen FI. Drawing of the medial aspect of a head of a deer, Cervus sp. the canalis incecivus is indicated by a straw, in this species the opening of the VNO is through the palate, while in mouse it is in the nasal cavity. FgII. Drawing of an isolated vomeronasal organ; the lumen is outlined by a stippled line. FgIII. Cross section of the vomeronasal organ.* ***B.*** *Cross section of the ventral region of the nasal septum of a mouse, at the level of the middle of the vomeronasal organ. The organ is encapsulated in the vomer capsule. The sensory epithelium is on the medial wall and the non-sensory epithelium, composed by large blood vessels and cavernous tissue, in the lateral wall.* ***C.*** *Two colors in situ hybridization (ISH) with the Gαi2 probe (apical VSNs, green) and the Gαo probe (Basal VSNs, red) in a coronal section of a VNO. Apical neurons co-express V1R receptors with Gαi2 protein while basal neurons co-express V2R receptors with Gαo protein (See text for details). [A & B modified from (Trotier and Døving, 1998). C modified from (Leinders-Zufall et al., 2014)].*

In mammals, only two clear examples of pheromones activating specific receptors have been described: the male pheromone exocrine gland-secreting peptide1 (ESP1) activates the V2Rp5 vomeronasal receptor (Haga et al., 2010) (see later); and the male pheromone (Z)-5-tetradecen-1-ol activates the Olfr288 OR in the MOE (Yoshikawa et al., 2013). Although a limited number of functional pheromone-receptor couples have been described, several studies have demonstrated the effect of pheromones in mice. For example, it is known that adult female mice modify or suppress their estrous cycle when housed in groups and isolated from males, called Lee-Boot effect (Van der Lee and Boot,

1955); male urine can restore and synchronize the estrus cycle of non-cycling females, known as Whitten effect (Whitten, 1959), or accelerate puberty onset in females (Vandenbergh effect) (Vandenbergh et al., 1975). In addition, the exposure of a recently mated female mouse to a male, different from the stud, prevents implantation of fertilized eggs (Bruce effect), implying that the stud or its individual odor must be memorized at the moment of mating in order to be recognized later (Bruce, 1959). These pheromonal effects are commonly believed to be mediated by stimuli present in urine that act via the vomeronasal system. Urines are known to contain a variety of small, volatile pheromones (Novotny et al., 1984), as well as sulfated steroids and proteins, all thought to play a role in pheromone communication (Tirindelli et al., 2009).

For a long time it was considered that the two main chemoreceptor organs in the nasal cavity, the MOE and the VNO, play separate roles in chemodetection, with the MOE sensing volatile odorant molecules and the VNO sensing pheromones. More recent data clearly show that this strict functional division should be discarded; indeed both chemosensory organs can detect both pheromones and odorant molecules (Baxi et al., 2006; Johnston, 1992; Omura and Mombaerts, 2014; Yoshikawa et al., 2013). Nevertheless the main role of the VNO is the detection of pheromones and regulation of animal behavior.

1.3 Vomeronasal Sensory Neurons

1.3.1 Morphology and classification

Vomeronasal sensory neurons (VSNs) are the main component of the vomeronasal sensory epithelium. VSNs are bipolar neurons with a rounded soma that project a long dendrite that finishes in a knob with microvilli, this dendritic knob comes in contact with the fluids inside the lumen of the VNO. Most of the components of the machinery necessary for signal transduction are present in the knob/microvilli of the VSNs. From the opposite side of the soma a long axon projects to the central nervous system, specifically to the accessory olfactory bulb (AOB) (Rodriguez et al., 1999). The VSNs are divided in two different populations inside the sensory epithelium, basal and apical neurons, showing several differences between them. These two populations are located in two anatomically different regions inside the sensory epithelium, the basal neurons are located near the basal lamina and the apical neurons are located near the lumen surface. They also express different signaling proteins. Basal neurons express the Gαo isoform in combination mainly with the V2R class receptors while apical neurons express Gαi2 isoform mainly in combination with the V1R class receptors (Fig 3C) (Berghard and Buck, 1996; Dulac and Axel, 1995; Herrada and Dulac, 1997; Matsunami and Buck, 1997; Ryba and Tirindelli, 1997). Finally, these two populations project their axons to different regions inside the AOB (see also later) (Rodriguez et al., 1999).

1.3.2 Receptors in VSNs

The discovery of ORs in 1991 showed that the proteins responsible for detecting odors in the main olfactory epithelium are coded by an extremely large multigene family, with around 1000 members in the mouse, that encodes seven transmembrane domain proteins (Buck and Axel, 1991). As the expression of the OR multigene family was thought to be restricted to the MOE, it was proposed that the receptor protein expressed in VNO

should be from a different family. The discovery of a first multigene family coding for the putative receptors in VNO came out in 1995 (Dulac and Axel, 1995), later known as V1R receptors and related to VSNs expressing Gαi2 protein. Two years later a second multigene family was discovered coding for other putative VNO receptors (V2R) associated to VSNs expressing Gαo protein (Herrada and Dulac, 1997; Matsunami and Buck, 1997; Ryba and Tirindelli, 1997). Finally a third family of receptors was described for the VNO, the formyl peptide receptors (FPR) family (Liberles et al., 2009; Riviere et al., 2009).

1.3.2.1 V1R receptors.

Catherine Dulac and Richard Axel identified the first multigene family coding for V1Rs using a single-cell subtractive approach (Dulac and Axel, 1995). V1Rs are G protein-coupled receptor (GPCRs) with seven transmembrane domains, V1Rs are classified inside the class A or rhodopsin-like family of GPCRs (Rodriguez, 2016). As described previously, V1Rs expression is restricted to apical neurons from the VNO, sharing the same pattern of expression of Gαi2 protein (Fig 3C). In mammals, V1R genes have a very simple structure. They possess a first (and sometimes second) noncoding exon(s) followed by a final exon that contains the whole V1R coding sequence (Rodriguez, 2016). A total of 392 genes are present in the mouse genome, among which 239 have an intact open reading frame. Their products have been organized into 12 subfamilies (V1Ra to V1Rl) (Fig 4A), with members inside the same family sharing at least 40% amino acid sequence identity (Rodriguez, 2016; Rodriguez et al., 2002). The expression pattern of individuals V1Rs shows punctuated distribution marking between 1 – 4% of the VSN, this observation, and the non-overlapping expression of several V1Rs indicated that VSNs follow the one cell-one receptor rule, where just one receptor is expressed in a given VSNs, similar to OR expression in OSNs in the MOE (Dulac and Axel, 1998) and SO (Tian and Ma, 2004). The V1R-expressing neurons project their axons to the anterior part of the AOB (see later). The direct role of V1R receptors in VNO chemoreception was demonstrated by deletion of a cluster that contained almost all genes coding for V1R1a and V1R1b receptors, leading to deficient pheromone responses (Del Punta et al., 2002a).

1.3.2.2 V2R receptors

V2R receptors are also GPCRs, but different from V1Rs, they belong to the class C family, also known as the metabotropic glutamate receptor family. While V1Rs are expressed just in apical neurons, V2R expression is restricted to basal neurons expressing the Gαo protein (Herrada and Dulac, 1997; Matsunami and Buck, 1997; Ryba and Tirindelli, 1997). The coding sequence of V2R genes is split into multiple exons, with a single, large exon coding the seven-transmembrane part of the receptor. The mouse genome comprises 121 potentially functional V2Rs. V2R gene products are usually classified into four families (V2RA – V2RD, Fig 4B) (Francia et al., 2015; Ishii and Mombaerts, 2011; Rodriguez, 2016; Silvotti et al., 2007; Yang et al., 2005). Unlike all the other olfactory receptors, V2Rs do not follow the "monogenic rule". All V2R-expressing VSNs express a member of the V2RC family, plus one from another V2R family (A,B or D), meaning that all basal cells express at least two V2R proteins, one from the C family and one from the A, B or D family. (Francia et al., 2015; Ishii and Mombaerts, 2011; Silvotti et al., 2007). V2RC family is composed by 7 members (Vmn2r1-7). A detailed evaluation of the V2RC family expression in basal VSNs showed two different populations: one expressing Vmn2r1 (called also C1 family); and the

other one combinatorially co-expressing the other members of the C family (Vmn2r2-7 or C2 family). The two different populations of basal neurons co-express, in non-random manner, one member of the other V2R families (A, B or D), showing a multigenic expression of V2Rs in basal VSNs (Silvotti et al., 2011). Moreover V2R-expressing VSNs co-express a family of nine non-classical class I major histocompatibility (MHC) genes, H2-Mv genes. H2-Mv expression shows a spatial segregation, with more basal V2R neurons expressing H2-Mv while more apical V2R neurons do not express H2-Mv genes (Ishii and Mombaerts, 2008; Leinders-Zufall et al., 2014). The functional role of H2-Mv in VSNs is linked with pheromone detection. In 2014, Leinders-Zufall and co-workers deleted the whole cluster of H2-Mv genes in mouse germline and evaluated the physiological response of VSNs to peptides and proteins, the classical ligands for basal VSNs. They found that cells which normally express H2-Mv proteins displayed a decreased sensitivity to a ligand when H2-Mv genes were deleted, while cells that normally do not express H2-Mv genes showed no changes in the sensitivity when H2-Mv genes were deleted. Furthermore, they found deficits in sexual and aggressive behaviors in mice lacking H2-Mv genes. They concluded that H2-Mv genes are required for ultrasensitive chemodetection by a subset of cells (Leinders-Zufall et al., 2014).

Some single compounds are known to be V2R agonist. The first ones to be identified were the major histocompatibility complex (MHC) class 1 peptides that activates V2R-expressing VSNs at sub-picomolar concentrations (Leinders-Zufall et al., 2004, 2009, 2014). V2Rs are also activated by exocrine gland-secreting peptides (ESPs) and major urinary proteins (MUPs). The direct proof of V2R chemoresponsivity came mainly from two different works. Deletion of the gene coding for V2R1b result in a deficit for sensing peptide stimuli, specifically stimulation with MHC class 1 peptides (Leinders-Zufall et al., 2009). While deletion of the gene coding for V2Rp5 receptor disrupt responses to the male-specific ESP1 (Haga et al., 2010). Interestingly, it was shown that cells expressing the V2R1b receptor detects MHC peptides and exhibited combinatorial activation with overlapping specificities. In a given cell, response to peptides was broad, but very specific, being able to distinguish between peptides differing in just one amino acid (Leinders-Zufall et al., 2009). A given peptide activates a subset of V2R1b-expressing neuron and neurons lacking V2R1b were not able to respond to any MHC peptide, indicating that V2R1b receptor is necessary to activate the neuron. The diversity in the ligand-response observed in VSNs stimulated with peptides from the MHC could be given by the combinatorial co-expression of receptor from the V2RC family (Silvotti et al., 2007, 2011).

1.3.2.3 Formyl peptide receptors FPR

In 2009 two groups independently identified a new family of chemoreceptors (Liberles et al., 2009; Riviere et al., 2009). This family is composed of formyl peptide receptors (FPRs) that are seven-transmembrane GPCRs belonging to class A, or rhodopsin-like (Spehr, 2016). FPRs are found in all mammals and are encoded in mice by seven genes. Through quantitative RT–PCR and in situ analysis it was found that Fpr-rs1, Fpr-rs3, Fpr-rs4, Fpr-rs6 and Fpr-rs7 transcripts were exclusively observed in vomeronasal tissue extracts, in situ hybridization showing strong and punctate expression of FPRs in the sensory epithelium. Double in situ hybridizations, using a large panel of probes recognizing most chemoreceptors expressed by VSNs, failed to find co-expression of FPRs with members of other families or other members inside FPR family (Riviere et al., 2009), indicating that

FPRs follows the "monogenic rule", or one cell-one receptor. FPR-rs1 is expressed in Gαo-expressing neurons (i.e. basal neurons), whereas the other VNO FPRs (3, 4, 6 and 7) are expressed in Gαi2-expressing neurons (i.e. apical neurons). Stimulation of vomeronasal sensory epithelium with FPRs agonist formyl peptide fMLF, uPAR, or lipoxin A4 showed an increase in intracellular calcium concentration, indicating that VSNs can sense these compounds which are a possible link to pathogens, or to inflammation, which may result from an immune response to germs, a new possible role for the VNO (Riviere et al., 2009).

1.3.2.4 Olfactory receptors in the VNO

As previously mentioned, for a long time the most accepted view of the mammalian olfactory systems was that odorants are detected only in the MOE, whereas pheromones are detected in the VNO. Sam and colleagues (2001) first showed that VSNs can be activated by volatile compounds, suggesting that certain odorants may act in mammals as semiochemicals that influence behavior (Sam et al., 2001). After the report that VSNs can detect volatile odorants, Nakahara and colleagues (2016) evaluated the expression of ORs in the VNO, using RNA sequencing. They found that three ORs are expressed in the VNO, with two of them showing similar or lower expression levels than in the MOE, and one being more expressed in the VNO than in the MOE, the Olfr692 gene. Interestingly, Olfr692-expressing cells were activated by pup odors, and co-expressed TrpC2, V2R clade C, and Gαo transcripts, while they did not express CNGA2, V2R clades ABD nor Gαolf transcripts, suggesting that they represent a distinct and novel subpopulation of chemosensory cells in the adult mouse vomeronasal system (Nakahara et al., 2016).

1.4 Ligands for VSNs

1.4.1 Urinary volatiles

Several primer pheromone effects in laboratory mice are now well known. These include the Whitten, Bruce and Vandenbergh effects. These three phenomena are associated with the effect of male mouse urine on females. In the Whitten effect, male urine promotes a regular four to five day estrous cycle in female mice (Whitten, 1959). In the Bruce effect, urine from an unfamiliar male mouse will cause failure of implantation and pregnancy in a female recently mated with another male (Bruce, 1959). The Vandenbergh effect concerns the acceleration in the onset of puberty and first estrus in pre-pubertal female mice exposed to urine of males (Vandenbergh et al., 1975). Although it was known that urine was responsible for those effects, the nature and identity of the specific molecule was not known. Identification of diverse volatiles pheromones present in the mouse urine was carried by Novotny and colleagues (Jemiolo et al., 1989; Novotny et al., 1980, 1984, 1986, 1999). They identified, among others, 2-heptanone, α and β farnesenes and 2,5-dimethylpyrazine as volatile pheromones regulating animal behavior. Volatile pheromones evoked high affinity responses in both MOE and apical VNO sensory neurons (Kelliher et al., 2006; Zufall and Leinders-Zufall, 2000) although the relative roles of these detection systems are still unclear (Liberles, 2014).

1.4.2 Major urinary proteins (MUPs)

Major urinary proteins (MUPs), also named α2 urinary globulins in rat, belong to the lipocalin superfamily (Cavaggioni and Mucignat-Caretta, 2000). MUPS are mainly

synthesized in the liver and excreted with urine. Male mouse urine contains a higher concentration of MUPs than females. Although MUPs are also expressed in exocrine glands such as mammary, parotid, sublingual, submaxillary, lachrymal, nasal, and in modified sebaceous glands like preputial and perianal glands, their biological effects have been exclusively demonstrated when these proteins were purified from urine or added to urine that does not possess pheromonal activity (i.e., of a pre-pubertal or castrated mouse) (Chamero et al., 2007; Zhou and Rui, 2010). MUPS were first thought to function as transporters or stabilizers of pheromones or other semiochemicals, but now it is known that also MUPs themselves can be pheromones.

MUPs have a central cavity, lined with hydrophobic residues that constitute the site of binding of apolar ligands, especially pheromonal molecules. All lipocalins contain a tryptophan residue in the position 19 (Trp19) which may contributes to ligand binding but also to protein stability (Beynon and Hurst, 2004). The role of the binding of volatile pheromones to MUPs could be related with the protection of ligands from degradation, and with a slow release of pheromone to the air, allowing the message to persist for a longer time in the environment (Beynon and Hurst, 2004).
MUPs do not only have a role as carriers of pheromones, but also stimulate directly VSNs and regulate behavior by themselves. In 2007 Chamero and coworkers, through calcium imaging experiments, evaluated the effect of purified MUPs on isolated VSNs. They reported an increase in cytosolic calcium and determined that the MUP protein activates a sensory neuron subfamily characterized by the expression of the G protein Gαo subunit and Vmn2r putative pheromone receptors (V2Rs). Recombinant MUP1 promotes inter-male aggression in the absence of pheromones. Therefore, MUPs themselves also act as non-volatile pheromones in addition to being pheromone carriers (Chamero et al., 2007). In addition, Roberts and collaborators (2010) showed that MUP20, or darcin, a single atypical male-specific MUP, is involved in female's fixed sexual attraction to male. The recognition of darcing by a female elicits a flexible response, where the animal that enters in contact with darcing from a specific male, can learn and memorize the odor and be more attracted to it in future encounters, indicating that female sexual attraction is both, inherent and learned (Roberts et al., 2010). It has been shown that MUPs are also responsible for recognition of self and non-self cues, working in a combinatorial mode (Kaur et al., 2014).

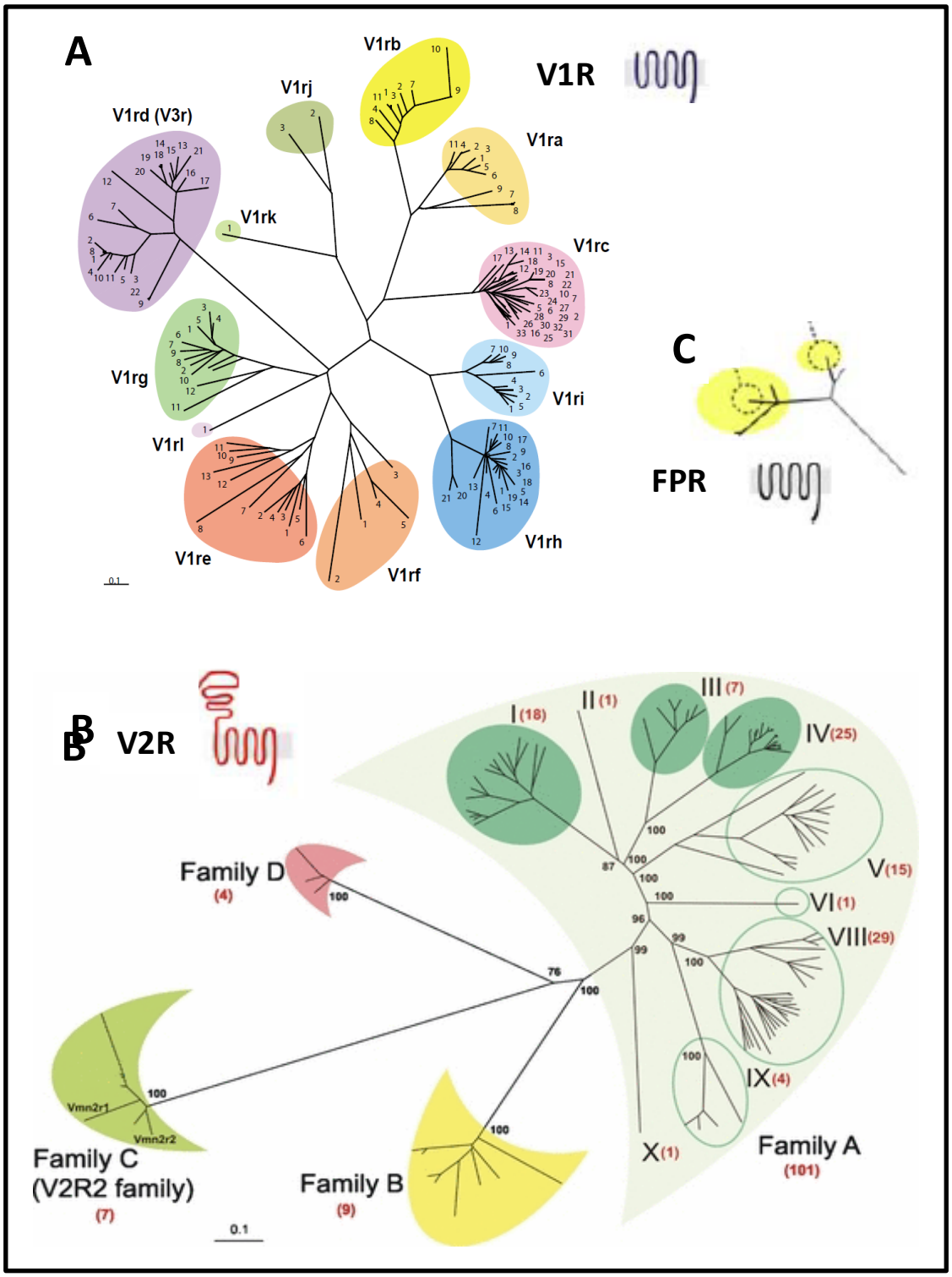

Figure 4. Mouse vomeronasal receptors. A. Type I vomeronasal receptors (V1R) repertoire. *Unrooted phylogenetic tree representing the 137 V1r genes, with 12 families readily distinguishable (From V1Ra to V1Rl).* ***B. Type II vomeronasal receptors (V2R) repertoire.*** *Unrooted phylogenetic tree of the mouse V2R genes with 4 families (from V2RA to V2RD). Family-A clades are represented by open and closed circles. The number of intact genes of each family or clade is indicated in brackets.* ***C. Formyl peptide receptors (FPRs) repertoire.*** *Phylogenetic tree of the mouse FPR genes with 5 families expressed in VSNs. FPR1 are expressed in apical neurons while FPR3, 4, 6 & 7 are expressed in basal neurons. [A. modified from (Rodriguez et al., 2002). B. modified from (Silvotti et al., 2007). C. modified from (Rodriguez, 2016)].*

1.4.3 Exocrine gland-secreting peptides (ESPs)

Non-volatile pheromones are present also in tears and saliva. In rodents, some exocrine glands, such as extraorbital, Harderian and submaxillary glands, secrete a family of peptides called exocrine gland-secreting peptides (ESPs) The ESP family is absent from the human genome (Tirindelli et al., 2009). In 2005 it was found that VSNs can be stimulated by a male-specific 7-kDa peptide, ESP1, secreted from the extra-orbital lacrimal gland of mice. ESP1 is secreted from the eyes of a male and is transferred to the female VNO, where it stimulates V2Rp5 expressing VSNs and causes enhancement in lordosis in females, which is the typical female sexual receptive behavior (Kimoto et al., 2005, 2007, Haga et al. 2010). Interestingly, it has been recently demonstrated that ESP1 is one of the key factor responsible for the Bruce effect (pregnancy block)(Hattori et al., 2017).

ESPs show sexual dimorphism and strain differences in mice. This dimorphism and the reception in the VNO suggest that the ESP family can convey information about sex and individual identity via the vomeronasal system (Haga et al., 2010; Kimoto et al., 2007). ESPs can also carry information about age of the animal. It was shown that ESP22 is secreted from the lacrimal gland and released into tears of 2–3 week old mice. Upon detection, ESP22 activates high affinity sensory neurons in the VNO, and downstream limbic neurons in the medial amygdala. ESP22 works as a powerful inhibitory effect on adult male mating behavior, and its effect is lost in mice lacking TRPC2, a key component of the vomeronasal signal transduction (see later) (Ferrero et al., 2013)

1.4.4 Class I major histocompatibility complex peptides (MHC peptides)

In addition to the well-established role of peptide ligands of the major histocompatibility complex (MHC) class I molecules for self-non self-recognition, MHC peptides also work as sensory stimuli for VSNs (Leinders-Zufall et al., 2004). This is possible because peptide/MHC complexes are not always retained at the cell surface, they are released into the extracellular space and appear in the urine and other bodily secretions (Singh et al., 1987). In 2004 it was shown that Class I MHC peptides at sub-picomolar concentration can directly activate VSNs, specifically basal neurons expressing V2R receptors and Gαo protein, and are able to affect the behavior of the mouse (Leinders-Zufall et al., 2004).

Interestingly, responses to peptides were not altered in TRPC2 KO mice when compared with WT mice, suggesting that class I MHC peptides transduction signaling was independent of TRPC2 channels, the main channel responsible for signaling transduction in VSNs (see later) (Kelliher et al., 2006).

1.4.5 Sulfated Steroids

Another group of molecules able to stimulate VSNs are sulfated steroids. Their activity as ligands of VRs was described by Nodari and co-workers (Kimoto et al., 2007). They fractioned the female urine by chromatography and evaluated the ability of those fractions to elicit reproducible responses in VSNs using multi-electrode array (MEA) recordings. They found that most of the compounds which activated VSNs had low molecular weight, moderate hydrophobicity, low volatility, and a negative electric charge. Purification and structural analysis of those compounds revealed the presence of multiple sulfated steroids. Interestingly, when the activity of sulfatase-treated urine fractions was evaluated, a loss of more than 80% of activity was detected, indicating that sulfated

compounds are the most active ligands for VSNs in female mouse urine (Celsi et al., 2012; Kimoto et al., 2007). Later, Isogai and co-workers (2011) investigated the detection of a mix of synthetic sulfated steroids by the VNO of male mice and found that VSNs expressing V1R receptors of the V1Ref and V1Rjk clades were specifically activated. Furthermore, they suggested that V1R receptors can distinguish distinct structural classes of steroids and that V1Rs may serve as detectors of the physiological status of an animal (Isogai et al., 2011).

1.5 Signaling transduction in VSNs

The mechanisms of sensory signal transduction in VSNs are still not completely known. However, some steps and proteins involved in this process have been described. It has been demonstrated that the VSNs respond to stimuli, mainly pheromones, producing a depolarization of the membrane potential, an increase of cytosolic calcium and increase in firing frequency (Kelliher et al., 2006; Leinders-Zufall et al., 2004; Liman et al., 1999; Lucas et al., 2003; Zufall and Leinders-Zufall, 2000). In VSNs, the binding of chemicals with vomeronasal receptors occurs in the microvilli, at the apical region of the neuron's dendrite. In rodents, these neurons express one or a few members of three families of G protein–coupled receptors: V1Rs, V2Rs, and formyl peptide receptors (FPRs) (Dulac and Axel, 1995; Francia et al., 2015; Herrada and Dulac, 1997; Liberles et al., 2009; Martini et al., 2001; Matsunami and Buck, 1997; Riviere et al., 2009; Ryba and Tirindelli, 1997). Figure 5 shows a schematic view of the putative signal transduction processes in VSNs.

The binding of the ligand to vomeronasal receptors activates a G protein-regulated and cyclic-nucleotide-independent signaling pathway involving phospholipase C activation, which leads to the activation of a transient receptor potential canonical 2 (TRPC2) channel, highly expressed in the knob microvilli of VSNs, allowing the influx of sodium and calcium ions (Liman et al., 1999; Munger et al., 2001; Zufall and Leinders-Zufall, 2000). As a secondary event, the rise in calcium is likely boosted by IP_3-dependent calcium release from internal stores (Kim et al., 2011) and gating of an unknown calcium conductance by a polyunsaturated fatty acid metabolite of DAG, probably arachidonic acid (AA) (Spehr et al., 2002). As a multifaceted messenger, calcium has been shown to act on several targets, including calcium-activated chloride channels, likely TMEM16A and/or TMEM16B (Billig et al., 2011), calcium-activated cation channels (CAN) (Liman, 2003; Spehr et al., 2009), and calcium-dependent potassium channels (BK, SK) (Kim et al., 2012; Zhang et al., 2008).

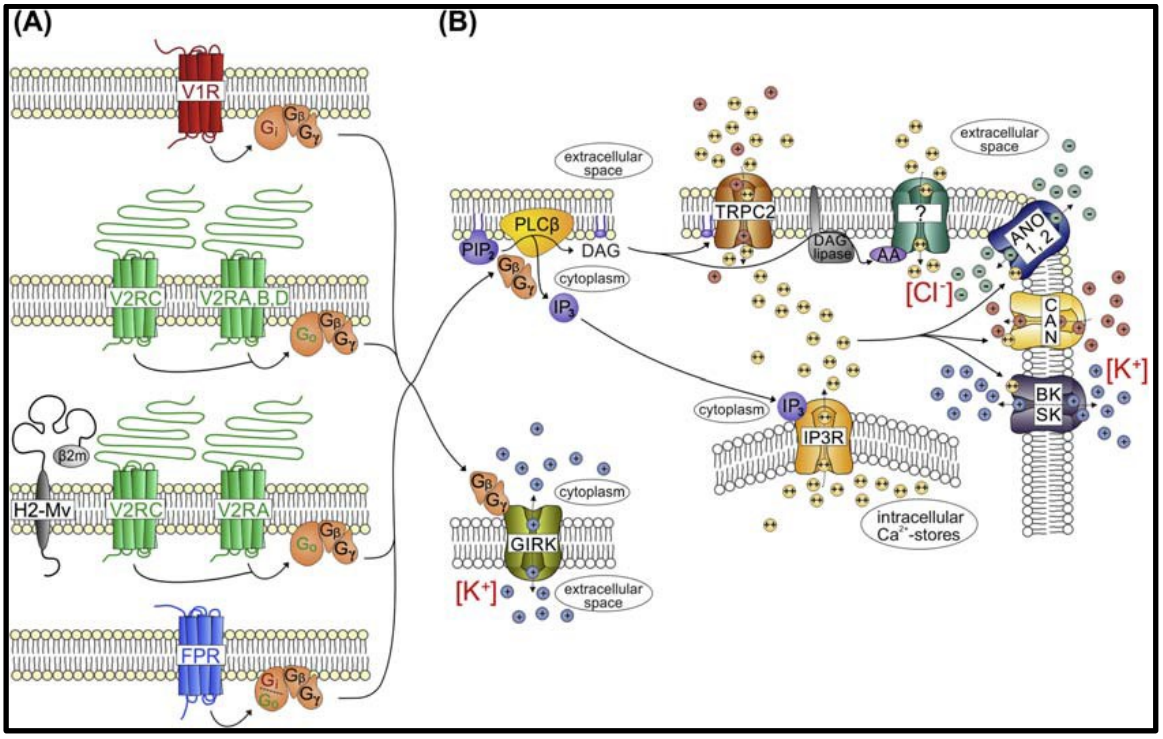

Figure 5 Signal transduction mechanisms involved in vomeronasal signaling*. A.** *Schematic view of putative signal transduction pathways implemented in the mouse vomeronasal organ. Four general "receptor identities" are found in vomeronasal sensory neurons (VSNs): V1R- and G protein α-subunit (Gαi2)-expressing neurons, VSNs coexpressing two V2Rs and Gαo. This neuronal population is subdivided into cells either expressing a family-A, -B, or -D receptor together with a broadly expressed member of the V2RC subfamily, or neurons coexpressing a family-A and family-C V2R in concert with a nonclassical major histocompatibility complex protein (H2-Mv; associated with β2-microglobulin) as well as formyl peptide receptor (FPR)-rs-expressing VSNs that, depending on the specific receptor type, coexpress either Gαi2 or Gαo.* ***B. *Downstream receptor activation, current models presume G protein-dependent activation of phospholipase C (PLCβ), cleavage of phosphatidylinositol-4,5-bisphosphate (PIP2) into soluble inositol-1,4,5-trisphosphate (IP3) and membrane-bound diacylglycerol (DAG), eventually resulting in gating of primary transduction channels that are formed, in part, by the transient receptor potential channel TRPC2. As a secondary event, the rise in calcium is likely boosted by IP3-dependent calcium release from internal stores and gating of an unknown calcium conductance by a polyunsaturated fatty acid metabolite of DAG, probably arachidonic acid (AA). As a multifaceted messenger, calcium has been shown to act on several targets, including calcium-activated chloride channels, likely TMEM16A and/or TMEM16B, calcium-activated cation channels (CAN), and calcium-dependent potassium channels (BK, SK). Microvillar membranes are indicated by yellow lipid polar head groups (filled circles), whereas putative soma/dendritic membranes are marked by open circles [Taken from (Spehr, 2016)].*

1.5.1 G proteins

For many years the demonstration of the involvement of G protein activation after ligand binding with vomeronasal receptors was missing. G protein activation was hypothesized on the basis of the specific co-expression, in the VSN knob/microvilli, of G-protein α-subunits (Gαo and Gαi2) and V1R and V2R receptors (Berghard and Buck, 1996). The direct proof that Gαo is important for the chemoreception process in VSNs arrived in 2014 when a conditional knockout mouse for Gαo protein was created. These mice show a striking reduction in the sensory response of V2R-positive VSNs to specific stimuli as MHC class 1 peptides, MUPs and ESP1, while the response to mitochondrial formyl peptide, activating Gαi2-expressing neurons, were not affected in the Gαo null mice,

indicating that Gαo is essential for signaling, subsequent membrane depolarization, and calcium influx in basal VSNs (Oboti et al., 2014).

Concerning the role of Gαi2 protein in VNO chemoreception, in 2003 it was shown that deletion of this protein produce alterations in behaviors for which an intact VNO is known to be important (Norlin et al., 2003). But it is important to notice that no functional measurements in single VSNs were performed in this study. Furthermore, a global deletion of a widely expressed protein, as Gαi2, could induce a great variety of defects. Direct evidence of the functional role of Gαi2 in V1R-expressing neurons is still lacking (Spehr, 2016). One G protein β-subunit (Gβ2) and two γ-subunits (Gγ2 and Gγ8) have been identified in the VNO (Rünnenburger et al., 2002; Ryba and Tirindelli, 1997; Tirindelli and Ryba, 1996). Gγ2 immunoreactivity is localized to the apical layer of the VNO, while Gγ8-expressing neurons are preferentially restricted to the basal layer. In 2013 Montani and co-workers showed that deletion of Gγ8 protein in mice, produce a slow but remarkable loss of basal VSNs starting from the fourth postnatal week, with a 40% reduction of cells at 2 months and 70% at 1 year. Interestingly, Gγ8 deletion specifically leads to a reduced pheromone-mediated aggressiveness in both males and females, defining the important role of Gγ8 in the maintenance of the VSNs population and in the mechanism of pheromone signaling that regulates aggressive behaviors (Montani et al., 2013).

1.5.2 Phospholipase C (PLC)

Different pharmacological and biochemical data showed that some responses of VSNs to stimuli are mediated by PLC activation. Indeed, Holy and colleagues (2000) measured the electrical activity of mouse VSNs in response to urine using multielectrode array recordings and showed that the PLC inhibitor U73122 blocked spiking responses to urine, whereas the inactive structural analogous U73343 did not produce a measurable effect. Similar results were obtained by Spehr and colleagues (2002) monitoring the activity of rat VSNs upon urine stimulation using calcium imaging. PLC hydrolyzes phosphatidylinositol-4,5-bisphosphate (PIP2) into inositol-1,4,5-trisphosphate (IP3) and diacylglycerol (DAG). Additional evidence of the involvement of PLC in the transduction cascade comes from biochemical studies showing that stimulation of VSNs with urine induced the production of IP3 in several species (Krieger et al., 1999; Kroner et al., 1996; Sasaki et al., 1999; Thompson et al., 2004). More recently RNA-seq data showed that different PLCβ isoforms were expressed by VSNs. Interestingly, it seems that the different PLCβ isoforms are responsible for the response to different stimuli. Indeed, PLCβ2 is directly involved in the response to MUPs while others isoforms, mainly PLCβ4, are involved in non-MUPs stimuli (Dey et al., 2015; Spehr, 2016).

Activation of PLCβ promotes cleavage of PIP2 into IP3 and diacylglycerol (DAG), but the role of the products of PLCβ activation is still under debate. Several different roles have been attributed, including activation of calcium release from internal stores by IP3 (Kim et al., 2011), activation of a DAG-gated channel (Lucas et al., 2003), activation of an arachidonic acid-gated channel (Spehr et al., 2002), and others. However, the role of IP3 in signal transduction is not clear. Indeed, urine-stimulated calcium increase in rat VSNs was not affected by the block of IP3 receptor (Spehr et al., 2002), although the presence of IP3 in the patch pipette induced a nonselective cation current in about 50% of the recorded rat VSNs (Inamura et al., 1997). Recently, Chamero and coworkers (2017)

showed that VSNs can still be activated in type-3 IP3 receptor null mice (Chamero et al., 2017), increasing the evidence that IP3 signaling could be involved in secondary signaling process, as adaptation or activation of other channels. As mentioned before, a general characteristic of VSN activation is the internal increase in cytosolic calcium that can play many roles in the signal transduction process.

1.5.3 Transient receptor potential canonical 2 (TRPC2) channel in VSNs.

The activation of the sensory transduction in the olfactory epithelium leads to the activation and opening of a cyclic nucleotide-gated channel (CNG channel) as described before. During some time researchers tried to find a cyclic nucleotides-gated current in VSNs to elucidate the signaling pathway in VSNs. Excised patches from dendritic knob of VSNs perfused with cAMP or cGMP at saturating concentration failed to develop any current. The same results were found dialyzing the neurons with cyclic nucleotides in whole cell configuration (Liman and Corey, 1996). The impossibility of finding any current activated by cyclic nucleotides in VSNs lead to the proposal of a different signaling pathway involving activation of TRP ion channels VSNs (Holy et al., 2000; Liman et al., 1999). In 1999 Liman *et al* found that the mRNA coding for the TRPC2 member of the TRP channels is present in all the VSNs and that the protein is highly expressed in the microvilli, proposing for the first time that TRP channels are the responsible for the depolarizing current after stimulation in VSNs (Liman et al., 1999). After TRPC2 was proposed as a candidate for the channel activated during signaling transduction in VSNs, the knockout mice for TRPC2 was generated and it was shown that the VSNs lose the capability to respond to urine stimulation (Stowers et al., 2002). In addition to the loss of responsiveness to urine in the TRPC2 KO, it was shown that the channel is important for the survival of the cell during maturation, since more than the 50% of cells were lost in 1 month old KO mice. As expected, behavioral disorders were also observed in the TRPC2 KO mice; but mating behavior was not affected by the mutation. The pheromone male-male aggression behavior was completely abolished, as well as the lack in sex discrimination for mating behavior (Stowers et al., 2002). TRPC2 protein is highly enriched in the VNO sensory microvilli, but early notions of strict VNO specificity have recently been challenged. Expression of TRPC2 in VNO was first described in rats by Liman in 1999 (Liman et al., 1999) showing the specificity of the channel for VNO system. But TRPC2 expression was not evaluated in mice, the species that was subject to gene knockout experiments (Stowers et al., 2002). Surprisingly when Omura and Mombaerts evaluated the expression of TRPC2 in mice, they found that it is expressed also in mouse MOE (Omura and Mombaerts, 2014), necessitating the reinterpretation of the conventional VSN-specific version of the behavioral phenotypes of TRPC2-KO mice.

Besides the possible interpretations of behavioral experiments and effects of knocking out the TRPC2 channels in mice, something that is largely accepted is the main role that TRPC2 is playing in vomeronasal chemoreception. The activation mechanism of TRPC2 in mice was resolved in 2003 by Lucas and colleagues; they reported a DAG-gated calcium permeant cationic current, activated independently of calcium or protein kinase C. They also demonstrate that ablation of the TRPC2 gene causes a severe deficit in the DAG-gated channel, indicating that TRPC2 encodes a principal subunit of this channel and that the primary electrical response to pheromones depends on DAG but not Ins(1,4,5)P, calcium stores, or arachidonic acid (Lucas et al., 2003).

1.5.4 Calcium-activated chloride channels in VSNs

The opening of the cationic channel TRPC2 in VSNs leads to the depolarization of the membrane potential and the increase of cytosolic calcium concentration. The increase in cytosolic calcium plays several roles in signaling transduction involving the activation of other ion channels and enzymes. In 2010, Yang & Delay tested the presence of calcium-activated chloride currents in dissociated VSNs during the response to urine stimulation, using perforated patch clamp with gramicidin to prevent alterations of the internal chloride concentration. During urine stimulation the cells developed an inward current with reversal potential near -20 mV. This current was reduced to near 25% in the presence of the typical chloride channels blocker DIDS at 30 µM, and to near 30% in the presence of niflumic acid at 300 µM. When they changed the external chloride concentration, a change in the reversal potential of the current was measured, confirming the involvement of chloride channels in response to urine stimulation. To confirm if the current was elicited by the increase of intracellular calcium, and considering the permeability of TRPC2 channels to calcium, they measured the current in the absence of extracellular calcium and they found that the DIDS-sensible current was eliminated, indicating that it is generated by the increase of calcium coming from outside the neuron and not from internal stores. It was the first time that it was proposed that calcium-activated chloride currents amplify the urine responses in VSNs (Yang and Delay, 2010). In contrast with Yang and Delay results, another study showed that calcium-activated chloride currents can be activated both by calcium entry through TRPC2 channels and calcium released from internal stores (Kim et al., 2011). In addition of the source of calcium activating the chloride currents, Kim and colleagues also showed that a TRPC2-independent pathway requiring calcium-activated chloride currents is activated during urine stimulation, indicating that calcium-activated chloride channels are working not only as amplifier of transduction currents but also as an independent pathway. In the works form Yang and Delay (2010) and Kim et al., (2011) the activation of calcium-activated chloride currents was studied using indirect ways to activate channels, as the increase in cytoplasmic calcium concentration was a secondary effect of urine stimulation. The presence of calcium-activated chloride channels in the apical portion of VSNs was confirmed by Dibattista and co-workers in 2012 (Dibattista et al., 2012). To investigate the physiological role played by the increase in intracellular calcium concentration in the apical region of VSNs, they produced localized, rapid, and reproducible increases in calcium concentration with flash photolysis of caged calcium and measured calcium-activated currents with the whole cell voltage-clamp technique. They provided a direct demonstration that a large chloride current can be directly activated by calcium in the apical region of mouse VSNs using a method that provides a temporal and spatial control of calcium release, such as photolysis of caged calcium (Dibattista et al., 2012).

1.5.5 Other ion channels

The second messengers in the VSNs signaling pathway can elicit a great variety of regulatory effects in the neurons, e.g. activation of other ionic channels. Calcium-activated cationic channels (I_{CAN}) were first reported in hamster VSNs, showing a half activation with near 500 µM of calcium concentration at negative potentials (Liman, 2003). Later calcium-activated cationic currents were reported in excised patches from the knob of about 12% mouse VSNs (Spehr et al., 2009), being activated with 50 µM

calcium concentration. An interesting open question is the possible role of arachidonic acid (AA) in sensory transduction. Spehr and colleagues (2002) first showed that AA was able to produce an increase in intracellular calcium concentration in rat VSNs. Zhang and colleagues (2010) reported that AA was able to activate a calcium-dependent calcium permeable channel in inside-out patches excised from dendritic knob of mouse VSNs that is independent of TRPC2. Moreover, pharmacological blockage of DAG lipase, an enzyme necessary to the production of AA upon PLC activation, induced a reduction of urine-induced current (Zhang et al., 2010), although another report failed to detect any effect of DAG lipase inhibition (Lucas et al., 2003). In 2012, Kim et al., (Kim et al., 2012) found that also potassium ions play an active role during signaling transduction in VSNs after stimulus presentation. Urine stimulation of VSNs, from TRPC2 KO mice, in absence of chloride ions showed a current carried by potassium ions. They found that two potassium channels were highly expressed in VSNs, the small conductance calcium-activated potassium channel (SK); and the G protein–activated inwardly rectifying potassium channel (GIRK). Later, through a pharmacological approach and using KO mice they showed that those two channels were activated after urine stimulation. Paradoxically, they found a depolarizing role of those potassium currents after urine stimulation, given the high potassium concentration (50mM) in the mucus filling the VNO (Kim et al., 2012). Another potassium channel that was reported to be involved in signaling transduction in VSNs was the large conductance calcium-activated potassium channels (BK). It was found that BK channel was activated via AA production and that repetitive applications of AA potentiated BK activation. It has been proposed that BK channels play a role in urine adaptation in VSNs, preventing the rapid and repetitive firing of action potentials (Zhang et al., 2008).

Another channel has been reported to play a possible role in the membrane properties and excitability regulation of the VSNs, the hyperpolarization-activated cyclic nucleotide-gated (HCN) channels (Cichy et al., 2015; Dibattista et al., 2008). As described previously (see 1.5), VSNs use mainly a DAG/IP3 second messenger cascade for signal transduction but it has been shown that also the level of cAMP in VSNs changes after pheromone stimulation (Luo et al., 1994; Rössler et al., 2000). Dibattista et al., (Dibattista et al., 2008) performed an electrophysiological characterization and evaluated the physiological role of the inward rectifying currents *(I_h)* in mouse VSNs. They described that I_h currents in VSNs are modulated by cAMP and that I_h can modulate the resting membrane potential and the neuron excitability. Furthermore, they found that VSNs express HCN2 and HCN4 isoforms that are possibly the responsible for I_h currents in VSNs (Dibattista et al., 2008). A physiological role for HCN channels was proposed by Cichy et al., (Cichy et al., 2015). They reported the modulation of VSNs excitability by extracellular pH, where extracellular acidification is a potent activator of vomeronasal I_h and suggested that HCN channels can control the gain of signal transduction in VSNs (Cichy et al., 2015).

1.5.6 Sensory adaptation in VSNs

Another role of the cytosolic increase of calcium during signal transduction is the adaptation of the system and sensitivity regulation given by calcium-calmodulin. The TRPC2 channel has a calmodulin binding domain in the amino terminal of the protein and the binding process is calcium dependent (Yildirim et al., 2003). Since TRPC2 plays a primary role during the signaling transduction in VSNs, Spehr et al. (2009) specifically evaluated the role of calmodulin in VSNs. It was found that calmodulin was able to

modulate a diacylglycerol-analog SAG activated current recorded directly from excised patch from the knob of VSNs, the SAG-activated current was probably TRPC2 current due to its similarities. The calcium-calmodulin regulation of the current was then evaluated directly in VSNs activated with different stimuli such as urine, 2-heptanone and MHC-peptides. The adaptation process in the presence of a prolonged stimulation, or during paired stimulation, was eliminated by the commonly used calmodulin's antagonist ophiobolin A and CALP2. All these results revealed that calcium-calmodulin plays an important role in VSN adaptation (Spehr et al., 2009).

1.5.7 Internal chloride concentration in VSNs

As described above, several studies pointed out the presence and importance of calcium-activated chloride currents in VSNs (Dibattista et al., 2012; Kim et al., 2011; Yang and Delay, 2010). The possible role of calcium-activated chloride currents in vomeronasal signal transduction is directly linked with the internal and external concentration of chloride ions. Depending on the equilibrium potential for chloride ions, the current generated by calcium could be depolarizing, amplifying the signal, or hyperpolarizing, reducing the signal. In 2015 Yu and colleagues (Kim et al., 2015), using the fluorescent ion indicator N-[ethoxycarbonylmethyl]-6-methoxy-quinolinium bromide (MQAE) measured the internal chloride concentration in the soma of VSNs, founding that it was near 85 mM, which, assuming a high external chloride concentration between 55 and 84mM (chloride concentration in mucus from MOE) (Billig et al., 2011; Reuter et al., 1998), gives a depolarizing role to the calcium-activated chloride currents. After urine stimulation, a decrease was observed in the internal chloride concentration arriving to near 60 mM, confirming the efflux of chloride after VSN stimulation. The decrease in chloride concentration was unexpectedly high; the current necessary to change the ionic concentration of an ion in a cell with a diameter near 10 µm by 20 mM, would be about 1 ampere. If we consider the high membrane resistance in VSNs, being typically few Gigaohms (Dibattista et al., 2008; Ghiaroni et al., 2003; Liman and Corey, 1996; Shimazaki et al., 2006; Ukhanov et al., 2007), that current would produce a very huge change in membrane potential, at the level of Gigavolts, something not very plausible in a common signal transduction process. If the real change in chloride concentration is around 20 mM after urine stimulation it could indicate the presence of another mechanism to regulate the internal chloride concentration.

Given that the transduction machinery, including the calcium-activated chloride channels, is mainly expressed in the microvilli of the dendritic knob, it is more accurate to measure the cytosolic chloride concentration directly in the knob. In 2016, Spehr and colleagues (Untiet et al., 2016) measured the cytosolic chloride concentration directly from the dendritic knob using quantitative fluorescence lifetime imaging microscopy (FLIM) of MQAE. They reported an internal chloride concentration near 42 mM, a lower value than 80 mM measured in the soma by (Kim et al., 2015), but still giving a depolarizing role to the chloride current after calcium activation, if it is assumed that the external chloride concentration is between 55 and 84 mM, similar to the concentration found in the mucus of the MOE (Billig et al., 2011; Reuter et al., 1998). In addition, it was found that chloride shows a concentration gradient along the VSN apico-basal dendritic axes, indicative of active chloride accumulation in VSN knobs (Untiet et al., 2016). The internal chloride accumulation could be caused by the activity of diverse Na–K–Cl (NKCC) cotransporter and/or K–Cl (KCC) cotransporters that are expressed in VSNs (Untiet et al., 2016; Yang and

Delay, 2010). Expression of NKCCs and KCCs chloride co-transporters in VSNs has been examined using RT-PCR, transcriptome-wide single neuron analysis and immunocytochemistry (Untiet et al., 2016; Yang and Delay, 2010). Specifically, it has been found that NKCC1 was the chloride transporter most prevalently expressed across VSNs and most abundantly expressed within VSNs (Untiet et al., 2016; Yang and Delay, 2010). NKCC1 is also abundantly expressed in the main olfactory epithelium and involved in olfactory neuron chloride accumulation (Kaneko et al., 2004; Reisert et al., 2005). KCC3 and KCC4 transporters have been shown to be also expressed in the majority of VSNs (Untiet et al., 2016), indicating that either or both chloride cotransporter(s) could add to chloride accumulation in VSN knobs.

1.6 Axonal projection of VSNs

As described in previous sections, VSNs inside the sensory epithelium can be divided in at least two populations, basal and apical neurons, with apical neurons expressing receptors of the V1R-family and basal neurons expressing receptors of the V2R-family (Dulac and Axel, 1995; Herrada and Dulac, 1997; Matsunami and Buck, 1997; Ryba and Tirindelli, 1997). The segregated localization of V1R- and V2R-expressing VSN cell bodies in the VNO is maintained at the level of their axonal projections to the accessory olfactory bulb (AOB). V1R-expressing VSNs that have their cell bodies in the apical layer of the VNO project axons to the anterior portion of the AOB, whereas basally located V2R-expressing VSNs innervate the posterior region of the AOB (Fig 6A-B) (Belluscio et al., 1999; Brignall and Cloutier, 2015; Halpern, 1987; Liberles et al., 2009; Riviere et al., 2009; Rodriguez et al., 1999; Wagner et al., 2006). In rodents, both the MOB and the AOB have a similar laminar organization with a superficial nerve layer formed by the axonal projections of the chemosensory neurons, a layer of neuropil structures termed glomeruli that represents the first order synaptic region between sensory neurons and mitral cell dendrites, and the external and internal plexiform layers that are regions where soma of, respectively, mitral/tufted and granule cells reside (Fig 6C) (Meisami and Bhatnagar, 1998). The wiring pattern of apical neurons/anterior AOB and basal neurons/posterior AOB is not maintained at the level of mitral cell projections, which directly innervate multiple nuclei of the limbic system, bypassing cortical structures (Halpern, 1987; Kang et al., 2006; Martínez-Marcos and Halpern, 1999; Mohedano-Moriano et al., 2008; Salazar and Brennan, 2001; Scalia and Winans, 1975; Von Campenhausen and Mori, 2000; Winans and Scalia, 1970). Neurons located in nuclei innervated by mitral cells project to multiple areas of the hypothalamus that are linked to aggression, parental behavior, and reproduction, including the ventromedial hypothalamus (Brignall and Cloutier, 2015; Newman and Winans, 1980; Scalia and Winans, 1975; Von Campenhausen and Mori, 2000).

In the AOB, glomeruli are very diffusely organized, surrounded by a small number of periglomerular cells, and highly variable in size (10-30 µm of diameter in mice). Neurons expressing the same receptor coalesce into 10–30 glomeruli. Moreover, the capacity to converge and to form these glomeruli depends on the possibility to express a specific vomeronasal receptor gene, deletion of VRs leads to the improper axon connections to glomeruli in the AOB, suggesting that the receptor proteins themselves play a role in axonal wiring to the bulb (Belluscio et al., 1999; Rodriguez et al., 1999). An additional layer of axonal organization has been proposed to exist within the posterior region of the

AOB (Fig 6B). A subset of basal VSNs expresses members of a family of non-classical class I major histocompatibility Mhc genes, known as H2-Mv genes, which have been shown to regulate VRs cell surface expression (Ishii and Mombaerts, 2008, 2011).

Mitral cells located in either the anterior or posterior half of the external plexiform layer (EPL) of the AOB project their apical dendrites to glomeruli located in the homonymous half of the AOB (Fig 6C) (Brignall and Cloutier, 2015; Larriva-Sahd, 2008; Yonekura and Yokoi, 2008), suggesting that the spatial segregation of V1R and V2R glomerular inputs along the anterior–posterior axis of the AOB may be maintained at the level of the mitral cell layer. However, a subset of mitral cells located at the anterior–posterior border of the AOB has been reported to project their apical dendrites to the opposite half of the AOB (Fig 6C-II) (Yonekura and Yokoi, 2008). Mitral cells can project their dendrites to glomeruli expressing the same VR (homotypic) or different VRs (heterotypics) (Fig 6C I-III) (Del Punta et al., 2002b).

Axonal projection of apical and basal neurons to the anterior and posterior region, respectively, of the AOB is regulated by the expression of several adhesion molecules. The semaphoring-neuropilin complex is one of the ligand–receptor pairs that contribute to this process. The class 3 semaphorin receptor Nrp-2 is selectively expressed in apical VSNs axons, which are repelled in vitro by explants of the posterior half of the AOB, suggesting that this region secretes a chemorepellent capable of preventing entry of apical axons into the posterior AOB (Cloutier et al., 2002). In addition to apical VSN axons being repelled from the posterior AOB due to Nrp-2 activity, apical VSN axons also respond to an attractive signal in the anterior region of the AOB which involves ephirin-A5 and EphA6. Apical axons express ephrin-A5 at their surface, while the EphA6 receptor is more highly expressed in the anterior region of the AOB. A subset of EphrinA5 knockout mice exhibits apical VSN axon mistargeting to the posterior AOB defining a requirement for ephrinA5 in VSN axon targeting (Knoll et al., 2001). Basal VSN axons, which do not express Nrp-2, express Robo-2, a receptor for the Slit family of secreted chemorepulsive axon guidance cues, and deletion of Robo-2 lead to a mistargeting of basal axons to the anterior AOB (Knöll et al., 2003; Prince et al., 2009)

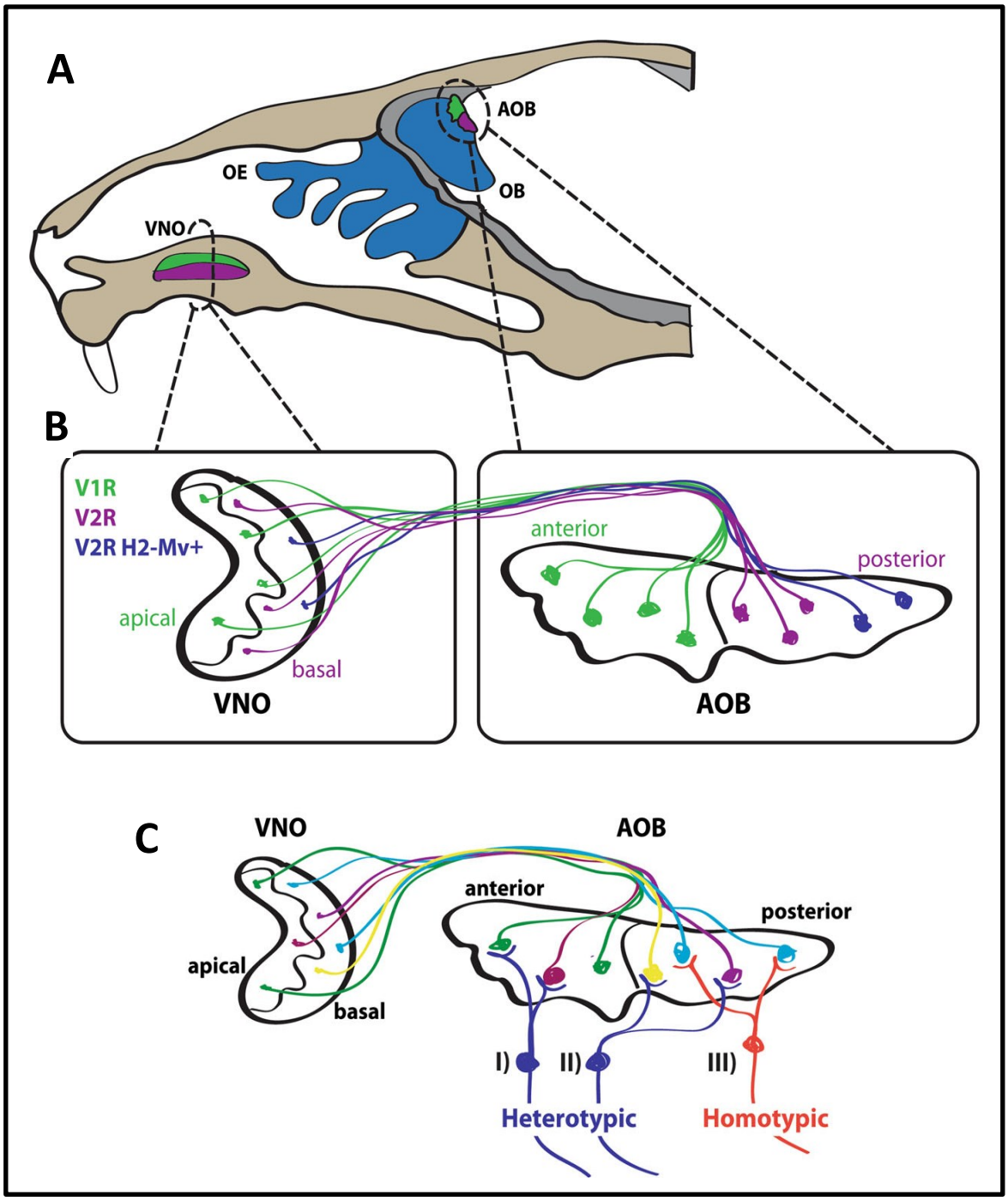

Figure 6. Axonal projection of the mouse vomeronasal system. A. *VSNs project axons to the AOB located on the caudal region of the OB. The sensory epithelium of the VNO is divided into apical (green), and basal (purple) regions. The AOB is also subdivided into two regions, the anterior (green) and posterior (purple) sections.* ***B.*** *Apical VSNs express V1R receptors and project their axons to the anterior region of the AOB (green). In contrast, basally VSNs express V2R receptors and innervate the posterior region of the AOB (purple). A third population of VSNs located in the basal region of the VNO expresses both V2Rs and H2-Mvs (blue). This population of VSNs projects its axons to a posterior subdomain within the posterior region of the AOB.* ***C.*** *VSN axons entering the AOB synapse onto dendrites of mitral cells whose cells bodies are located within the external plexiform layer (EPL) of the AOB. Mitral cells project their dendrites to multiple glomeruli in the AOB to form both homotypic (III), if they are connected with glomeruli expressing a given VR, and heterotypic (I) connections, if they project dendrites to multiple glomeruli innervated by populations of VSN axons expressing different VRs. Some mitral cells located near the anterior–posterior border of the AOB can project their dendrites to the opposite half of the glomerular layer (II). AOB accessory olfactory bulb, OB olfactory bulb, OE olfactory epithelium, VNO vomeronasal organ [taken from (Brignall and Cloutier, 2015)].*

1.7 TMEM16 channels

1.7.1 TMEM16 proteins as calcium-activated chloride channels.

Calcium-activated chloride channels are fundamental mediators in numerous physiological processes including trans-epithelial secretion, cardiac and neuronal excitation, sensory transduction, smooth muscle contraction and fertilization. All the calcium-activated chloride channels involved in those physiological process share common characteristics such as voltage dependence of calcium activation and a preference for permeating large anions (Duran et al., 2010; Hartzell et al., 2004; Huang et al., 2012). Surprisingly, the identity of the genes coding for the calcium-activated chloride channels was hidden for a long time and some candidates were proposed; ClC family, bestrophin family or tweety, but none of them fitted completely the physiological characteristics of native calcium-activated chloride channels (Hartzell et al., 2004). Specifically, calcium-activated chloride currents were first described in frog OSNs (Kleene and Gesteland, 1991), and later in OSNs from many other animals (Schild and Restrepo, 1998). Bestrophin-2 was proposed as the calcium-activated chloride channel in OSNs, but it was shown that calcium-activated chloride currents were not affected by the deletion of bestrophin-2 (Pifferi et al., 2009a).

In 2008 three different groups reported the molecular identity of calcium-activated chloride channels. These laboratories from three continents took different approaches but all reported the same protein, TMEM16A, as a bona fide calcium-activated chloride channel (Caputo et al., 2008; Schroeder et al., 2008; Yang et al., 2008). Later studies indicated that at least two members of the TMEM16 family, TMEM16A and TMEM16B, are calcium-activated chloride channel (Pifferi et al., 2009b; Stephan et al., 2009; Stöhr et al., 2009). Given the eight putative transmembrane domains of TMEM16 members and the ability of TMEM16A to form calcium-activated chloride channels, Yang and coworkers called this family Anoctamin family (from anionic and eight transmembrane domains). The term Anoctamin, or ANO to identify a single member (e.g. ANO1 for TMEM16A), is not correct for two main reasons: 1) not all the family members code for chloride channels, as for example TMEM16F which works as a phospholipid scramblase (Suzuki et al., 2010), and 2) the recent X-ray structure of a TMEM16 homologue from *Nectria haematococca* (nhTMEM16) shows it has ten transmembrane domains (Brunner et al., 2014). Given these recent results, I am going to avoid the use of Anoctamin or ANO to refer to TMEM16 proteins. The TMEM16 family is composed by 10 members, 2 of them are calcium-activated chloride channels (members A and B), and some other members have been shown to work as lipid scramblases combined with ion channel activity (Benarroch, 2017; Whitlock and Hartzell, 2017).

1.7.2 TMEM16B in MOE

In vertebrate OSNs, signaling by a calcium-activated chloride conductance in the cilia is the final step of a well-characterized signal transduction pathway (Firestein, 2001; Kleene, 2008). When odors bind to receptor proteins in the ciliary membrane, a G protein signaling cascade is activated, producing an increase in the internal cAMP concentration through the activation of adenylyl cyclase. The open probability of CNG channels increases causing an influx of calcium and sodium. The rise in cytosolic calcium

concentration due to calcium influx through the CNG channels activates calcium-activated chloride channels on the cilia. The chloride current at the cilia of ORNs is inward, hence excitatory, carrying up to 80% of the odorant-induced receptor current in rodents, studied under voltage clamp condition (Firestein, 2001; Reisert et al., 2005). Although, the calcium-activated chloride currents were found, characterized and their role in olfactory transduction was studied thoroughly in the early 90's, the molecular identity of the protein responsible for the current was not known for a long time. In 2009 Stephan and colleagues identified TMEM16B in a proteomic screen of OSN cilia membranes and provided molecular and electrophysiological evidence indicating that TMEM16B constitutes the long-sought olfactory calcium-activated chloride channel that may mediate signal amplification (Stephan et al., 2009). Later it was shown, by immunohistochemistry, that TMEM16B protein is expressed in the OSN cilia (Hengl et al., 2010; Rasche et al., 2010; Sagheddu et al., 2010). Confirmation that TMEM16B is the channel responsible for calcium-activated chloride currents in OSN arrived with the TMEM16B KO mouse. Billig et al. (2011) reported that by eliminating TMEM16B the calcium-activated chloride currents were completely eliminated in OSNs. Surprisingly, they found that electro-olfactogram (EOG) recordings of TMEM16B KO mice were reduced by only up to ~40%, and TMEM16B KO mice were able to smell normally (Billig et al., 2011). Recently, Pietra et al. (2016) reexamined the role of the TMEM16B channel in OSNs by further extending the experimental analysis and comparing additional aspects of olfactory function in TMEM16B KO versus WT mice. It was found that TMEM16B plays an important role in several aspects in the olfactory system. OSNs from TMEM16B KO showed a different firing pattern when compared with WT; spontaneous activity was reduced; and when OSNs from TMEM16B KO were stimulated by odors they responded with a higher firing activity than those from WT mice; the axonal targeting to the olfactory bulb was also affected by the loss of TMEM16B protein, with the appearance of more glomeruli for one specific receptor. Interestingly, TMEM16B KO mice showed an olfactory defect when evaluated through behavioral tests, showing a reduction in the ability to find previously unknown buried food. Altogether, these results showed that TMEM16B is relevant for the normal development and function of the olfactory system (Dibattista et al., 2017; Pietra et al., 2016).

OSNs express two variants of the tmem16b gene, isoform A and Isoform B, differing in its N-terminus length (Ponissery Saidu et al., 2014). In addition, TMEM16B expressed in the olfactory epithelium presents alternative splicing at exon 4, generating TMEM16B variants either with or without exon 4. The exon 4–containing transcripts are present in greater abundance than the exon 4–lacking transcripts. The N-terminus variants showed different calcium sensitivity while the exon 4 is required for channel function in a heterologous system (Ponissery Saidu et al., 2014).

1.7.3 TMEM16 proteins in VSNs

As shown before, the study of calcium-activated chloride currents in VNO started just few years ago with the works of Yang and Delay, Kim et al, and Dibattista et al (Dibattista et al., 2012; Kim et al., 2011; Yang and Delay, 2010). Furthermore, the presence of calcium-activated chloride channels in the apical portion of VSNs was confirmed by local photorelease of caged calcium (Dibattista et al., 2012). As at the beginning for the MOE, the molecular identity of the protein responsible for the currents in the VNO was not

known. Some studies reported that two members of the TMEM16 family, TMEM16A and TMEM16B, are expressed in the VNO and specifically in the microvilli of the VSNs (Billig et al., 2011; Dauner et al., 2012; Dibattista et al., 2012; Rasche et al., 2010). Although both channels are co-expressed in VSNs microvilli and calcium-activated chloride currents have been reported in VSNs, a clear electrophysiological characterization of those currents is still missing, as well as the identity of the channel. Billig et al. (2011) reported that calcium-activated chloride currents were eliminated in the TMEM16B KO mouse (Billig et al., 2011). However, it is important to notice that Billig et al. (2011) compared a very small number of cells (WT n=7, TMEM16B KO n=5) and reported that a residual current was still present in some neurons.

2. AIMS

The specific aims of this work were:

- To provide an electrophysiological characterization of calcium-activated chloride currents in mouse VSNs.
- To identify the molecular identity of the channels mediating calcium-activated chloride currents in VSNs.
- To determine the effect of eliminating calcium-activated chloride currents on spontaneous and evoked activity in VSNs.

3. MATERIALS AND METHODS.

3.1 Animals.

Mice were handled in accordance with the guidelines of the Italian Animal Welfare Act and European Union guidelines on animal research, under a protocol approved by the ethic committee of SISSA. 2–3-mo-old mice were anaesthetized by CO_2 inhalation and decapitated before VNO removal.

To obtain mice in which TMEM16A expression was specifically eliminated in mature vomeronasal sensory neurons, we crossed floxed TMEM16A$^{fl/fl}$ mice, whose generation has been previously described in detail [(Faria et al., 2014; Schreiber et al., 2015); provided by J. Rock, University of California, School of Medicine, San Francisco], with mice expressing Cre recombinase under the control of the olfactory marker protein (OMP) promoter [OMP-Cre mice; (Li et al., 2004); provided by P. Mombaerts, Max Planck Research Unit for Neurogenetics, Frankfurt, Germany]. Our conditional TMEM16A knockout mice (TMEM16A cKO) were homozygous for the floxed TMEM16A alleles and heterozygous for Cre and OMP. C57BL/6 or TMEM16Afl/fl mice were used as controls.

3.2 Dissociation of mouse vomeronasal sensory neurons

The vomer capsule containing the VNO was removed as described previously (Arnson and Holy, 2011; Dean et al., 2004; Liman and Corey, 1996; Shimazaki et al., 2006). Vomeronasal sensory neurons were dissociated from the VNO with the enzymatic-mechanical dissociation protocol described in Dibattista et al. (Dibattista et al., 2008, 2012), or with the following slight modifications. In brief, the removed vomer capsule was put into a Petri dish containing divalent-free PBS (Sigma-Aldrich) solution where the VNO was extracted and transferred to a tube containing PBS with 1 mg/ml collagenase (type A), incubated at 37°C for 20 min, and transferred twice to Ringer's solution with 5% fetal bovine serum for 5 min. The tissue was then cut into small pieces with tiny scissors and gently triturated with a fire-polished Pasteur pipette. Neurons were plated on Petri dishes (WPI) coated with concanavalin A (type V; Sigma-Aldrich) and stored at 4°C.

3.3 Patch-clamp recordings and ionic solutions in isolated VSNs.

Dissociated VNSs were viewed using an inverted microscope (IMT-2 or IX70; Olympus) with 20× or 40× objectives and identified by their bipolar shape, as illustrated in Fig. 1 of Dean et al. (Dean et al., 2004). Patch pipettes, pulled from borosilicate capillaries (WPI) with a PC-10 puller (Narishige), had a resistance of 3–6 MΩ for whole-cell and 6–8 MΩ for excised patch recordings.

Currents were recorded with an Axopatch 1D, 200B or 700B amplifier controlled by Clampex 9 or 10 via a Digidata 1332A or 1440 (Molecular Devices). Data were low-pass filtered at 2 or 5 kHz and sampled at 10 kHz. Experiments were performed at room temperature (20–25°C). For whole-cell recordings, the standard extracellular mammalian Ringer's solution contained (mM): 140 NaCl, 5 KCl, 2 $CaCl_2$, 1 $MgCl_2$, 10 HEPES, 10 glucose,

and 1 sodium pyruvate, pH 7.4. The intracellular solution filling the patch pipette contained (mM): 140 CsCl, 10 HEPES, and 10 HEDTA, adjusted to pH 7.2 with CsOH, and no added calcium for the nominally 0-calcium solution, or various added calcium concentrations, as calculated with the program WinMAXC (C. Patton, Stanford University, Stanford, CA), to obtain free calcium in the range between 0.5 and 13 µM (Patton et al., 2004), as described previously (Pifferi et al., 2006, 2009a). The composition of the intracellular solutions containing 2 mM calcium was (mM) 140 CsCl, 10 HEPES, 2 $CaCl_2$ or 145 NaCl, 10 HEPES, and 2 $CaCl_2$, as in Liman (2003). No significant difference was observed among currents activated by the two solutions containing 2 mM calcium. For ionic selectivity experiments, NaCl in the extracellular mammalian Ringer's solution was replaced with equimolar choline chloride, Na-gluconate, or NaSCN. Niflumic acid (NFA), CaCCinh-A01 (Tocris Bioscience), and anthracene-9-carboxylic acid (A9C) were prepared in DMSO as stock solutions at 200 mM, 20 mM, or 1 M, respectively, and diluted to the final concentrations in Ringer's solution. A gravity perfusion system was used to exchange solutions.

In most whole-cell recordings, we applied voltage steps from a holding potential of 0 mV ranging from -100 to 100 (or 160 mV), followed by a step to -100 mV. A single-exponential function was fitted to instantaneous tail currents to extrapolate the current value at the beginning of the step to -100 mV. For inside-out recordings, the solution in the patch pipette contained (mM): 140 NaCl, 10 HEDTA, and 10 HEPES, pH 7.2. The bathing solution at the intracellular side of the patch contained (mM): 140 NaCl, 5 EGTA or 10 HEDTA, and 10 HEPES, pH 7.2, and no added calcium for the nominally 0-calcium solution, or various added calcium concentrations, as calculated with the program WinMAXC (C. Patton, Stanford University, Stanford, CA), to obtain free calcium in the range between 0.18 and 100 µM (Patton et al., 2004).

Rapid solution exchange in inside-out patches was obtained with the perfusion Fast-Step (SF-77B; Warner Instruments). For I-V relations of calcium-activated currents, a double voltage ramp from -100 to 100 mV and back to -100 mV was applied at 1 mV/ms. The two I-V relations were averaged, and leak currents measured with the same ramp protocol in calcium-free solutions were subtracted. For dose–response experiments, a patch was exposed for 1 s to solutions with increasing calcium concentration. The bath was grounded through a 3 M KCl agar bridge connected to an Ag/AgCl reference electrode. Liquid junction potentials were calculated using Clampex's Junction Potential Calculator (Molecular Devices), based on the JPCalc program developed by Barry (1994), and applied voltages were corrected offline for the calculated values.

3.4 Preparation of acute slices of mouse vomeronasal organ

Acute slices of mouse VNO were prepared as described previously (Shimazaki et al., 2006). In brief, the VNO was removed and transferred to ice-cold artificial cerebrospinal fluid (ACSF). The capsule and all cartilaginous tissues were carefully removed and the two halves of the VNO were isolated from the vomer bone. Each half of the VNO was then separately treated. The VNO was embedded in 3% low-grade agar (A7002 Sigma) prepared in ACSF once the agar had cooled to 38°C. Upon solidification, the agar block was fixed in a glass Petri dish and sliced with a vibratome (Vibratome 1000 Plus Sectioning System) at 200 -250 µm in oxygenated ACSF solution. Slices were then left to recover for >30 min before electrophysiological experiments were initiated.

3.5 Patch clamp recording in VSNs from acute slices

For whole-cell recordings, the intracellular solution filling the patch pipette contained (mM): 110 K-Gluconate, 30 KCl, 10 NaCl, 1 $MgCl_2$, 0.023 $CaCl_2$, 10 HEPES, and 10 EGTA, adjusted to pH 7.2 with KOH. The cell was kept at a holding potential of -70 mV from where 10 mV steps were applied from -100 mV to +40 mV. To test the membrane resistance a -10 mV step was applied from the holding potential and the steady-state current was measured to calculate the membrane resistance. Series resistance was not compensated. Resting membrane potential was measured in current clamp mode under I=0 configuration, shortly after obtaining the whole-cell configuration.

Slices were viewed with an upright microscope (Olympus BX51WI) by infrared differential contrast optics with water immersion 20X or 60X objectives. The murine slice preparation maintained the VNO cross-sectional structure, many individual vomeronasal sensory neurons (VSNs) could be clearly distinguished by their morphology. Patch pipettes, pulled from borosilicate capillaries (WPI) with a PC-10 puller (Narishige), had a resistance of 3–6 MΩ for whole-cell and loose-patch recordings. Currents were recorded with a Multiclamp 700B amplifier controlled by Clampex 10 via a Digidata 1440 (Molecular Devices). Data were low-pass filtered at 2 kHz and sampled at 10 kHz. Experiments were performed at room temperature (20–25°C). The recording chamber was continuously perfused with oxygenated (95% O_2, and 5% CO_2) artificial cerebrospinal fluid (ACSF) contained (mM): 120 NaCl, 20 $NaHCO_3$, 3 KCl, 2 $CaCl_2$, 1 $MgSO_4$, 10 HEPES, 10 glucose pH 7.4 by gravity flow. The slice was anchored to the base of the recording chamber using a home-made U-shaped silver wire, holding down the agar support without touching the slice itself.

3.6 Loose-patch extracellular recording in VSNs from acute slices

Extracellular recordings from the soma of VSNs were obtained in the loose-patch configuration with seal resistances of 40-100 MΩ. Pipette solution was ACSF, as the bath solution, and the recordings were made in voltage-clamp mode with a holding potential of 0 mV. Data were low-pass filtered at 2 kHz and sampled at 10 kHz. Stimulation was focally delivered through a multi-barrelled stimulation pipettes system (ALA-VM8, ALA Scientific Instruments) working with gravity pressure. The tip of the perfusion head, with a diameter of 360 µm, was placed ~500 µm away from the slice. The time delay of the stimulus was measured using high-potassium solution. It took around 300 ms from the opening of the valve to the start of the activity in the neuron. To avoid mechanical artifact, the slice was constantly perfused with ACSF and the flow out of the pipette was switched between ACSF and stimulus solutions, resulting in a constant flow across the epithelium and sharp concentration transients, undiluted by the bath ACSF. It was possible to record from single VSNs, just in few cases two neurons were recorded at the same time from a single electrode but the single action potentials of the two different cells were clearly different in size and shape.

3.7 Urine collection and solutions for VSNs stimulation.

Urine was collected from both sexes of adult (>2 months) C57BL/6 mice, filtered with a 0.2-µm filter and frozen at -80°C. Before use, male and female urines were mixed in 1:1 ratio and the mixture was diluted to 1:50 in ACSF (pH 7.4). Mouse urine contains urea and potassium ions, which could potentially cause neurons to fire by direct membrane

depolarization. As a negative control we used artificial urine diluted 1:50 (Holy et al., 2000), artificial urine contains (mM): 100 NaCl; 40 KCl; 20 NH_4OH; 4 $CaCl_2$; 2.5 $MgCl_2$; 15 NaH_2PO_4; 20 $NaHSO_4$; 333 urea; pH 7.4 adjusted with NaOH. As a positive control we used high-potassium solutions (25 mM KCl) by substituting equimolar quantities of KCl for NaCl. Urine and artificial urine were presented in 10-seconds pulses, the inter-stimulus interval was at least 4 minutes to avoid desensitization or adaptation process (Spehr et al., 2009). High-potassium was presented in 3 or 5-seconds pulses.

3.8 Chemicals

All compounds and chemicals were obtained from Sigma-Aldrich, unless otherwise stated.

3.9 Analysis of electrophysiological data

IgorPro software (WaveMetrics) and Clampfit (Molecular Devices) were used for data analysis and figure preparation. Data are presented as mean ± SEM. Because most of the data were not normally distributed (Shapiro–Wilk test), statistical significance was determined using Wilcoxon-Mann Whitney test or Kolmogorov-Smirnov test. p-values of <0.01 were considered statistically significant. For data normally distributed t-test was used (Fig 1D).

For spike detection, recordings were filtered offline with a high-pass filter at 2 Hz to eliminate slow changes in the baseline. Individual action potentials were identified by an event detection using an arbitrary threshold, and each event was confirmed by shape inspection. The start time of each event was taken as the time for that individual action potential. Mean spontaneous firing frequency was calculated as the number of spikes divided by the duration of the recording. Inter-spike interval (ISI) was calculated measuring the time between consecutive spikes (second to first, third to second, and so forth). To construct the ISI distribution during spontaneous activity we calculated the ISI for all spikes in 158 recordings of 90 s each from 20 WT VSNs, and 161 recordings of 90 s each from 22 TMEM16A cKO VSNs. Then we grouped the ISIs in 5 ms bins and divided the value of each bin by the total number of calculated ISIs for each group. The y-axes value in Fig 2C represents the percentage of spikes in each bin, the area under the curve is 100 %. ISI distribution during odor-evoked activity was calculated from the spikes during the 10 s stimulus presentation and calculating the ISI as described for spontaneous activity but with 10 ms bins (Fig 4D). Average firing rate (Fig 3 bottom) was calculated dividing each recording (Fig 3 Middle) in 1 s bins and counting the number of spikes per bin. The histogram represents the mean ± SEM of all repeats for one single VSN.

As VSNs usually shows spontaneous activity in bursts (Arnson and Holy, 2011), it was difficult to identify a urine response from a single recording. To avoid false positives we applied at least 4 repetitive stimulations. Each recording was 90 s long divided in: 40 s of pre-stimulus, 10 s of stimulus, and 40 s of post-stimulation. To analyze the response to urine for a single cell we took the basal period (40 s pre-stimulation) and stimulus period (10 s of stimulation), and we calculated the basal and stimulation frequency for each trace. We defined a threshold level as: $BF + 2*\sigma^2$; where BF is the average of basal frequency for all the traces and σ^2 is the standard deviation of the basal frequency. A cell was considered responsive to urine if: 1) the average spike frequency during the

stimulations (SF) was higher than the threshold and 2) there was not response in artificial urine.

3.10 Immunohistochemistry

VNO sections and immunohistochemistry were obtained as described previously (Dibattista et al., 2012). The following primary antibodies were used: rabbit anti-TMEM16A (1:50; Abcam), goat anti-TMEM16A (1:50; Santa Cruz Biotechnology, Inc.), rabbit anti-TMEM16B (1:100; Santa Cruz Biotechnology, Inc.), and goat anti-TRPC2 (1:50; Santa Cruz Biotechnology, Inc.). The following secondary antibodies obtained from Invitrogen were used: donkey anti–rabbit Alexa Fluor 488 (1:500) and donkey anti–goat Alexa Fluor 594 (1:500). Immunoreactivity was visualized with a confocal microscope (TCS SP2; Leica). Images were acquired using Leica software (at 1,024 × 1,024–pixel resolution) and were not modified other than to balance brightness and contrast. Nuclei were stained by DAPI (1:500), and signals were enhanced for better visualization of the vomeronasal epithelium. Control experiments without the primary antibodies gave no signal.

4. RESULTS

4.1 Conditional knockout of TMEM16A/anoctamin1 abolishes the calcium-activated chloride current in mouse vomeronasal sensory neurons

Published March 16, 2015

Conditional knockout of TMEM16A/anoctamin1 abolishes the calcium-activated chloride current in mouse vomeronasal sensory neurons

Asma Amjad,[1]* Andres Hernandez-Clavijo,[1]* Simone Pifferi,[1]* Devendra Kumar Maurya,[1] Anna Boccaccio,[2] Jessica Franzot,[1] Jason Rock,[3] and Anna Menini[1]

[1]Neurobiology Group, SISSA, Scuola Internazionale Superiore di Studi Avanzati, 34136 Trieste, Italy
[2]Istituto di Biofisica, National Research Council, 16149 Genova, Italy
[3]Department of Anatomy, University of California, San Francisco, School of Medicine, San Francisco, CA 94143

Pheromones are substances released from animals that, when detected by the vomeronasal organ of other individuals of the same species, affect their physiology and behavior. Pheromone binding to receptors on microvilli on the dendritic knobs of vomeronasal sensory neurons activates a second messenger cascade to produce an increase in intracellular Ca^{2+} concentration. Here, we used whole-cell and inside-out patch-clamp analysis to provide a functional characterization of currents activated by Ca^{2+} in isolated mouse vomeronasal sensory neurons in the absence of intracellular K^+. In whole-cell recordings, the average current in 1.5 µM Ca^{2+} and symmetrical Cl^- was −382 pA at −100 mV. Ion substitution experiments and partial blockade by commonly used Cl^- channel blockers indicated that Ca^{2+} activates mainly anionic currents in these neurons. Recordings from inside-out patches from dendritic knobs of mouse vomeronasal sensory neurons confirmed the presence of Ca^{2+}-activated Cl^- channels in the knobs and/or microvilli. We compared the electrophysiological properties of the native currents with those mediated by heterologously expressed TMEM16A/anoctamin1 or TMEM16B/anoctamin2 Ca^{2+}-activated Cl^- channels, which are coexpressed in microvilli of mouse vomeronasal sensory neurons, and found a closer resemblance to those of TMEM16A. We used the Cre–loxP system to selectively knock out TMEM16A in cells expressing the olfactory marker protein, which is found in mature vomeronasal sensory neurons. Immunohistochemistry confirmed the specific ablation of TMEM16A in vomeronasal neurons. Ca^{2+}-activated currents were abolished in vomeronasal sensory neurons of TMEM16A conditional knockout mice, demonstrating that TMEM16A is an essential component of Ca^{2+}-activated Cl^- currents in mouse vomeronasal sensory neurons.

INTRODUCTION

Chemosensation is used by animals to obtain information from the environment and to regulate their behavior. In most mammals, both the main olfactory epithelium and the vomeronasal epithelium are involved in chemodetection (Brennan, 2009; Tirindelli et al., 2009; Touhara and Vosshall, 2009). Sensory neurons in these epithelia detect chemicals and, through different second messenger–mediated transduction pathways, generate action potentials that are transmitted to different regions of olfactory bulbs. In vomeronasal sensory neurons, the binding of chemicals with vomeronasal receptors occurs in the microvilli, at the apical region of the neuron's dendrite. In rodents, these neurons express one or a few members of three families of G protein–coupled receptors: V1Rs, V2Rs, and formyl peptide receptors (FPRs) (Dulac and Axel, 1995; Herrada and Dulac, 1997; Matsunami and Buck, 1997; Ryba and Tirindelli, 1997; Martini et al., 2001; Liberles et al., 2009; Rivière et al., 2009; Francia et al., 2014). The binding of molecules to vomeronasal receptors activates a phospholipase C pathway, which leads to the influx of Na^+ and Ca^{2+} ions mainly through the transient receptor potential canonical 2 (TRPC2) channel present in the microvilli (Liman et al., 1999; Zufall et al., 2005; Munger et al., 2009), and/or to Ca^{2+} release from intracellular stores (Kim et al., 2011).

The vomeronasal organ (VNO) plays an important role in the detection of pheromones. Stimulation of the VNO with urine, which contains a rich blend of pheromones, or with individual pheromones, produces a transient increase in intracellular Ca^{2+} concentration in vomeronasal sensory neurons (Holy et al., 2000; Leinders-Zufall et al., 2000, 2004, 2009; Chamero et al., 2007, 2011; Haga et al., 2010; Kim et al., 2011; Celsi et al., 2012). The intracellular Ca^{2+} increase has several physiological effects, including activation of ion channels (Liman, 2003; Spehr et al., 2009; Yang and Delay, 2010;

*A. Amjad, A. Hernandez-Clavijo, and S. Pifferi contributed equally to this paper.

Correspondence to Anna Menini: menini@sissa.it

D.K. Maurya's present address is Dept. of Molecular Biology, Umea University, 901 87 Umea, Sweden.

Abbreviations used in this paper: A9C, anthracene-9-carboxylic acid; FPR, formyl peptide receptor; NFA, niflumic acid; OMP, olfactory marker protein; TRPC2, transient receptor potential canonical 2; VNO, vomeronasal organ.

The Rockefeller University Press $30.00
J. Gen. Physiol. Vol. 145 No. 4 285–301
www.jgp.org/cgi/doi/10.1085/jgp.201411348

Published March 16, 2015

Kim et al., 2011, 2012; Dibattista et al., 2012) and modulation, through binding to calmodulin, of sensory adaptation (Spehr et al., 2009).

Previous studies in vomeronasal sensory neurons identified the presence of Ca^{2+}-activated currents; some studies found Ca^{2+}-activated nonselective cation currents (Liman, 2003; Spehr et al., 2009), whereas other studies found Ca^{2+}-activated Cl^- currents (Yang and Delay, 2010; Kim et al., 2011; Dibattista et al., 2012). In hamster vomeronasal sensory neurons, Liman (2003) measured Ca^{2+}-activated nonselective cation currents with half-activation occurring at 0.51 mM Ca^{2+} at −80 mV. In mouse vomeronasal sensory neurons, Spehr et al. (2009) showed that 50 µM Ca^{2+} activated nonselective cation currents in patches from dendritic knobs from a small population of neurons (12.5%; 7 out of 56). Other recent studies showed that Ca^{2+}-activated Cl^- channels contribute to the response of mouse vomeronasal neurons to urine (Yang and Delay, 2010; Kim et al., 2011). Furthermore, the presence of Ca^{2+}-activated Cl^- channels in the apical portion of vomeronasal sensory neurons was confirmed by local photorelease of Ca^{2+} from caged Ca^{2+} (Dibattista et al., 2012) and by the expression of TMEM16A and TMEM16B (Dibattista et al., 2012), two proteins forming Ca^{2+}-activated Cl^- channels (Caputo et al., 2008; Schroeder et al., 2008; Yang et al., 2008; Pifferi et al., 2009a; Stephan et al., 2009; Stöhr et al., 2009; Scudieri et al., 2012; Pedemonte and Galietta, 2014). The aim of this study was to further characterize the ionic nature (in the absence of intracellular K^+ to avoid the contribution of Ca^{2+}-activated K^+ currents) of Ca^{2+}-activated currents in mouse vomeronasal sensory neurons and to identify the molecular identity of the channels mediating these currents. We performed recordings both in whole-cell and in inside-out patches from dendritic knobs/microvilli of mouse vomeronasal neurons, and we measured only Ca^{2+}-activated Cl^- currents with biophysical properties more similar to those of TMEM16A than of TMEM16B. To investigate the role of TMEM16A in vomeronasal neurons, we generated conditional knockout mice for TMEM16A, as the constitutive TMEM16A knockout mice die soon after birth (Rock et al., 2008). Our results demonstrate the presence of Ca^{2+}-activated Cl^- currents in the apical portion of vomeronasal sensory neurons of WT mice, confirm that TMEM16A is expressed in mature neurons, and show that TMEM16A is a necessary component of Ca^{2+}-activated Cl^- channels in mouse vomeronasal sensory neurons.

MATERIALS AND METHODS

Animals

Mice were handled in accordance with the Italian Guidelines for the Use of Laboratory Animals (Decreto Legislativo 27/01/1992, no. 116) and European Union guidelines on animal research (no. 86/609/EEC). 2–3-mo-old mice were anaesthetized by CO_2 inhalation and decapitated before VNO removal.

To obtain mice in which TMEM16A expression was specifically eliminated in mature vomeronasal sensory neurons, we crossed floxed TMEM16A$^{fl/fl}$ mice, whose generation has been described in detail (Faria et al., 2014; Schreiber et al., 2014), with mice expressing *Cre* recombinase under the control of the olfactory marker protein (*OMP*) promoter (OMP-Cre mice; Li et al., 2004; provided by P. Mombaerts, Max Planck Institute of Biophysics, Frankfurt, Germany). Our conditional TMEM16A knockout mice (TMEM16A cKO) were homozygous for the floxed *TMEM16A* alleles and heterozygous for *Cre* and *OMP*. C57BL/6 or TMEM16A$^{fl/fl}$ mice were used as controls. In the following, WT mice correspond to C57BL/6 mice.

Dissociation of mouse vomeronasal sensory neurons

The vomer capsule containing the VNO was removed as described previously (Liman and Corey, 1996; Dean et al., 2004; Shimazaki et al., 2006; Arnson et al., 2010). Vomeronasal sensory neurons were dissociated from the VNO with the enzymatic-mechanical dissociation protocol described in Dibattista et al. (2008, 2012), or with the following slight modifications. In brief, the removed vomer capsule was put into a Petri dish containing divalent-free PBS (Sigma-Aldrich) solution where the VNO was extracted and transferred to a tube containing PBS with 1 mg/ml collagenase (type A), incubated at 37°C for 20 min, and transferred twice to Ringer's solution with 5% fetal bovine serum for 5 min. The tissue was then cut into small pieces with tiny scissors and gently triturated with a fire-polished Pasteur pipette. Neurons were plated on Petri dishes (WPI) coated with poly-L-lysine and concanavalin A (type V; Sigma-Aldrich) and stored at 4°C.

Patch-clamp recordings and ionic solutions

Vomeronasal sensory neurons were viewed using an inverted microscope (IMT-2 or IX70; Olympus) with 20× or 40× objectives and identified by their bipolar shape, as illustrated in Fig. 1 of Dean et al. (2004). Patch pipettes, pulled from borosilicate capillaries (WPI) with a PC-10 puller (Narishige), had a resistance of ∼3–6 MΩ for whole-cell and 6–8 MΩ for excised patch recordings. Currents were recorded with an Axopatch 1D or 200B amplifier controlled by Clampex 9 or 10 via a Digidata 1332A or 1440 (Molecular Devices). Data were low-pass filtered at 2 or 5 kHz and sampled at 10 kHz. Experiments were performed at room temperature (20–25°C).

For whole-cell recordings, the standard extracellular mammalian Ringer's solution contained (mM): 140 NaCl, 5 KCl, 2 $CaCl_2$, 1 $MgCl_2$, 10 HEPES, 10 glucose, and 1 sodium pyruvate, pH 7.4. The intracellular solution filling the patch pipette contained (mM): 140 CsCl, 10 HEPES, and 10 HEDTA, adjusted to pH 7.2 with CsOH, and no added Ca^{2+} for the nominally 0-Ca^{2+} solution, or various added Ca^{2+} concentrations, as calculated with the program WinMAXC (C. Patton, Stanford University, Stanford, CA), to obtain free Ca^{2+} in the range between 0.5 and 13 µM (Patton et al., 2004), as described previously (Pifferi et al., 2006, 2009b). The composition of the intracellular solutions containing 2 mM Ca^{2+} was (mM) 140 CsCl, 10 HEPES, 2 $CaCl_2$ or 145 NaCl, 10 HEPES, and 2 $CaCl_2$, as in Liman (2003). No significant difference was observed among currents activated by the two solutions containing 2 mM Ca^{2+}. For ionic selectivity experiments, NaCl in the extracellular mammalian Ringer's solution was replaced with equimolar choline chloride, Na-gluconate, or NaSCN. Niflumic acid (NFA), $CaCC_{inh}$-A01 (Tocris Bioscience), and anthracene-9-carboxylic acid (A9C) were prepared in DMSO as stock solutions at 200 mM, 20 mM, or 1 M, respectively, and diluted to the final concentrations in Ringer's solution. A gravity perfusion system was used to exchange solutions.

Published March 16, 2015

In most whole-cell recordings, we applied voltage steps from a holding potential of 0 mV ranging from −100 to 100 (or 160 mV), followed by a step to −100 mV. A single-exponential function was fitted to instantaneous tail currents to extrapolate the current value at the beginning of the step to −100 mV.

For inside-out recordings, the solution in the patch pipette contained (mM): 140 NaCl, 10 HEDTA, and 10 HEPES, pH 7.2. The bathing solution at the intracellular side of the patch contained (mM): 140 NaCl, 5 EGTA or 10 HEDTA, and 10 HEPES, pH 7.2, and no added Ca^{2+} for the nominally 0-Ca^{2+} solution, or various added Ca^{2+} concentrations, as calculated with the program WinMAXC (C. Patton, Stanford University, Stanford, CA), to obtain free Ca^{2+} in the range between 0.18 and 100 µM (Patton et al., 2004).

Rapid solution exchange in inside-out patches was obtained with the perfusion Fast-Step (SF-77B; Warner Instruments). For I-V relations of Ca^{2+}-activated currents, a double voltage ramp from −100 to 100 mV and back to −100 mV was applied at 1 mV/ms. The two I-V relations were averaged, and leak currents measured with the same ramp protocol in Ca^{2+}-free solutions were subtracted. For dose–response experiments, a patch was exposed for 1 s to solutions with increasing Ca^{2+} concentration.

The bath was grounded through a 3-M KCl agar bridge connected to a Ag/AgCl reference electrode. Liquid junction potentials were calculated using Clampex's Junction Potential Calculator (Molecular Devices), based on the JPCalc program developed by Barry (1994), and applied voltages were corrected offline for the calculated values.

Chemicals, unless otherwise stated, were purchased from Sigma-Aldrich.

Analysis of electrophysiological data

IGOR Pro software (WaveMetrics) was used for data analysis and figures. Data are presented as mean ± SEM and the number of neurons (n). Because most of the data were not normally distributed (Shapiro–Wilk test), statistical significance was determined using Wilcoxon Signed Rank test or Krustal–Wallis test. When a statistically significant difference was determined with Krustal–Wallis analysis, Dunn–Hollander–Wolfe test was done to evaluate which data groups showed significant differences. P-values of <0.05 were considered statistically significant. For the sake of clarity, capacitive transients were trimmed in some traces.

Immunohistochemistry

VNO sections and immunohistochemistry were obtained as described previously (Dibattista et al., 2012). The following primary antibodies were used: rabbit anti-TMEM16A (1:50; Abcam), goat anti-TMEM16A (1:50; Santa Cruz Biotechnology, Inc.), rabbit anti-TMEM16B (1:100; Santa Cruz Biotechnology, Inc.), and goat anti-TRPC2 (1:50; Santa Cruz Biotechnology, Inc.). The following secondary antibodies obtained from Invitrogen were used: donkey anti–rabbit Alexa Fluor 488 (1:500) and donkey anti–goat Alexa Fluor 594 (1:500). Immunoreactivity was visualized with a confocal microscope (TCS SP2; Leica). Images were acquired using Leica software (at 1,024 × 1,024–pixel resolution) and were not modified other than to balance brightness and contrast. Nuclei were stained by DAPI, and signals were enhanced for better visualization of the vomeronasal epithelium. Control experiments without the primary antibodies gave no signal.

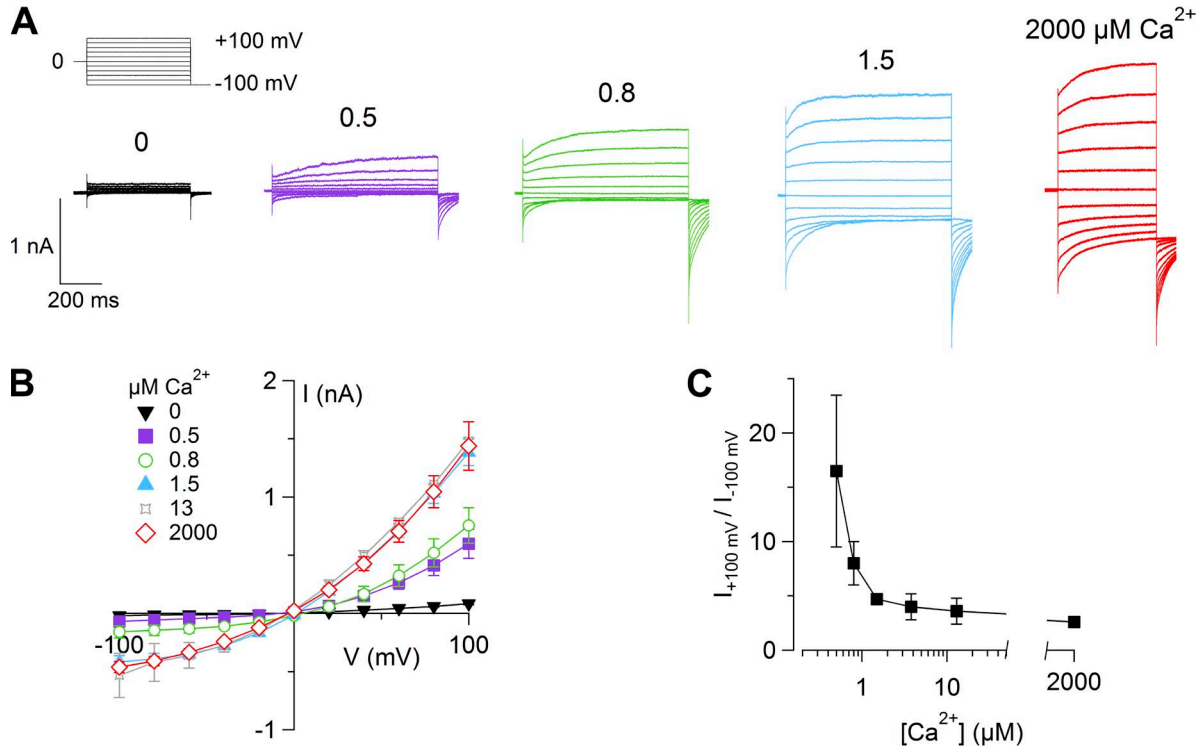

Figure 1. Ca^{2+}-activated currents in mouse vomeronasal sensory neurons. (A) Representative whole-cell currents recorded from different neurons with a pipette solution containing the indicated $[Ca^{2+}]_i$ (for the trace in 2 mM Ca^{2+}, the intracellular solution contained 140 mM NaCl). The holding voltage was 0 mV and voltage steps from −100 to 100 mV with 20-mV increments, followed by a step to −100 mV, were applied as indicated in the top part of the panel. (B) Average steady-state I-V relationships from several neurons at the indicated $[Ca^{2+}]_i$ (n = 3–28). (C) Average ratios between steady-state currents measured at 100 and −100 mV at various $[Ca^{2+}]_i$ (n = 3–28). Data in B and C are represented as mean ± SEM.

Published March 16, 2015

RESULTS

Ca^{2+}-activated Cl^- currents in isolated mouse vomeronasal sensory neurons

We first studied Ca^{2+}-activated currents in isolated mouse vomeronasal sensory neurons using the whole-cell voltage-clamp configuration with intracellular solutions containing different amounts of free $[Ca^{2+}]_i$, ranging from nominally 0 Ca^{2+} up to 2 mM Ca^{2+}. To avoid contributions from Ca^{2+}-activated K^+ currents, the intracellular monovalent cation was Cs^+ (or Na^+ in some experiments in the presence of 2 mM Ca^{2+}).

Fig. 1 A shows currents activated by voltage steps between −100 and 100 mV from a holding voltage of 0 mV. The average current in the presence of nominally 0 Ca^{2+} was 82 ± 9 pA at 100 mV and −20 ± 7 pA at −100 mV (n = 6). When neurons were dialyzed with a solution containing 0.5 µM Ca^{2+}, large currents were recorded in several neurons at positive voltages, with an average value at steady state of 545 ± 96 pA (range of 133 to 1,060 pA) at 100 mV, and −50 ± 17 pA (range of −21 to −163 pA) at −100 mV (n = 10). Further increases in $[Ca^{2+}]_i$ produced currents of higher amplitudes, reaching the average of 1,503 ± 146 pA (range of 615 to 3,530 pA) at 100 mV (n = 28) in the presence of 1.5 µM Ca^{2+}. The average current amplitude did not further increase for $[Ca^{2+}]_i$ up to 2 mM.

The I-V relations measured at steady state were outwardly rectifying (Fig. 1, B and C), and the rectification index, calculated as the ratio between current at 100 and −100 mV, decreased from 16 ± 7 at 0.5 µM Ca^{2+} to 5.5 ± 0.6 at 1.5 µM Ca^{2+} and 3.2 ± 0.3 at 2 mM Ca^{2+}, showing that the I-V relation is Ca^{2+} dependent and becomes more linear as $[Ca^{2+}]_i$ increases.

All together, we tested 178 neurons with various $[Ca^{2+}]_i$ and found that 70% of the neurons (124 out of 178) had a Ca^{2+}-activated current. The remaining 30% of the neurons (54 out of 178) did not have Ca^{2+}-activated currents but showed transient voltage-gated inward currents (likely Na^+ currents) in response to a depolarizing step to 0 mV from a holding potential of −100 mV.

In the presence of Ca^{2+}, voltage steps induced currents composed of an instantaneous component and a time-dependent relaxation (Figs. 1 A and 2, A and B). The instantaneous component is related to channels open at the holding potential of 0 mV, whereas the time-dependent component is the result of the activation of the channel at a given voltage step, indicating that these channels are regulated both by Ca^{2+} and by voltage.

The time-dependent component was fit by a single-exponential function to calculate the time constant of activation, τ_{act}. At 100 mV, τ_{act} in the presence of 0.5 µM Ca^{2+} was 235 ± 29 ms (n = 7), decreased to 156 ± 15 ms (n = 8) at 0.8 µM Ca^{2+}, and to 46 ± 6 ms (n = 6) at 1.5 µM Ca^{2+} (Fig. 2, A–C). At all the tested intracellular Ca^{2+} concentrations, the activation kinetics did not show voltage dependence in the range between 80 and 160 mV (not depicted).

We examined the deactivation kinetics by measuring the decay of the instantaneous current after a step from 100 to −100 mV (Fig. 2, A, B, and D). The best fit of the current decay was obtained with two exponential functions with average τ_{deact1} = 4.1 ± 0.7 ms and τ_{deact2} = 50 ± 4 ms (n = 7) at 0.5 µM Ca^{2+}. Increasing $[Ca^{2+}]_i$ to 1.5 µM produced a slower decay of the current, with average τ_{deact1} = 7 ± 1 ms and τ_{deact2} = 100 ± 11 ms (n = 5).

These results show that an increase in $[Ca^{2+}]_i$ accelerates activation and slows deactivation.

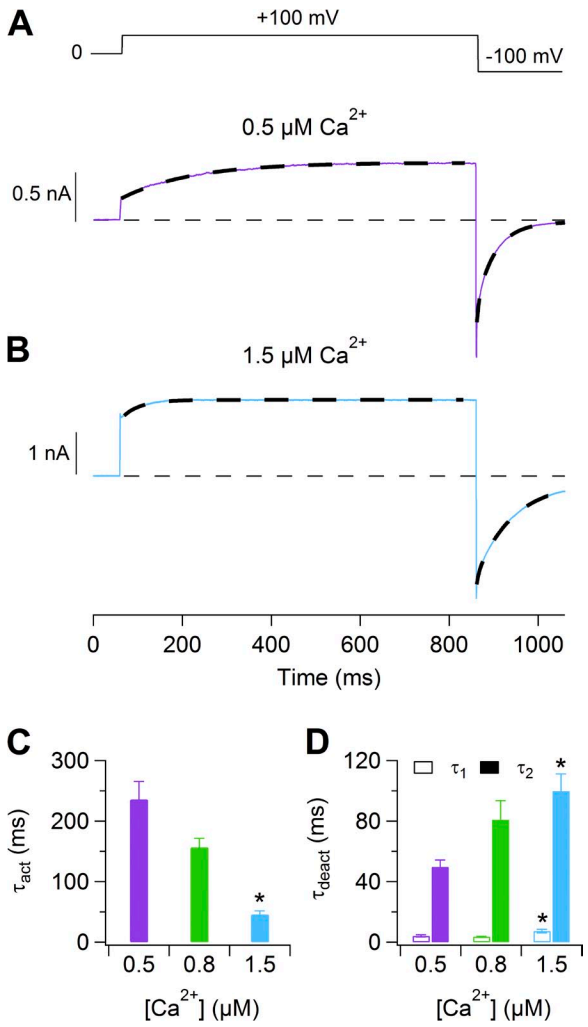

Figure 2. Activation and deactivation kinetics of Ca^{2+}-activated currents. (A and B) Representative currents with 0.5 and 1.5 µM $[Ca^{2+}]_i$, respectively. The voltage was stepped from 0 to 100 mV and then to −100 mV. Dashed lines are the fit of activation or deactivation time constants obtained, respectively, with a single- or double-exponential function. (C and D) Average activation (from 0 to 100 mV) or deactivation (from 100 to −100 mV) time constants at the indicated $[Ca^{2+}]_i$ (n = 5–7). Data in C and D are represented as mean ± SEM (*, P < 0.05; Dunn–Hollander–Wolfe test after Krustal–Wallis analysis between 0.5 and 1.5 µM).

Published March 16, 2015

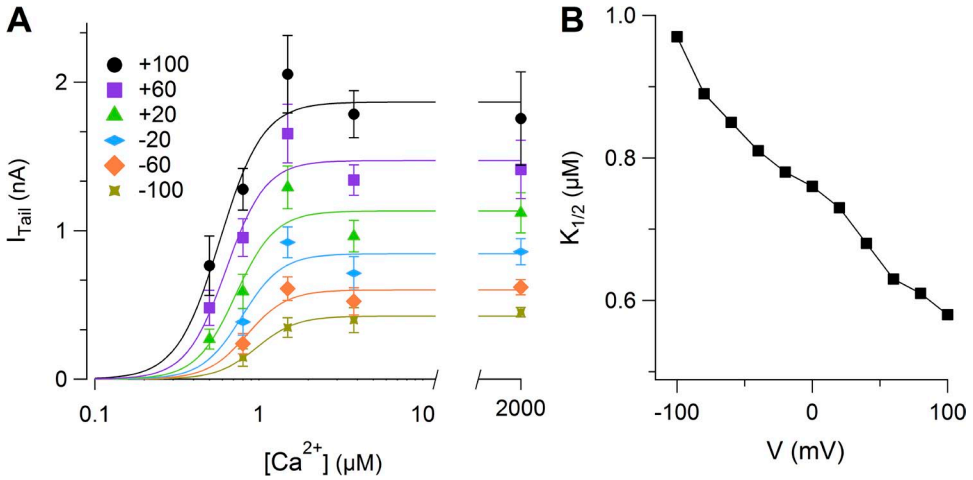

Figure 3. Ca^{2+} sensitivity. (A) Average instantaneous tail currents measured at −100 mV after a prepulse varying from −100 to 100 mV plotted versus $[Ca^{2+}]_i$ (n = 4–8). The continuous lines are the fit with the Hill equation (Eq. 1). (B) $K_{1/2}$ values plotted versus the prepulse voltage. Data in A are represented as mean ± SEM.

To analyze the Ca^{2+} dependence of current activation, we measured dose–response relations by calculating instantaneous tail currents at −100 mV after prepulses ranging from −100 to 100 mV with a duration between 200 and 800 ms (Fig. 3 A). The average instantaneous tail currents were plotted versus $[Ca^{2+}]_i$ and fit at each voltage by the Hill equation:

$$I = I_{max}\left[Ca^{2+}\right]_i^{nH} \Big/ \left(\left[Ca^{2+}\right]_i^{nH} + {K_{1/2}}^{nH}\right), \quad (1)$$

where I is the current, I_{max} is the maximal current, $K_{1/2}$ is the $[Ca^{2+}]_i$ producing 50% of I_{max}, and n_H is the Hill coefficient.

Fig. 3 B shows that $K_{1/2}$ decreased with membrane depolarization from 0.97 µM at −100 mV to 0.58 µM at 100 mV. The Hill coefficient was not voltage dependent with a value ranging between 3 and 4. These results show that Ca^{2+} sensitivity is slightly voltage dependent and that binding of more than 3 Ca^{2+} ions is necessary to open the channel. It should be noted, however, that the current amplitudes at high Ca^{2+} concentrations were sometimes smaller than those at 1.5 µM Ca^{2+} (Fig. 3 A), and that this current decrease may have slightly affected the estimation of n_H and $K_{1/2}$. A decline of currents at high Ca^{2+} concentrations has been described previously in some native Ca^{2+}-activated Cl^- currents (Kuruma and Hartzell, 2000; Qu et al., 2003), as well as in some splice variants of TMEM16A (Ferrera et al., 2009; Yang et al., 2014).

To estimate the voltage dependence of channel activation (G-V relation), we increased the amplitude of voltage steps to 160 mV and calculated instantaneous tail currents at −100 mV. G-V relations were fit by the Boltzmann equation:

$$G = G_{max} \Big/ \left\{1 + \exp\left[z\left(V_{1/2} - V\right)F/RT\right]\right\}, \quad (2)$$

where G is the conductance, G_{max} is the maximal conductance, z is the equivalent gating charge associated with voltage-dependent channel opening, $V$is the membrane potential, $V_{1/2}$ is the membrane potential producing 50% of G_{max}, F is the Faraday constant, R is the gas constant, and T is the absolute temperature.

Fig. 4 A shows the average G-V relations at the indicated $[Ca^{2+}]_i$. Continuous lines were obtained from a global fit of the average G-V relations with the same G_{max}. The average $V_{1/2}$ was 197 ± 39 mV (n = 4) at 0.5 µM

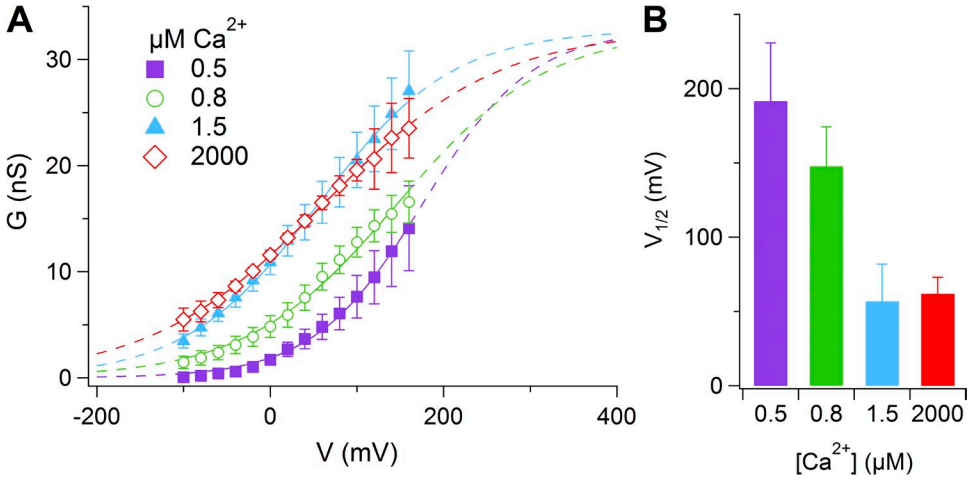

Figure 4. Voltage dependence of Ca^{2+}-activated currents. (A) Average conductances at the indicated $[Ca^{2+}]_i$ measured from instantaneous tail currents at −100 mV after prepulses from −100 to 160 mV plotted versus the prepulse voltage (n = 4–8). The continuous lines are the fit with the Boltzmann equation (Eq. 2). (B) Average $V_{1/2}$ values plotted versus $[Ca^{2+}]_i$ (n = 4–8). Data are represented as mean ± SEM.

Published March 16, 2015

Ca^{2+} and became 70 ± 25 mV (n = 6) at 1.5 µM Ca^{2+} (Fig. 4 B), whereas the equivalent gating charge was not largely modified (z = 0.39 and 0.34, respectively).

These results show that an increase in $[Ca^{2+}]_i$ caused a leftward shift of the G-V relation. Thus, the conductance depends both on $[Ca^{2+}]_i$ and voltage, and depolarization can activate more channels as $[Ca^{2+}]_i$ is increased.

To investigate if the Ca^{2+}-activated currents are caused by cation channels, we first substituted Na^+ in the Ringer's solution with choline, as this large organic cation is

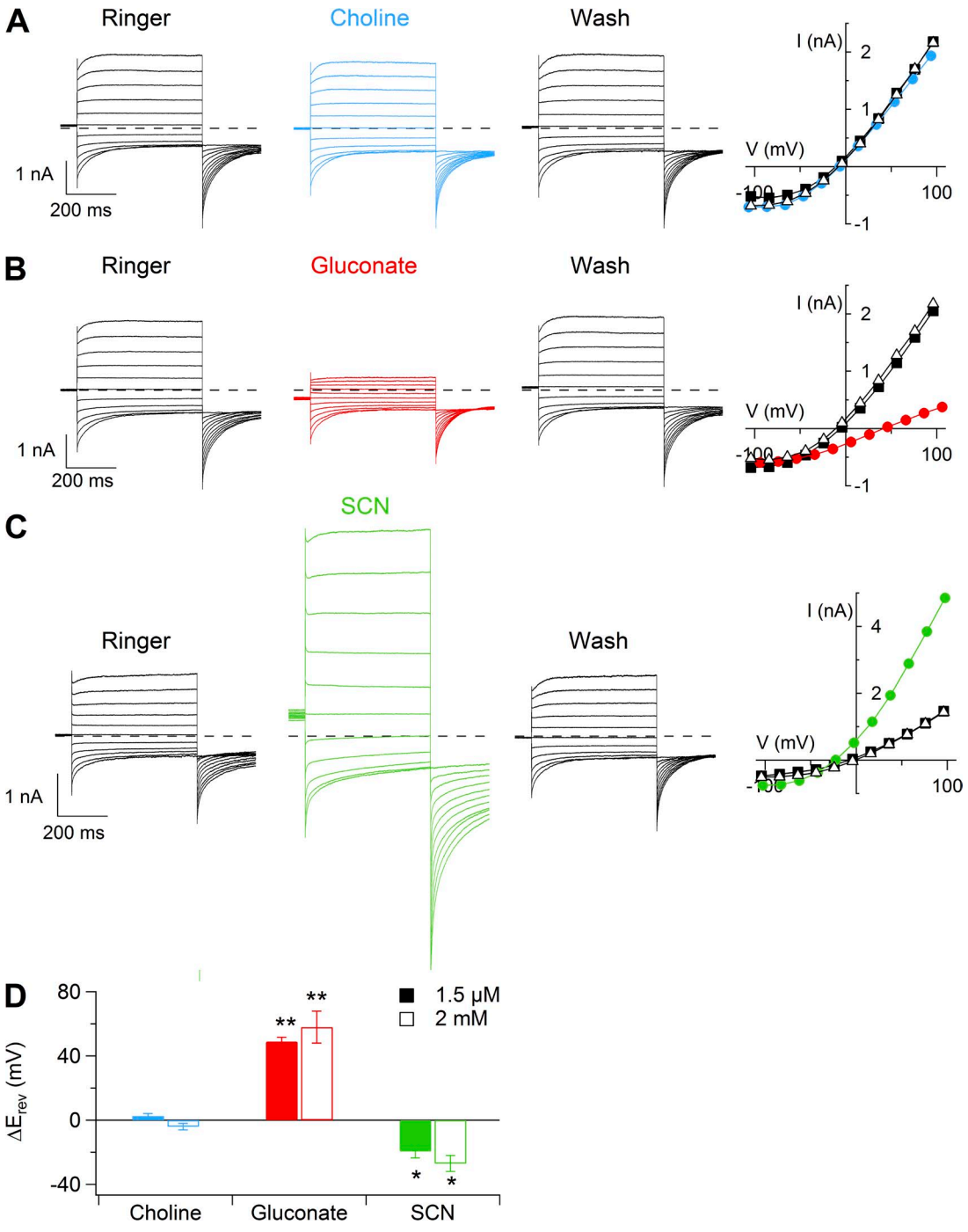

Figure 5. Ionic selectivity of Ca^{2+}-activated currents. Representative whole-cell recordings obtained with an intracellular solution containing 1.5 µM Ca^{2+}. Voltage protocol as in Fig. 1 A. Each neuron was exposed to a Ringer's solution containing NaCl, choline-Cl (A), Na-gluconate (B), or NaSCN (C), followed by washout in Ringer's solution with NaCl. Dashed lines indicate zero current. Steady-state I-V relationships measured at the end of the voltage steps are shown at the right of each set of recordings. (D) Average reversal potential shift upon substitution of extracellular NaCl with choline-Cl, Na-gluconate, or NaSCN in 1.5 µM (closed bars; n = 5–10) or 2 mM Ca^{2+} (open bars; n = 4). Data in D are represented as mean ± SEM (**, P < 0.01; *, P < 0.05; Wilcoxon Signed Rank test).

Published March 16, 2015

usually impermeant in cation channels (Hille, 2001). Fig. 5 A shows representative recordings at 1.5 µM Ca^{2+} in the presence of NaCl, after replacement of Na^+ with choline, and in NaCl after washout. Steady-state I-V relations plotted in Fig. 5 B show that the replacement of Na^+ with choline did not modify the I-V relation. Similar results were obtained with 2 mM Ca^{2+}. The average reversal potential in choline-Cl was −10 ± 4 mV (n = 5), not significantly different from the value of −7 ± 2 mV (n = 5) measured in NaCl. The average shift of reversal potential in choline-Cl with respect to NaCl was not significantly different in 1.5 µM or 2 mM Ca^{2+} (Fig. 5 D), indicating that the Ca^{2+}-activated current at both Ca^{2+} concentrations was not a cation current.

Anion selectivity was then tested by replacing 140 mM NaCl with equimolar amounts of Na-gluconate or NaSCN (Fig. 5, C and E). When Cl^- was replaced with gluconate in the presence of 1.5 µM Ca^{2+}, we measured an average shift of V_{rev} of 49 ± 3 mV (n = 10), whereas in the presence of SCN^- the V_{rev} shift was −20 ± 3 mV (n = 8). Similar values were obtained in the presence of 2 mM Ca^{2+} (Fig. 5 D). The average permeability ratios for anions (P_X/P_{Cl}) were: SCN^- (2.6) > Cl^- (1.0) > gluconate (0.1).

We investigated whether the more permeant anion SCN^- modifies the voltage dependence of channel activation and the gating kinetics, as observed in several native Ca^{2+}-activated Cl^- currents (Greenwood and Large, 1999; Perez-Cornejo et al., 2004), as well as in heterologously expressed TMEM16A and TMEM16B (Xiao et al., 2011; Betto et al., 2014). Fig. 6 (A and B) shows recordings and I-V relations from a vomeronasal neuron in the presence of 0.5 µM Ca^{2+} when NaCl was replaced with NaSCN. The G-V relation was shifted toward more negative potentials when Cl^- was substituted with SCN^- (Fig. 6 C). The average $V_{1/2}$ from several neurons significantly changed from 168 ± 6 mV in Cl^- to 39 ± 14 mV in SCN^- (n = 3). Moreover, τ_{act} in the presence of 0.5 µM Ca^{2+} became significantly faster in SCN^-, with an average value at 100 mV of 94 ± 12 ms (n = 3), compared with 282 ± 49 ms (n = 3) in Cl^- (Fig. 6 E). Also, the deactivation time constants, measured as in Fig. 2 D, were significantly modified upon anion substitution (Fig. 6 F), with average values of τ_{deact1} = 4.2 ± 0.9 ms and τ_{deact2} = 57 ± 2 ms (n = 3) in SCN^-, slower than the values in Cl^- measured in the same neurons: τ_{deact1} = 10 ± 2 ms and τ_{deact2} = 183 ± 16 ms (n = 3).

To assess the pharmacological profile of Ca^{2+}-activated Cl^- currents in vomeronasal sensory neurons, we measured the extracellular blockage properties of 300 µM NFA, 10 µM $CaCC_{inh}$-A01, and 1 mM A9C, commonly used blockers of Ca^{2+}-activated Cl^- currents (De La Fuente et al., 2008; Hartzell et al., 2009; Huang et al.,

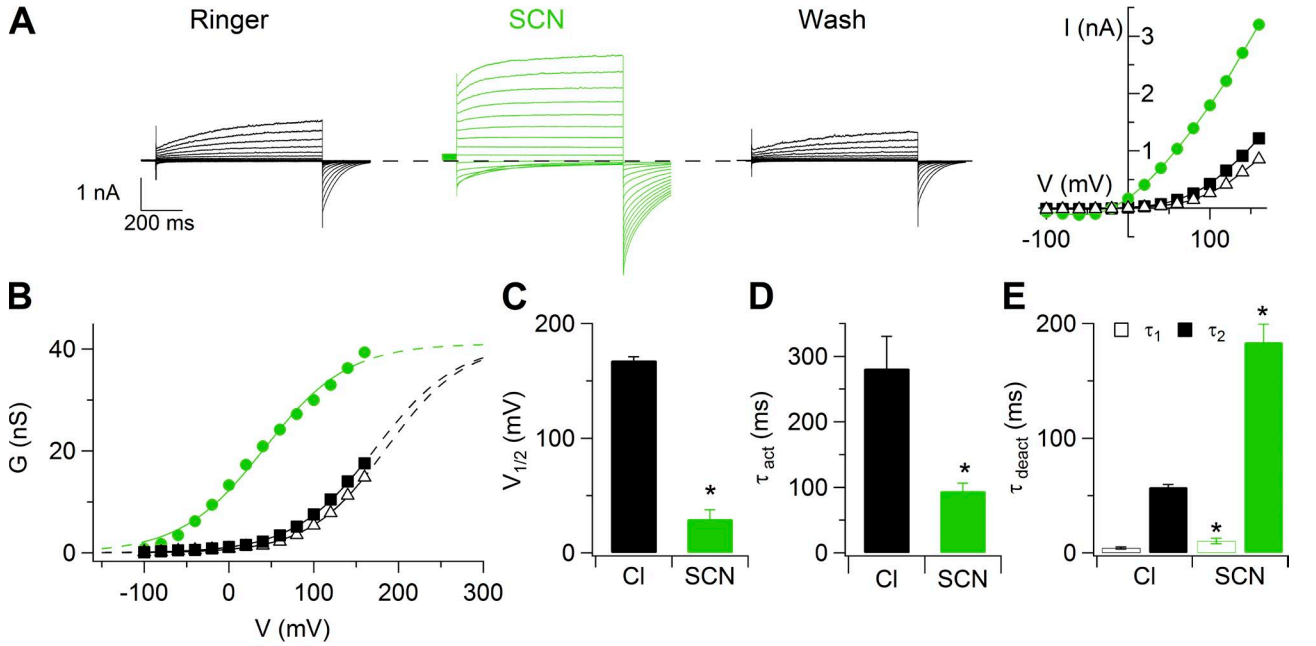

Figure 6. Change of voltage dependence in the presence of SCN^-. (A) Representative whole-cell recordings obtained with an intracellular solution containing 0.5 µM Ca^{2+}. The same neuron was exposed to a Ringer's solution containing NaCl or NaSCN, followed by washout in Ringer's solution with NaCl. Voltage steps of 800-ms duration were given from a holding voltage of 0 mV to voltages between −100 and 160 mV in 20-mV steps, followed by a step to −100 mV. Dashed lines indicate zero current. Steady-state I-V relationships measured at the end of the voltage steps. (B) Conductances measured from instantaneous tail currents at −100 mV after prepulses from −100 to 160 mV plotted versus the prepulse voltage. Data from the recordings shown in A. (C) Average $V_{1/2}$ in Cl^- or SCN^- (n = 3). (D and E) Average activation and deactivation time constants in Cl^- or SCN^- (n = 3). Data in C–E are represented as mean ± SEM (*, P < 0.05; Wilcoxon Signed Rank test).

Published March 16, 2015

2012). Fig. 7 shows that all three compounds induced a reversible block of the outward currents activated by 1.5 µM Ca^{2+}, whereas inward currents were blocked only by NFA and $CaCC_{inh}$-A01. The percentage of current in the presence of each compound relative to control was measured both at 2 ms after the voltage step (early current) and at the end of the voltage step (late current), as shown in Fig. 7 (G and H). At 100 mV, the percentage of late currents was 29 ± 5 for NFA, 38 ± 5 for $CaCC_{inh}$-A01, and 29 ± 7 for A9C (Fig. 7 G; n = 5–7), and similar values were obtained by measuring the early currents (Fig. 7 H). At −100 mV, both NFA and $CaCC_{inh}$-A01 partially blocked the inward late currents with the following percentages: 48 ± 13 for NFA and 46 ± 7 for $CaCC_{inh}$-A01 (Fig. 7 G). These values were not significantly different when measured as early currents (Fig. 7 H). On the contrary, A9C did not significantly affect the inward early current at −100 mV but greatly potentiated the inward late current with a percentage of 200 ± 55 (Fig. 7, G and H).

These results show that, in the presence of 1.5 µM Ca^{2+}, 300 µM NFA and 10 µM $CaCC_{inh}$-A01 produced

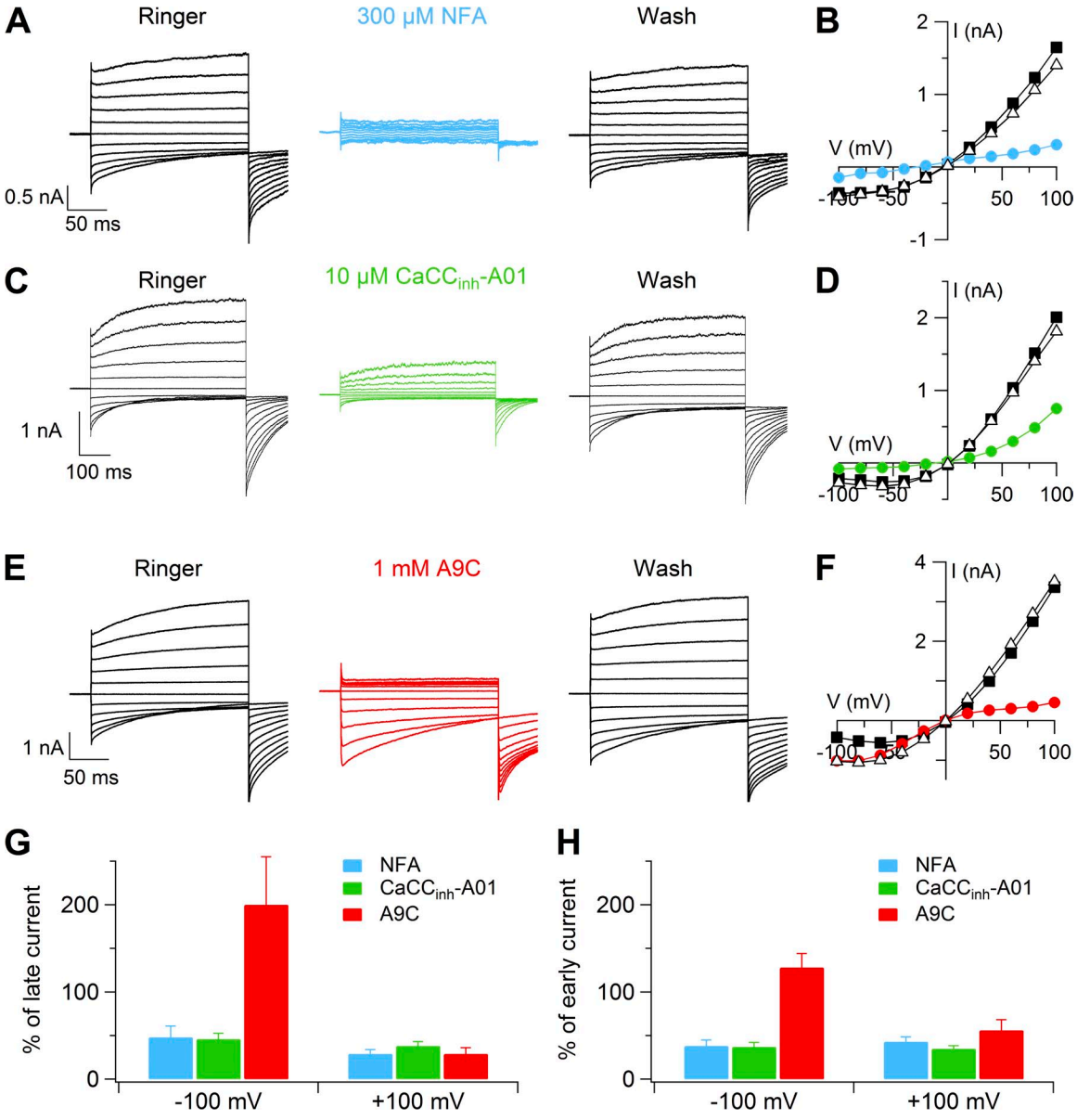

Figure 7. Pharmacology of Ca^{2+}-activated currents. Representative whole-cell recordings obtained with an intracellular solution containing 1.5 µM Ca^{2+}. Voltage protocol as in Fig. 1 A. Each neuron was exposed to a Ringer's solution to 300 µM NFA (A), 10 µM $CaCC_{ihn}$-A01 (C), or 1 mM A9C (E), and again to Ringer's solution. (B, D, and F) I-V relationships measured at the end of the voltage steps from the recordings shown on the left. (G and H) Average percentages of currents measured in the presence of each compound relative to control at the end of the voltage step (G; late current) or 2 ms after the voltage step (H; early current) at −100 or 100 mV (n = 5–7). Data in G and H are represented as mean ± SEM.

Published March 16, 2015

similar current inhibitions at 100 and −100 mV both for early and late currents. 1 mM A9C had an anomalous effect, blocking the current at 100 mV and largely potentiating late currents at −100 mV.

Collectively, these results show that the Ca^{2+}-activated currents measured in vomeronasal sensory neurons are mainly anion currents.

TMEM16A and TMEM16B are coexpressed in microvilli of vomeronasal sensory neurons (Dibattista et al., 2012), and their individual heterologous expression shows some similar electrophysiological properties—indeed, they cannot be distinguished by their ionic selectivity (Adomaviciene et al., 2013) or by their pharmacological profile (Pifferi et al., 2009a; Bradley et al., 2014)—as well as some important differences: TMEM16A have a higher Ca^{2+} sensitivity and slower activation kinetics than TMEM16B (Caputo et al., 2008; Schroeder et al., 2008; Yang et al., 2008; Pifferi et al., 2009a; Stephan et al., 2009; Ferrera et al., 2011: Cenedese et al., 2012; Pedemonte and Galietta, 2014). We found that whole-cell properties of Ca^{2+}-activated Cl^- currents in vomeronasal neurons are more similar to those of heterologous TMEM16A than TMEM16B.

Ca^{2+}-activated Cl^- currents in inside-out excised patches from dendritic knob/microvilli of mouse vomeronasal sensory neurons

To further characterize Ca^{2+}-activated currents, we excised membrane patches in the inside-out configuration from dendritic knobs of vomeronasal neurons. Membrane patches were excised from the tips of the knobs and are likely to contain membranes from both the dendritic knob and from microvilli. Fig. 8 A shows the change of current at −50 mV when an inside-out patch was exposed to 100 µM Ca^{2+} for 2 s. Upon the application of 100 µM Ca^{2+}, the current rapidly reached a value of about −40 pA and remained stationary in the presence of Ca^{2+}, whereas it rapidly returned to the baseline value when Ca^{2+} was removed. The average current from several patches at −50 mV was −16 ± 5 pA (range of −6 to −40 pA; $n = 7$), and the average ratio between the current measured 2 s after Ca^{2+} application and the current measured shortly after Ca^{2+} application was 0.96 ± 0.02 ($n = 7$).

Fig. 8 B shows that the amplitude of Ca^{2+}-activated currents in inside-out patches decreased with time after patch excision. A similar current rundown has also been

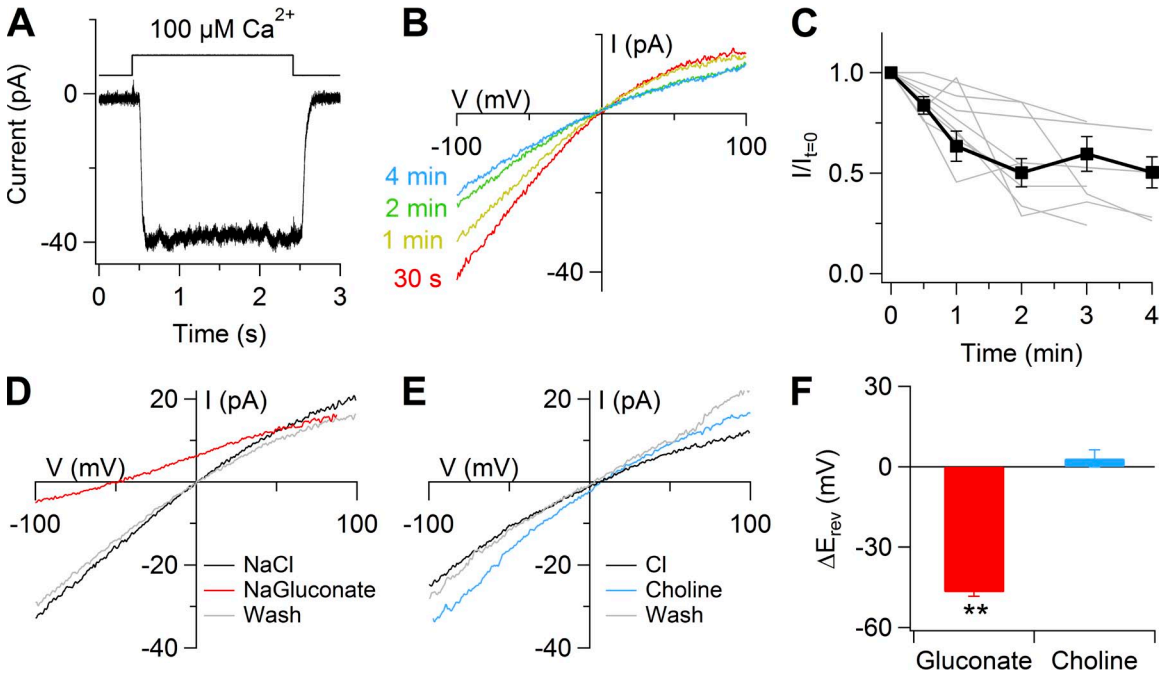

Figure 8. Rundown and ionic selectivity of Ca^{2+}-activated currents in inside-out patches from dendritic knob/microvilli of vomeronasal sensory neurons. (A) An inside-out patch was exposed to 100 µM Ca^{2+} for 2 s at the time indicated in the upper trace. Holding potential, −50 mV. Symmetrical NaCl solutions. (B) I-V relations from a voltage ramp protocol. Leakage currents measured in 0 Ca^{2+} were subtracted. The number next to each trace indicates the time of Ca^{2+} application after patch excision. (C) Average ratios between currents at −100 mV measured at the indicated times after patch excision and the current measured at patch excision ($n = 3$–10). Ratios of individual patches are in gray. (D and E) I-V relations activated by 100 µM Ca^{2+} from a voltage ramp protocol after subtraction of the leakage currents measured in 0 Ca^{2+}. The patch was exposed to bath solutions containing 140 mM NaCl, Na-gluconate (D), or choline-Cl (E), followed by washout with NaCl. Current traces in D and E were from the same patch. (F) Average reversal potential shift upon substitution of extracellular NaCl with Na-gluconate or choline-Cl ($n = 3$) (**, $P < 0.01$; Wilcoxon Signed Rank test). Error bars indicate SEM.

Published March 16, 2015

observed in other native Ca^{2+}-activated Cl^- currents, as well as in heterologous TMEM16A and TMEM16B currents (Kuruma and Hartzell, 2000; Qu and Hartzell, 2000; Reisert et al., 2003; Pifferi et al., 2009a,b; Stephan et al., 2009; Yu et al., 2014). Currents underwent an irreversible reduction until they reached an almost steady-state value (Fig. 8, B and C).

To determine the ion selectivity of the Ca^{2+}-activated current, we replaced NaCl in the bathing solution with Na-gluconate or with choline-Cl and measured the shift of reversal potential (Fig. 8, D–F). Currents were activated by 100 µM Ca^{2+}, and voltage ramps from −100 to 100 mV were applied. When Cl^- was replaced with gluconate, we measured an average shift of V_{rev} of −47 ± 2 mV ($n = 3$), whereas in the presence of choline-Cl, the shift of V_{rev} was 3 ± 3 mV ($n = 3$). Thus, replacement of Cl^- with gluconate shifted the reversal potential from near zero in symmetrical Cl^- to more negative values, as expected for Cl^--selective channels in our experimental conditions, showing that Ca^{2+}-activated currents were Cl^- selective.

To measure dose–response relations, we activated currents in excised inside-out patches with various Ca^{2+} concentration and measured current amplitudes after the rapid phase of rundown, when the current reached an almost steady-state value (Fig. 9, A–D). Fig. 9 C shows that $K_{1/2}$ decreased with membrane depolarization from 1.5 ± 0.2 µM at −100 mV to 1.1 ± 0.1 µM ($n = 5$) at 100 mV. The Hill coefficient was not voltage dependent with a value ranging between 2.4 and 3.2. The average ratio between currents at 100 and −100 mV was 1.3 ± 0.3 at 1 µM ($n = 5$) and 0.65 ± 0.05 at 100 µM ($n = 13$).

Collectively, these results demonstrate the presence of Ca^{2+}-activated Cl^- currents in the knob/microvilli of mouse vomeronasal sensory neurons. Moreover, the range of Ca^{2+} sensitivity and the absence of inactivation in the presence of a constant Ca^{2+} concentration indicate that properties of native currents are more similar to those of TMEM16A than TMEM16B (see also Discussion). Indeed, all isoforms of TMEM16B have been shown to inactivate in the continuous presence of Ca^{2+} at negative potentials (Pifferi et al., 2009a; Stephan et al., 2009; Ponissery Saidu et al., 2013), whereas TMEM16A current did not inactivate (Ni et al., 2014; Tien et al., 2014; Yu et al., 2014).

Conditional knockout of TMEM16A in vomeronasal sensory neurons

We have shown previously that TMEM16A and TMEM16B are coexpressed in microvilli of mouse vomeronasal sensory neurons (Dibattista et al., 2012), and we showed here that Ca^{2+}-activated Cl^- currents in vomeronasal sensory neurons are more similar to heterologous TMEM16A than TMEM16B. As the constitutive TMEM16A knockout is lethal soon after birth (Rock et al., 2008), we selectively abolished expression of TMEM16A in mature vomeronasal sensory neurons by crossing floxed $TMEM16A^{fl/fl}$ mice (Faria et al., 2014; Schreiber et al., 2014) with OMP-Cre mice (Li et al., 2004).

By immunohistochemistry, we confirmed our previous results that TMEM16A and TMEM16B are expressed at the apical surface of the vomeronasal epithelium of control WT mice (Fig. 10, A and B), whereas we showed

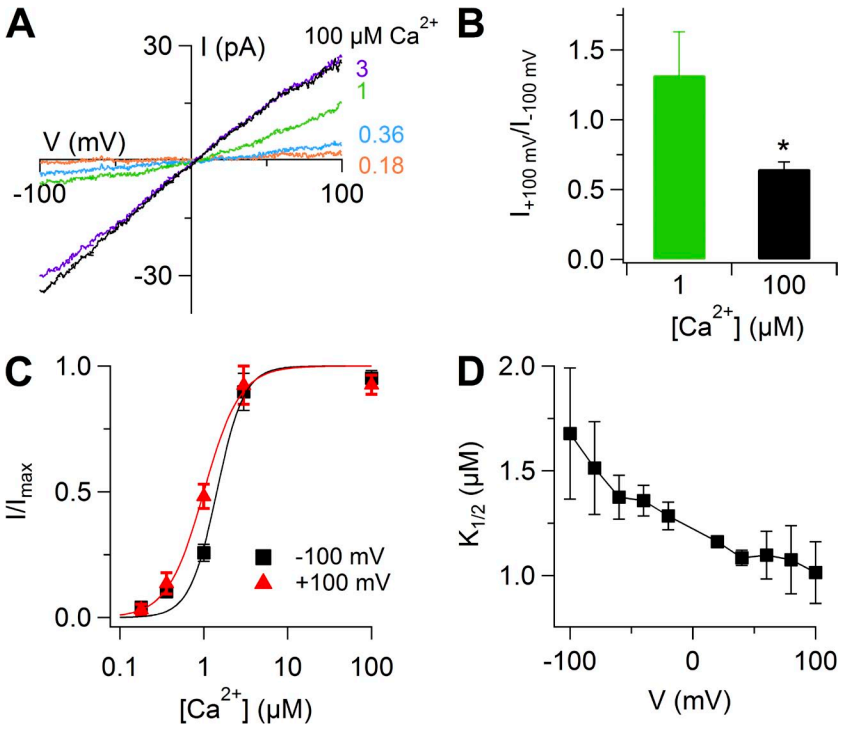

Figure 9. Dose–response relations of Ca^{2+}-activated currents in inside-out patches from the dendritic knob/microvilli of vomeronasal sensory neurons. (A) I-V relations from the same patch exposed to the indicated Ca^{2+} concentrations after subtraction of the currents measured in 0 Ca^{2+}. (B) Ratios between currents measured at 100 and at −100 mV at the indicated Ca^{2+} concentrations ($n = 5$–13). *, $P < 0.05$; Wilcoxon Signed Rank test. (C) Dose–response relations, obtained by normalized currents at −100 or 100 mV ($n = 5$). Continuous lines are the fit with the Hill equation (Eq. 1). (D) Mean $K_{1/2}$ values plotted versus voltage ($n = 5$). Error bars indicate SEM.

Published March 16, 2015

that TMEM16A immunoreactivity was absent in TMEM16A cKO mice (Fig. 10 C). Furthermore, we investigated by immunohistochemistry if the lack of TMEM16A affected the expression of TMEM16B and TRPC2, and found a normal pattern of expression for the two proteins (Fig. 10, D and F). In addition, we verified the specificity of *Tmem16A* ablation, by checking TMEM16A expression in lateral nasal glands and septal nasal glands, which do not express OMP and should therefore express TMEM16A. Indeed, Fig. 10 (G and H) shows expression of TMEM16A in the nasal glands of TMEM16A cKO mice.

These results demonstrate that the loss of TMEM16A is restricted to vomeronasal sensory neurons of cKO mice and confirm the specificity of the antibody against this protein. Furthermore, TMEM16B and TRPC2 are expressed at the apical surface of the vomeronasal epithelium in cKO as in WT mice.

To determine the contribution of TMEM16A to Ca^{2+}-activated Cl^- currents in vomeronasal sensory neurons, we measured currents in isolated neurons from TMEM16A cKO mice in the whole-cell configuration with intracellular solutions containing various amounts of free $[Ca^{2+}]_i$. Fig. 11 (A and B) shows the comparison between representative recordings from $TMEM16A^{fl/fl}$ and TMEM16A cKO mice. Currents were activated by voltage steps between −100 and 100 mV from a holding potential of 0 mV, followed by a step to −100 mV and return to 0 mV. The last part of the current trace elicited by the depolarizing voltage from −100 to 0 mV was used as a control of the viability of neurons, as it allowed the measurement of voltage-gated inward currents (likely Na^+ currents; insets of Fig. 11, A and B). The kinetics of currents activated by 1.5 µM Ca^{2+} in neurons from $TMEM16A^{fl/fl}$ mice resembled those measured in control WT mice (Figs. 11 A and 1 A), whereas currents in vomeronasal neurons from TMEM16A cKO mice were not significantly different from currents in the absence of Ca^{2+} (Figs. 11, B and C, and 1 A). The inset of Fig. 11 B shows a representative voltage-gated current (elicited by a 0-mV step from −100 mV), indicating that the neuron was viable but did not have currents activated by Ca^{2+}. All together, we tested 40 viable neurons from 6 TMEM16A cKO mice at $[Ca^{2+}]_i$ varying from 0.5 µM to 2 mM Ca^{2+} and did not find a significant difference from currents measured in 0 Ca^{2+}. Furthermore, we measured currents in inside-out patches from dendritic knobs of vomeronasal neurons from TMEM16A

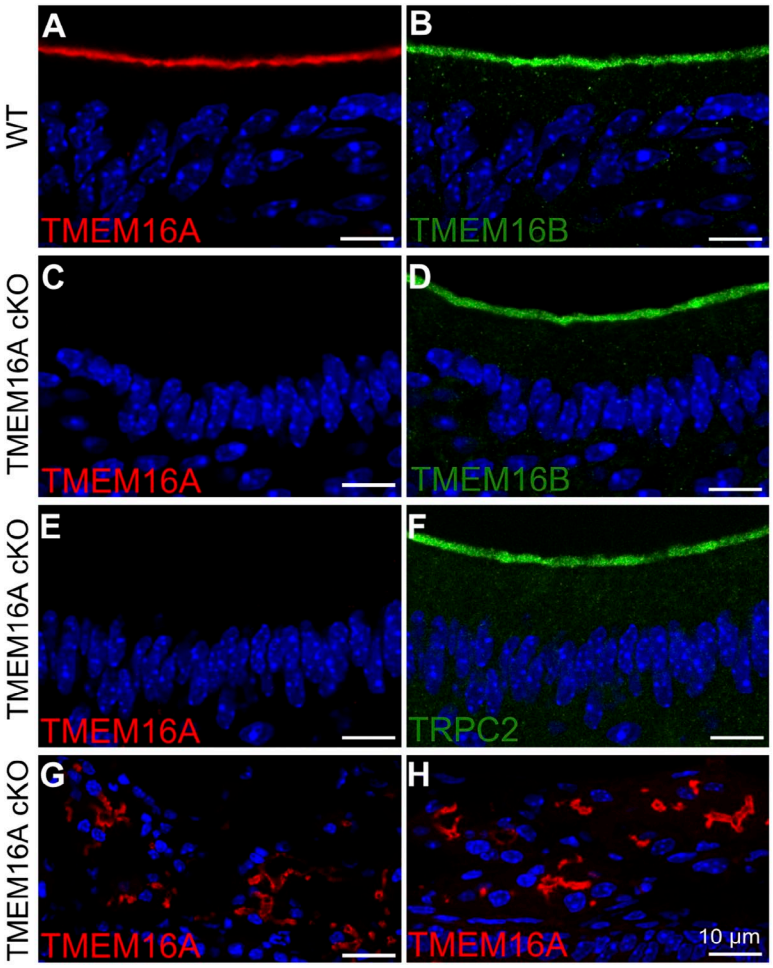

Figure 10. Immunostaining of sections of VNO in WT and TMEM16A cKO mice. (A and B) Confocal micrographs showing TMEM16A (red) and TMEM16B (green) expression at the apical surface of the vomeronasal epithelium in WT mice. (C–F) No immunoreactivity to TMEM16A was detectable at the apical surface of the vomeronasal epithelium in TMEM16A cKO mice, whereas TMEM16B and TRPC2 were normally detected. (G and H) As a control, expression of TMEM16A is shown in nasal septal glands (G) and lateral nasal glands (H) of cKO mice. Cell nuclei were stained by DAPI (blue). Bars, 10 µm.

Published March 16, 2015

cKO mice and did not find any measurable Ca^{2+}-activated current (not depicted).

These results demonstrate that TMEM16A is a necessary component of the Ca^{2+}-activated Cl^- current in vomeronasal sensory neurons.

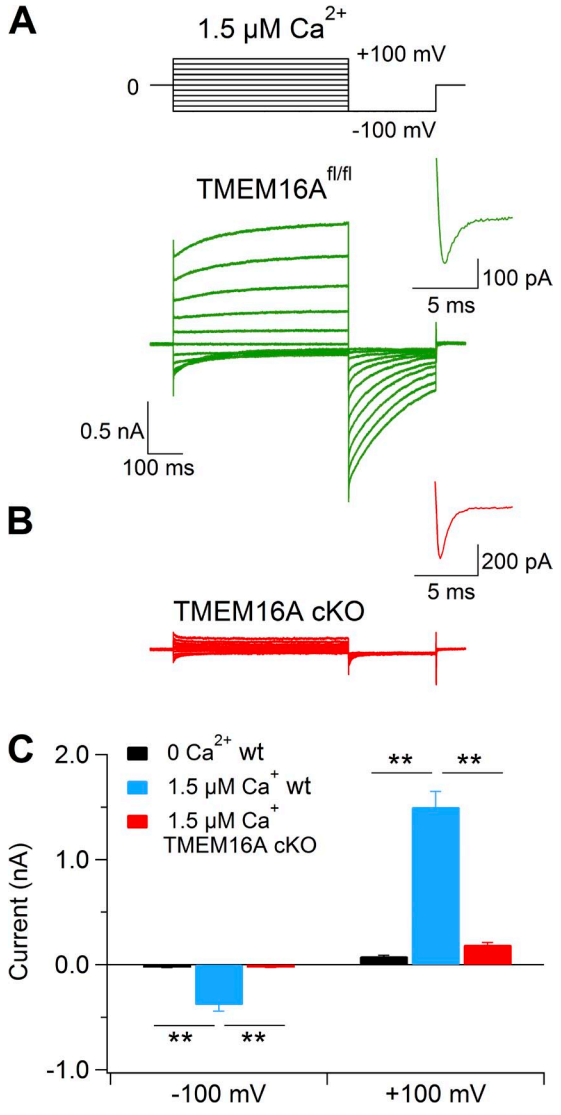

Figure 11. Lack of Ca^{2+}-activated currents in vomeronasal sensory neurons from TMEM16A conditional knockout mice. Representative whole-cell recordings obtained with an intracellular solution containing 1.5 µM Ca^{2+} from vomeronasal sensory neurons dissociated from $TMEM16A^{fl/fl}$ (A) or TMEM16A cKO (B) mice. Insets show the enlargement of the recordings of voltage-gated inward currents activated by a step to 0 mV from the holding potential of −100 mV, as indicated in the voltage protocol at the top of the figure. (C) Mean current amplitudes measured at −100 or 100 mV with intracellular pipette solution containing nominally 0 (black bar; $n = 6$) or 1.5 µM free Ca^{2+} from WT (blue bar; $n = 28$) or TMEM16A cKO mice (red bar; $n = 20$). Error bars indicate SEM (**, $P < 0.01$; Dunn–Hollander–Wolfe test after Krustal–Wallis analysis).

DISCUSSION

In this study, we have provided the first functional characterization of Ca^{2+}-activated Cl^- currents in isolated mouse vomeronasal sensory neurons both in whole-cell and in inside-out patches from the knobs/microvilli. A comparison among biophysical properties indicates that native currents are more similar to heterologous TMEM16A than to TMEM16B Ca^{2+}-activated Cl^- currents. Furthermore, conditional knockout of TMEM16A abolished Ca^{2+}-activated currents in mouse vomeronasal neurons, demonstrating that TMEM16A is a necessary component of Ca^{2+}-activated Cl^- currents in these neurons.

Ca^{2+}-activated currents

In whole-cell recordings, we measured Ca^{2+}-activated currents in 70% of the neurons (124/178), whereas we did not record any Ca^{2+}-activated current in the remaining neurons (30%; 54/178), although these neurons were considered viable, as they had transient voltage-gated inward currents (likely Na^+ currents). These currents were recorded with intracellular Cs^+ or Na^+ instead of K^+, i.e., under ionic conditions that prevented permeation through Ca^{2+}-activated K^+ channels. The absence of Ca^{2+}-activated currents in some neurons could simply be caused by inactivation or rundown of Ca^{2+}-activated channels, or to damage of the microvilli, where these channels should be mostly expressed (as it will be discussed later), but it also raises the question of whether a Ca^{2+}-activated current is present only in a subset of vomeronasal neurons. Indeed, the mouse vomeronasal epithelium contains two major populations of neurons, basal and apical, based on their location and on the expression of different receptors and proteins (Berghard and Buck, 1996; Jia and Halpern, 1996; Lau and Cherry, 2000; Martini et al., 2001; Leinders-Zufall et al., 2004; Liberles et al., 2009; Rivière et al., 2009). Apical neurons express receptors of the V1R or FPR families, the G protein α subunit Gαi2, and phosphodiesterase 4A, whereas basal neurons express receptors of the V2R or FPR families and the G protein α subunit Gαo. We have previously investigated by immunocytochemistry the percentage of apical and basal neurons obtained in our dissociated preparations using anti–phosphodiesterase 4A antibody as a marker for apical neurons, or anti-Gαo antibody as a marker for basal neurons, and found that on average, ∼74% of the dissociated neurons were apical (Celsi et al., 2012). Based on these results, it is very likely that most of our electrophysiological recordings were obtained from apical neurons, and it is possible to speculate that the 30% of neurons without Ca^{2+}-activated current could be basal neurons. However, in the dissociated preparations used for electrophysiological recordings, we could not determine by visual inspection whether a neuron was apical or basal, nor we could perform immunocytochemistry after the recordings, as neurons were

Published March 16, 2015

often lost after pipette retrieval. It is important to note that TMEM16A and TMEM16B are coexpressed both in apical and basal neurons (Dibattista et al., 2012). Thus, we favor the interpretation that all neurons have Ca^{2+}-activated currents and that the absence of these currents in some neurons was likely caused by channel inactivation or rundown or to damage of the microvilli, although we cannot exclude the possibility that Ca^{2+}-activated currents are present only in a subset of vomeronasal neurons.

Cationic and anionic Ca^{2+}-activated currents

Previous studies on vomeronasal sensory neurons have reported the presence of Ca^{2+}-activated currents, in the absence of intracellular K^+, with different ionic selectivity: nonselective cation currents or anion currents.

Ca^{2+}-activated nonselective cation currents have been recorded in the hamster (Liman, 2003) and in the mouse (Spehr et al., 2009), although they showed different Ca^{2+} sensitivities. In the hamster, whole-cell dialysis with 0.5–2 mM Ca^{2+} produced currents with an average amplitude of −177 pA at −80 mV, and half-activation of this current required a high Ca^{2+} concentration of 0.5 mM at −80 mV (Liman, 2003). In the mouse, nonselective cation currents were recorded in inside-out patches only in a subpopulation of neurons (12.5%) in the presence of 50 µM Ca^{2+} (Spehr et al., 2009). In a previous study by our group (Dibattista et al., 2012), we used photolysis of caged Ca^{2+} to increase Ca^{2+} concentration in the apical region (dendritic knob and microvilli) of mouse vomeronasal neurons, and we did not detect any cation current, but we measured Ca^{2+}-activated Cl^- currents with an average amplitude of −261 pA at −50 mV. In that study, we pointed out that the highest Ca^{2+} concentration obtained from photolysis of caged Ca^{2+} was probably ∼10–20 µM, lower than the values used to activate the nonselective cation currents in the previous studies (Liman, 2003; Spehr et al., 2009), and that perhaps a higher Ca^{2+} concentration could activate nonselective cation currents. However, in the present study, we dialyzed neurons also using high Ca^{2+} concentrations in the pipette, reaching 2 mM, and did not record any cation current. Indeed, the substitution of extracellular NaCl with choline-Cl did not cause a significant shift in the reversal potential both with 1.5 µM and 2 mM of intracellular Ca^{2+}, whereas the substitution of NaCl with Na-gluconate caused a shift in the reversal potential, as expected for Cl^- currents. The substitution of extracellular Cl^- with SCN^- showed that this anion is more permeant than Cl^- and also altered the voltage dependence of the Ca^{2+}-activated current, a common characteristic of Ca^{2+}-activated Cl^- channels (Perez-Cornejo et al., 2004; Xiao et al., 2011; Betto et al., 2014). Moreover, the typical Cl^- blockers NFA and $CaCC_{inh}$-A01 caused a reversible inhibition of the current. A9C had an anomalous effect, causing a current decrease at positive voltages and a current increase at negative voltages, consistent with previous results observed in Ca^{2+}-activated Cl^- channels in smooth muscle cells (Piper and Greenwood, 2003; Cherian et al., 2015).

Furthermore, we performed inside-out recordings from the knobs/microvilli of mouse vomeronasal neurons and demonstrated the presence of Ca^{2+}-activated Cl^- channels with electrophysiological properties similar to those of TMEM16A. We therefore suggest that the nonselective cation current measured in vomeronasal neurons from the hamster may be species specific. In the mouse, results obtained in 12.5% of inside-out patches from Spehr et al. (2009) could indicate that the presence of Ca^{2+}-activated nonselective cation channels is restricted to a very small subpopulation of vomeronasal neurons that was not present in our experiments.

Other studies have also reported evidence for Ca^{2+}-activated Cl^- currents in mouse vomeronasal sensory neurons. Yang and Delay (2010) used perforated patch recording on dissociated neurons and reported that the urine-activated current was partially blocked by some Cl^- channel blockers (NFA and DIDS), and was reduced by removing extracellular Ca^{2+} or by blocking intracellular Cl^- accumulation mediated by the NKCC1 cotransporter. Similar results were also obtained by Kim et al. (2011) using VNO slice preparations. At present, the source of intracellular Ca^{2+} increase is still unclear, as Yang and Delay (2010) showed that Ca^{2+} influx is necessary to activate a Cl^- current, whereas Kim et al. (2011) suggested that Cl^- currents could also be activated by Ca^{2+} release from internal store mediated by IP_3 in a TRPC2-independent manner. The presence of Ca^{2+}-activated Cl^- component in urine response indicates that these channels could play a role in vomeronasal transduction. However, at present, the Cl^- equilibrium potential in vomeronasal neurons in physiological conditions is unknown, preventing the possibility to determine if Ca^{2+}-activated Cl^- currents contribute to depolarization or hyperpolarization.

TMEM16A is a necessary component of the Ca^{2+}-activated Cl^- currents in mouse vomeronasal sensory neurons

Both the results of our whole-cell and inside-out experiments from mouse vomeronasal neurons showed the presence of Ca^{2+}-activated Cl^- currents with electrophysiological properties more similar to those of heterologous TMEM16A than TMEM16B currents. It is important to note that splice variants have been identified both for TMEM16A (Caputo et al., 2008; Ferrera et al., 2009, 2011) and for TMEM16B (Stephan et al., 2009; Ponissery Saidu et al., 2013), and it has been shown that some functional channel properties such as Ca^{2+} sensitivity and time and voltage dependence differ among the various isoforms of each protein (Ferrera et al., 2010; Huang et al., 2012; Pedemonte and Galietta, 2014).

In whole-cell recordings, we measured a kinetics of activation with a time constant of ∼235 ms at 100 mV in

0.5 μM Ca^{2+}, rather similar to the value of ∼300 ms measured in the same conditions for the TMEM16A (abc) isoform (Scudieri et al., 2013), but very different from the fast kinetics, with time constants of activation <10 ms, measured in the retinal isoforms of TMEM16B (Cenedese et al., 2012; Adomaviciene et al., 2013; Scudieri et al., 2013; Betto et al., 2014). However, time constants of activation for the olfactory isoforms of TMEM16B have not been estimated yet, and visual inspection of a whole-cell recording of the recently identified olfactory isoform B (Fig. 4 A of Ponissery Saidu et al., 2013) indicates that the kinetics could be slower than in the retinal isoforms.

In inside-out recordings, a comparison of dose–response relations shows that the Ca^{2+} concentration necessary for 50% activation of the maximal current at 60 or 70 mV had a value of 1.1 μM in our experiments, more similar to the value of 1.3 μM for TMEM16A (Adomaviciene et al., 2013) than to the value of 1.8–4 μM for TMEM16B (Pifferi et al., 2009a, 2012; Adomaviciene et al., 2013). Moreover, at the holding potential of −50 mV and in the presence of 100 μM Ca^{2+}, we did not measure a time-dependent decrease in the presence of Ca^{2+}, typical of all TMEM16B isoforms (Pifferi et al., 2009a, 2012; Stephan et al., 2009; Ponissery Saidu et al., 2013), but we observed a stationary current similar to the behavior of TMEM16A currents in inside-out patches (Ni et al., 2014; Tien et al., 2014; Yu et al., 2014).

To investigate the contribution of TMEM16A to Ca^{2+}-activated Cl^- currents in vomeronasal neurons, we obtained TMEM16A cKO mice and surprisingly found that Ca^{2+}-activated currents were abolished, demonstrating that TMEM16A is an essential component of Ca^{2+}-activated Cl^- currents in mouse vomeronasal sensory neurons. Immunohistochemistry showed the presence of TMEM16B at the apical surface of the vomeronasal epithelium TMEM16A cKO mice, indicating that the expression of TMEM16B does not depend on TMEM16A. At present, we do not know which splice variants are expressed in vomeronasal neurons, but Ponissery Saidu et al. (2013) showed that neurons of the main olfactory epithelium also express isoforms lacking the exon 4 sequence (named isoforms AΔ4 or BΔ4), which do not form functional channels by themselves but modulate channel properties of main olfactory isoforms (named A and B) when they are coexpressed. It is therefore tempting to speculate that vomeronasal neurons may express TMEM16B isoforms that do not form functional channels but could modulate the activity of TMEM16A. Previous results showed that TMEM16A coimmunoprecipitated with TMEM16B in heterologous systems, suggesting that these two proteins may form heteromers (Tien et al., 2014). Thus, native vomeronasal Ca^{2+}-activated Cl^- channels may be heteromers composed of two or more TMEM16A and TMEM16B isoforms. Moreover, our results show that TMEM16A is necessary to have functional channels in the VNO, whereas VNO TMEM16B isoforms may not form functional channels by themselves but could be modulatory subunits of heteromeric channels.

However, in a previous study, Billig et al. (2011) compared whole-cell recordings in vomeronasal sensory neurons from WT (n = 7) or knockout mice for TMEM16B ($Ano2^{-/-}$; n = 6) in the presence of 1.5 μM Ca^{2+} or 0 Ca^{2+} in the pipette, and reported that: "Currents of most $Ano2^{-/-}$ VSNs were indistinguishable from those we observed without Ca^{2+} (Fig. 5n), but a few cells showed currents up to twofold larger. Averaged current/voltage curves revealed that Ca^{2+}-activated Cl^- currents of VSNs depend predominantly on Ano2 (Fig. 5l). Although Ano1 is expressed in the VNO (Fig. 3a), its contribution to VSN currents seems minor." Thus, Billig et al. (2011) suggested that TMEM16B plays a prominent role in Ca^{2+}-activated currents in vomeronasal neurons. However, as the specific VNO TMEM16A and TMEM16B isoforms are presently unknown, there is an alternative possible explanation for the results observed by Billig et al. (2011); vomeronasal neurons may express one or more TMEM16A isoforms that do not form functional channels by themselves but may form functional heteromeric channels when coexpressed with specific TMEM16B isoforms.

Collectively, our data and those from Billig et al. (2011) raise the possibility that only heteromeric channels composed by the VNO-specific isoforms TMEM16A and TMEM16B are functional in vomeronasal neurons. In addition, we cannot exclude the possibility that different populations of neurons may express different isoforms at various levels, and that the two studies investigated different populations of vomeronasal neurons. Future experiments will have to identify the specific VNO isoforms and unravel their interactions.

We thank Peter Mombaerts (Max Planck Institute of Biophysics, Frankfurt, Germany) for providing OMP-Cre mice. We also thank Claudia Gargini (University of Pisa, Italy) for useful discussions, Gianluca Pietra for help with the production of cKO mice, and all members of the laboratory for discussions.

This study was supported by grants from the Italian Ministry of Education, University and Research (2010599KBR to A. Menini) and from the Fondazione Compagnia di San Paolo, Torino (2013.0922 to A. Boccaccio). S. Pifferi is a recipient of an EU Marie Curie Reintegration Grant (OLF-STOM n.334404).

The authors declare no competing financial interests.

Angus C. Nairn served as editor.

Submitted: 15 December 2014
Accepted: 10 February 2015

REFERENCES

Adomaviciene, A., K.J. Smith, H. Garnett, and P. Tammaro. 2013. Putative pore-loops of TMEM16/anoctamin channels affect channel density in cell membranes. *J. Physiol.* 591:3487–3505. http://dx.doi.org/10.1113/jphysiol.2013.251660

Arnson, H.A., X. Fu, and T.E. Holy. 2010. Multielectrode array recordings of the vomeronasal epithelium. *J. Vis. Exp.* 1:1845.

Barry, P.H. 1994. JPCalc, a software package for calculating liquid junction potential corrections in patch-clamp, intracellular, epithelial and bilayer measurements and for correcting junction potential measurements. *J. Neurosci. Methods.* 51:107–116. http://dx.doi.org/10.1016/0165-0270(94)90031-0

Berghard, A., and L.B. Buck. 1996. Sensory transduction in vomeronasal neurons: Evidence for Gαo, Gαi2, and adenylyl cyclase II as major components of a pheromone signaling cascade. *J. Neurosci.* 16:909–918.

Betto, G., O.L. Cherian, S. Pifferi, V. Cenedese, A. Boccaccio, and A. Menini. 2014. Interactions between permeation and gating in the TMEM16B/anoctamin2 calcium-activated chloride channel. *J. Gen. Physiol.* 143:703–718. http://dx.doi.org/10.1085/jgp.201411182

Billig, G.M., B. Pál, P. Fidzinski, and T.J. Jentsch. 2011. Ca^{2+}-activated Cl^- currents are dispensable for olfaction. *Nat. Neurosci.* 14:763–769. http://dx.doi.org/10.1038/nn.2821

Bradley, E., S. Fedigan, T. Webb, M.A. Hollywood, K.D. Thornbury, N.G. McHale, and G.P. Sergeant. 2014. Pharmacological characterization of TMEM16A currents. *Channels (Austin).* 8:308–320. http://dx.doi.org/10.4161/chan.28065

Brennan, P.A. 2009. Outstanding issues surrounding vomeronasal mechanisms of pregnancy block and individual recognition in mice. *Behav. Brain Res.* 200:287–294. http://dx.doi.org/10.1016/j.bbr.2008.10.045

Caputo, A., E. Caci, L. Ferrera, N. Pedemonte, C. Barsanti, E. Sondo, U. Pfeffer, R. Ravazzolo, O. Zegarra-Moran, and L.J.V. Galietta. 2008. TMEM16A, a membrane protein associated with calcium-dependent chloride channel activity. *Science.* 322:590–594. http://dx.doi.org/10.1126/science.1163518

Celsi, F., A. D'Errico, and A. Menini. 2012. Responses to sulfated steroids of female mouse vomeronasal sensory neurons. *Chem. Senses.* 37:849–858. http://dx.doi.org/10.1093/chemse/bjs068

Cenedese, V., G. Betto, F. Celsi, O.L. Cherian, S. Pifferi, and A. Menini. 2012. The voltage dependence of the TMEM16B/anoctamin2 calcium-activated chloride channel is modified by mutations in the first putative intracellular loop. *J. Gen. Physiol.* 139:285–294. http://dx.doi.org/10.1085/jgp.201110764

Chamero, P., T.F. Marton, D.W. Logan, K. Flanagan, J.R. Cruz, A. Saghatelian, B.F. Cravatt, and L. Stowers. 2007. Identification of protein pheromones that promote aggressive behaviour. *Nature.* 450:899–902. http://dx.doi.org/10.1038/nature05997

Chamero, P., V. Katsoulidou, P. Hendrix, B. Bufe, R. Roberts, H. Matsunami, J. Abramowitz, L. Birnbaumer, F. Zufall, and T. Leinders-Zufall. 2011. G protein Gαo is essential for vomeronasal function and aggressive behavior in mice. *Proc. Natl. Acad. Sci. USA.* 108:12898–12903. http://dx.doi.org/10.1073/pnas.1107770108

Cherian, O.L., A. Menini, and A. Boccaccio. 2015. Multiple effects of anthracene-9-carboxylic acid on the TMEM16B/anoctamin2 calcium-activated chloride channel. *Biochim. Biophys. Acta.* 1848:1005–1013. http://dx.doi.org/10.1016/j.bbamem.2015.01.009

De La Fuente, R., W. Namkung, A. Mills, and A.S. Verkman. 2008. Small-molecule screen identifies inhibitors of a human intestinal calcium-activated chloride channel. *Mol. Pharmacol.* 73:758–768. http://dx.doi.org/10.1124/mol.107.043208

Dean, D.M., A. Mazzatenta, and A. Menini. 2004. Voltage-activated current properties of male and female mouse vomeronasal sensory neurons: sexually dichotomous? *J. Comp. Physiol. A Neuroethol. Sens. Neural Behav. Physiol.* 190:491–499. http://dx.doi.org/10.1007/s00359-004-0513-8

Dibattista, M., A. Mazzatenta, F. Grassi, R. Tirindelli, and A. Menini. 2008. Hyperpolarization-activated cyclic nucleotide-gated channels in mouse vomeronasal sensory neurons. *J. Neurophysiol.* 100:576–586. http://dx.doi.org/10.1152/jn.90263.2008

Dibattista, M., A. Amjad, D.K. Maurya, C. Sagheddu, G. Montani, R. Tirindelli, and A. Menini. 2012. Calcium-activated chloride channels in the apical region of mouse vomeronasal sensory neurons. *J. Gen. Physiol.* 140:3–15. http://dx.doi.org/10.1085/jgp.201210780

Dulac, C., and R. Axel. 1995. A novel family of genes encoding putative pheromone receptors in mammals. *Cell.* 83:195–206. http://dx.doi.org/10.1016/0092-8674(95)90161-2

Faria, D., J.R. Rock, A.M. Romao, F. Schweda, S. Bandulik, R. Witzgall, E. Schlatter, D. Heitzmann, H. Pavenstädt, E. Herrmann, et al. 2014. The calcium-activated chloride channel Anoctamin 1 contributes to the regulation of renal function. *Kidney Int.* 85:1369–1381. http://dx.doi.org/10.1038/ki.2013.535

Ferrera, L., A. Caputo, I. Ubby, E. Bussani, O. Zegarra-Moran, R. Ravazzolo, F. Pagani, and L.J.V. Galietta. 2009. Regulation of TMEM16A chloride channel properties by alternative splicing. *J. Biol. Chem.* 284:33360–33368. http://dx.doi.org/10.1074/jbc.M109.046607

Ferrera, L., A. Caputo, and L.J.V. Galietta. 2010. TMEM16A protein: A new identity for Ca^{2+}-dependent Cl^- channels. *Physiology (Bethesda).* 25:357–363. http://dx.doi.org/10.1152/physiol.00030.2010

Ferrera, L., P. Scudieri, E. Sondo, A. Caputo, E. Caci, O. Zegarra-Moran, R. Ravazzolo, and L.J.V. Galietta. 2011. A minimal isoform of the TMEM16A protein associated with chloride channel activity. *Biochim. Biophys. Acta.* 1808:2214–2223. http://dx.doi.org/10.1016/j.bbamem.2011.05.017

Francia, S., S. Pifferi, A. Menini, and R. Tirindelli. 2014. Vomeronasal receptors and signal transduction in the vomeronasal organ of mammals. *In* Neurobiology of Chemical Communication. C. Mucignat-Caretta, editor. CRC Press, Boca Raton, FL. 297–324. http://dx.doi.org/10.1201/b16511-11

Greenwood, I.A., and W.A. Large. 1999. Modulation of the decay of Ca^{2+}-activated Cl^- currents in rabbit portal vein smooth muscle cells by external anions. *J. Physiol.* 516:365–376. http://dx.doi.org/10.1111/j.1469-7793.1999.0365v.x

Haga, S., T. Hattori, T. Sato, K. Sato, S. Matsuda, R. Kobayakawa, H. Sakano, Y. Yoshihara, T. Kikusui, and K. Touhara. 2010. The male mouse pheromone ESP1 enhances female sexual receptive behaviour through a specific vomeronasal receptor. *Nature.* 466:118–122. http://dx.doi.org/10.1038/nature09142

Hartzell, H.C., K. Yu, Q. Xiao, L.-T. Chien, and Z. Qu. 2009. Anoctamin/TMEM16 family members are Ca^{2+}-activated Cl^- channels. *J. Physiol.* 587:2127–2139. http://dx.doi.org/10.1113/jphysiol.2008.163709

Herrada, G., and C. Dulac. 1997. A novel family of putative pheromone receptors in mammals with a topographically organized and sexually dimorphic distribution. *Cell.* 90:763–773. http://dx.doi.org/10.1016/S0092-8674(00)80536-X

Hille, B. 2001. Ion Channels of Excitable Membranes. Third Edition. Sinauer Associates, Sunderland, MA. 814 pp.

Holy, T.E., C. Dulac, and M. Meister. 2000. Responses of vomeronasal neurons to natural stimuli. *Science.* 289:1569–1572. http://dx.doi.org/10.1126/science.289.5484.1569

Huang, F., X. Wong, and L.Y. Jan. 2012. International Union of Basic and Clinical Pharmacology. LXXXV: Calcium-activated chloride channels. *Pharmacol. Rev.* 64:1–15. http://dx.doi.org/10.1124/pr.111.005009

Jia, C., and M. Halpern. 1996. Subclasses of vomeronasal receptor neurons: differential expression of G proteins ($G_{i\alpha 2}$ and $G_{o\alpha}$) and segregated projections to the accessory olfactory bulb. *Brain Res.* 719:117–128. http://dx.doi.org/10.1016/0006-8993(96)00110-2

Kim, S., L. Ma, and C.R. Yu. 2011. Requirement of calcium-activated chloride channels in the activation of mouse vomeronasal neurons. *Nat. Commun.* 2:365. http://dx.doi.org/10.1038/ncomms1368

Kim, S., L. Ma, K.L. Jensen, M.M. Kim, C.T. Bond, J.P. Adelman, and C.R. Yu. 2012. Paradoxical contribution of SK3 and GIRK channels to the activation of mouse vomeronasal organ. *Nat. Neurosci.* 15:1236–1244. http://dx.doi.org/10.1038/nn.3173

Kuruma, A., and H.C. Hartzell. 2000. Bimodal control of a Ca^{2+}-activated Cl^- channel by different Ca^{2+} signals. *J. Gen. Physiol.* 115:59–80. http://dx.doi.org/10.1085/jgp.115.1.59

Lau, Y.E., and J.A. Cherry. 2000. Distribution of PDE4A and $G_{o\alpha}$ immunoreactivity in the accessory olfactory system of the mouse. *Neuroreport.* 11:27–30. http://dx.doi.org/10.1097/00001756-200001170-00006

Leinders-Zufall, T., A.P. Lane, A.C. Puche, W. Ma, M.V. Novotny, M.T. Shipley, and F. Zufall. 2000. Ultrasensitive pheromone detection by mammalian vomeronasal neurons. *Nature.* 405:792–796. http://dx.doi.org/10.1038/35015572

Leinders-Zufall, T., P. Brennan, P. Widmayer, P. Chandramani S., A. Maul-Pavicic, M. Jäger, X.H. Li, H. Breer, F. Zufall, and T. Boehm. 2004. MHC class I peptides as chemosensory signals in the vomeronasal organ. *Science.* 306:1033–1037. http://dx.doi.org/10.1126/science.1102818

Leinders-Zufall, T., T. Ishii, P. Mombaerts, F. Zufall, and T. Boehm. 2009. Structural requirements for the activation of vomeronasal sensory neurons by MHC peptides. *Nat. Neurosci.* 12:1551–1558. http://dx.doi.org/10.1038/nn.2452

Li, J., T. Ishii, P. Feinstein, and P. Mombaerts. 2004. Odorant receptor gene choice is reset by nuclear transfer from mouse olfactory sensory neurons. *Nature.* 428:393–399. http://dx.doi.org/10.1038/nature02433

Liberles, S.D., L.F. Horowitz, D. Kuang, J.J. Contos, K.L. Wilson, J. Siltberg-Liberles, D.A. Liberles, and L.B. Buck. 2009. Formyl peptide receptors are candidate chemosensory receptors in the vomeronasal organ. *Proc. Natl. Acad. Sci. USA.* 106:9842–9847. http://dx.doi.org/10.1073/pnas.0904464106

Liman, E.R. 2003. Regulation by voltage and adenine nucleotides of a Ca^{2+}-activated cation channel from hamster vomeronasal sensory neurons. *J. Physiol.* 548:777–787. http://dx.doi.org/10.1113/jphysiol.2002.037119

Liman, E.R., and D.P. Corey. 1996. Electrophysiological characterization of chemosensory neurons from the mouse vomeronasal organ. *J. Neurosci.* 16:4625–4637.

Liman, E.R., D.P. Corey, and C. Dulac. 1999. TRP2: A candidate transduction channel for mammalian pheromone sensory signaling. *Proc. Natl. Acad. Sci. USA.* 96:5791–5796. http://dx.doi.org/10.1073/pnas.96.10.5791

Martini, S., L. Silvotti, A. Shirazi, N.J. Ryba, and R. Tirindelli. 2001. Co-expression of putative pheromone receptors in the sensory neurons of the vomeronasal organ. *J. Neurosci.* 21:843–848.

Matsunami, H., and L.B. Buck. 1997. A multigene family encoding a diverse array of putative pheromone receptors in mammals. *Cell.* 90:775–784. http://dx.doi.org/10.1016/S0092-8674(00)80537-1

Munger, S.D., T. Leinders-Zufall, and F. Zufall. 2009. Subsystem organization of the mammalian sense of smell. *Annu. Rev. Physiol.* 71:115–140. http://dx.doi.org/10.1146/annurev.physiol.70.113006.100608

Ni, Y.-L., A.-S. Kuan, and T.-Y. Chen. 2014. Activation and inhibition of TMEM16A calcium-activated chloride channels. *PLoS ONE.* 9:e86734. http://dx.doi.org/10.1371/journal.pone.0086734

Patton, C., S. Thompson, and D. Epel. 2004. Some precautions in using chelators to buffer metals in biological solutions. *Cell Calcium.* 35:427–431. http://dx.doi.org/10.1016/j.ceca.2003.10.006

Pedemonte, N., and L.J.V. Galietta. 2014. Structure and function of TMEM16 proteins (anoctamins). *Physiol. Rev.* 94:419–459. http://dx.doi.org/10.1152/physrev.00039.2011

Perez-Cornejo, P., J.A. De Santiago, and J. Arreola. 2004. Permeant anions control gating of calcium-dependent chloride channels. *J. Membr. Biol.* 198:125–133. http://dx.doi.org/10.1007/s00232-004-0659-x

Pifferi, S., G. Pascarella, A. Boccaccio, A. Mazzatenta, S. Gustincich, A. Menini, and S. Zucchelli. 2006. Bestrophin-2 is a candidate calcium-activated chloride channel involved in olfactory transduction. *Proc. Natl. Acad. Sci. USA.* 103:12929–12934. http://dx.doi.org/10.1073/pnas.0604505103

Pifferi, S., M. Dibattista, and A. Menini. 2009a. TMEM16B induces chloride currents activated by calcium in mammalian cells. *Pflugers Arch.* 458:1023–1038. http://dx.doi.org/10.1007/s00424-009-0684-9

Pifferi, S., M. Dibattista, C. Sagheddu, A. Boccaccio, A. Al Qteishat, F. Ghirardi, R. Tirindelli, and A. Menini. 2009b. Calcium-activated chloride currents in olfactory sensory neurons from mice lacking bestrophin-2. *J. Physiol.* 587:4265–4279. http://dx.doi.org/10.1113/jphysiol.2009.176131

Pifferi, S., V. Cenedese, and A. Menini. 2012. Anoctamin 2/TMEM16B: a calcium-activated chloride channel in olfactory transduction. *Exp. Physiol.* 97:193–199. http://dx.doi.org/10.1113/expphysiol.2011.058230

Piper, A.S., and I.A. Greenwood. 2003. Anomalous effect of anthracene-9-carboxylic acid on calcium-activated chloride currents in rabbit pulmonary artery smooth muscle cells. *Br. J. Pharmacol.* 138:31–38. http://dx.doi.org/10.1038/sj.bjp.0705000

Ponissery Saidu, S., A.B. Stephan, A.K. Talaga, H. Zhao, and J. Reisert. 2013. Channel properties of the splicing isoforms of the olfactory calcium-activated chloride channel Anoctamin 2. *J. Gen. Physiol.* 141:691–703. http://dx.doi.org/10.1085/jgp.201210937

Qu, Z., and H.C. Hartzell. 2000. Anion permeation in Ca^{2+}-activated Cl^- channels. *J. Gen. Physiol.* 116:825–844. http://dx.doi.org/10.1085/jgp.116.6.825

Qu, Z., R.W. Wei, and H.C. Hartzell. 2003. Characterization of Ca^{2+}-activated Cl^- currents in mouse kidney inner medullary collecting duct cells. *Am. J. Physiol. Renal Physiol.* 285:F326–F335.

Reisert, J., P.J. Bauer, K.-W. Yau, and S. Frings. 2003. The Ca-activated Cl channel and its control in rat olfactory receptor neurons. *J. Gen. Physiol.* 122:349–364. http://dx.doi.org/10.1085/jgp.200308888

Rivière, S., L. Challet, D. Fluegge, M. Spehr, and I. Rodriguez. 2009. Formyl peptide receptor-like proteins are a novel family of vomeronasal chemosensors. *Nature.* 459:574–577. http://dx.doi.org/10.1038/nature08029

Rock, J.R., C.R. Futtner, and B.D. Harfe. 2008. The transmembrane protein TMEM16A is required for normal development of the murine trachea. *Dev. Biol.* 321:141–149. http://dx.doi.org/10.1016/j.ydbio.2008.06.009

Ryba, N.J., and R. Tirindelli. 1997. A new multigene family of putative pheromone receptors. *Neuron.* 19:371–379. http://dx.doi.org/10.1016/S0896-6273(00)80946-0

Schreiber, R., D. Faria, B.V. Skryabin, P. Wanitchakool, J.R. Rock, and K. Kunzelmann. 2014. Anoctamins support calcium-dependent chloride secretion by facilitating calcium signaling in adult mouse intestine. *Pflugers Arch.* In press. http://dx.doi.org/10.1007/s00424-014-1559-2

Schroeder, B.C., T. Cheng, Y.N. Jan, and L.Y. Jan. 2008. Expression cloning of TMEM16A as a calcium-activated chloride channel subunit. *Cell.* 134:1019–1029. http://dx.doi.org/10.1016/j.cell.2008.09.003

Scudieri, P., E. Sondo, L. Ferrera, and L.J.V. Galietta. 2012. The anoctamin family: TMEM16A and TMEM16B as calcium-activated chloride channels. *Exp. Physiol.* 97:177–183. http://dx.doi.org/10.1113/expphysiol.2011.058198

Scudieri, P., E. Sondo, E. Caci, R. Ravazzolo, and L.J.V. Galietta. 2013. TMEM16A-TMEM16B chimaeras to investigate the structure-function relationship of calcium-activated chloride channels. *Biochem. J.* 452:443–455. http://dx.doi.org/10.1042/BJ20130348

Shimazaki, R., A. Boccaccio, A. Mazzatenta, G. Pinato, M. Migliore, and A. Menini. 2006. Electrophysiological properties and modeling of murine vomeronasal sensory neurons in acute slice preparations. *Chem. Senses.* 31:425–435. http://dx.doi.org/10.1093/chemse/bjj047

Spehr, J., S. Hagendorf, J. Weiss, M. Spehr, T. Leinders-Zufall, and F. Zufall. 2009. Ca^{2+}-calmodulin feedback mediates sensory adaptation and inhibits pheromone-sensitive ion channels in the vomeronasal organ. *J. Neurosci.* 29:2125–2135. http://dx.doi.org/10.1523/JNEUROSCI.5416-08.2009

Stephan, A.B., E.Y. Shum, S. Hirsh, K.D. Cygnar, J. Reisert, and H. Zhao. 2009. ANO2 is the cilial calcium-activated chloride channel that may mediate olfactory amplification. *Proc. Natl. Acad. Sci. USA.* 106:11776–11781. http://dx.doi.org/10.1073/pnas.0903304106

Stöhr, H., J.B. Heisig, P.M. Benz, S. Schöberl, V.M. Milenkovic, O. Strauss, W.M. Aartsen, J. Wijnholds, B.H.F. Weber, and H.L. Schulz. 2009. TMEM16B, a novel protein with calcium-dependent chloride channel activity, associates with a presynaptic protein complex in photoreceptor terminals. *J. Neurosci.* 29:6809–6818. http://dx.doi.org/10.1523/JNEUROSCI.5546-08.2009

Tien, J., C.J. Peters, X.M. Wong, T. Cheng, Y.N. Jan, L.Y. Jan, and H. Yang. 2014. A comprehensive search for calcium binding sites critical for TMEM16A calcium-activated chloride channel activity. *eLife.* 3. http://dx.doi.org/10.7554/eLife.02772

Tirindelli, R., M. Dibattista, S. Pifferi, and A. Menini. 2009. From pheromones to behavior. *Physiol. Rev.* 89:921–956. http://dx.doi.org/10.1152/physrev.00037.2008

Touhara, K., and L.B. Vosshall. 2009. Sensing odorants and pheromones with chemosensory receptors. *Annu. Rev. Physiol.* 71:307–332. http://dx.doi.org/10.1146/annurev.physiol.010908.163209

Xiao, Q., K. Yu, P. Perez-Cornejo, Y. Cui, J. Arreola, and H.C. Hartzell. 2011. Voltage- and calcium-dependent gating of TMEM16A/Ano1 chloride channels are physically coupled by the first intracellular loop. *Proc. Natl. Acad. Sci. USA.* 108:8891–8896. http://dx.doi.org/10.1073/pnas.1102147108

Yang, C., and R.J. Delay. 2010. Calcium-activated chloride current amplifies the response to urine in mouse vomeronasal sensory neurons. *J. Gen. Physiol.* 135:3–13. http://dx.doi.org/10.1085/jgp.200910265

Yang, T., W.A. Hendrickson, and H.M. Colecraft. 2014. Preassociated apocalmodulin mediates Ca^{2+}-dependent sensitization of activation and inactivation of TMEM16A/16B Ca^{2+}-gated Cl^- channels. *Proc. Natl. Acad. Sci. USA.* 111:18213–18218. http://dx.doi.org/10.1073/pnas.1420984111

Yang, Y.D., H. Cho, J.Y. Koo, M.H. Tak, Y. Cho, W.-S. Shim, S.P. Park, J. Lee, B. Lee, B.-M. Kim, et al. 2008. TMEM16A confers receptor-activated calcium-dependent chloride conductance. *Nature.* 455:1210–1215. http://dx.doi.org/10.1038/nature07313

Yu, Y., A.-S. Kuan, and T.-Y. Chen. 2014. Calcium-calmodulin does not alter the anion permeability of the mouse TMEM16A calcium-activated chloride channel. *J. Gen. Physiol.* 144:115–124. http://dx.doi.org/10.1085/jgp.201411179

Zufall, F., K. Ukhanov, P. Lucas, E.R. Liman, and T. Leinders-Zufall. 2005. Neurobiology of TRPC2: from gene to behavior. *Pflugers Arch.* 451:61–71. http://dx.doi.org/10.1007/s00424-005-1432-4

1.1 Sensory information representation in mouse vomeronasal sensory neurons is modified by the calcium-activated chloride current TMEM16A

Sensory information representation in mouse vomeronasal sensory neurons is modified by the Ca^{2+}-activated Cl^- channel TMEM16A

Manuscript in preparation

Andres Hernandez-Clavijo conceived, designed, performed and analyzed the experiments, prepared figures, wrote the manuscript.

Simone Pifferi conceived, designed and evaluated experiments, wrote software for data analysis and the manuscript.

Anna Menini conceived, designed and evaluated experiments, wrote the manuscript.

Jason Rock (Department of Anatomy, University of California, School of Medicine, San Francisco, CA) provided floxed TMEM16A$^{fl/fl}$ mice.

Abstract

Calcium-activated chloride channels are expressed in several cells, including sensory neurons of the mouse vomeronasal organ, where pheromones bind to receptors located in microvilli activating a transduction cascade that leads to neuron depolarization and increase in firing activity. We have previously shown that calcium-activated chloride currents are abolished in vomeronasal sensory neurons from conditional knock out mice for TMEM16A (TMEM16A cKO). Thus, this mouse line is a good model to study the role of calcium-activated chloride currents in vomeronasal physiology. Here, we investigated the firing properties of vomeronasal sensory neurons in acute slices of the vomeronasal organ from wild type and TMEM16A cKO mice. Loose-patch recordings show that the firing pattern of spontaneous activity has less burst activity in sensory neurons from TMEM16A cKO with respect to WT mice, while the mean frequency is not affected by the lack of TMEM16A. Moreover, we measured an increase in firing rate in response to stimulation with dilute urine, a physiologically relevant stimulus for mouse, both in WT and TMEM16A cKO vomeronasal sensory neurons, indicating that neurons lacking calcium-activated chloride currents are still able to activate the signal transduction cascade. Importantly, we also observed significant changes in the pattern of firing activity in response to dilute urine, as the inter-spike interval distribution of evoked activity showed that vomeronasal sensory neurons from TMEM16A cKO fire with shorter intervals than WT neurons. These results indicate that deletion of TMEM16A in mouse vomeronasal sensory neurons induces a modification in the characteristics of the firing pattern during spontaneous and evoked activity, indicating that the calcium-activated chloride channel TMEM16A plays a role in the response to physiological stimuli.

Introduction

Most mammals detect pheromones by using at least two main chemoreceptive systems in the nasal cavity: the main olfactory epithelium and the vomeronasal epithelium (Tirindelli et al., 2009). The vomeronasal organ (VNO) is a cylindrical structure located in the lower region of the nasal cavity and is surrounded by a cartilaginous capsule that is opened in the anterior part and connected via a duct with the nasal cavity or oral cavity (Trotier and Døving, 1998). The VNO is composed by two epithelia, the non-sensory epithelium and the sensory epithelium, making a central lumen full of fluid in direct contact with the nasal cavity fluids. The sensory epithelium is a pseudostratified epithelium, mainly composed by vomeronasal sensory neurons (VSN), cells responsible to detect the stimuli.

VSNs respond to stimuli, mainly pheromones, producing a depolarization of the membrane potential, an increase of cytosolic calcium, and an increase in firing frequency (Celsi et al., 2012; Holy et al., 2000; Inamura et al., 1997; Kim et al., 2011; Leinders-Zufall et al., 2004; Riviere et al., 2009; Spehr et al., 2002; Stowers et al., 2002; Yang and Delay, 2010; Zhang et al., 2010; Zufall and Leinders-Zufall, 2000). The binding of the ligand to vomeronasal receptors activates a G protein regulated and cyclic-nucleotide-independent signaling pathway involving phospholipase C activation, which leads to the activation of a transient receptor potential canonical 2 (TRPC2) channel, highly expressed in the knob microvilli of VSNs, allowing the influx of sodium and calcium ions (Liman et al., 1999; Munger et al., 2001; Zufall and Leinders-Zufall, 2000), and/or to calcium release from intracellular stores (Kim et al., 2011). The increase in cytosolic calcium, through TRPC2 channels opening or release from internal stores, plays several roles in signal transduction involving the activation of other ion channels and enzymes.

Several studies identified the presence of calcium-activated chloride currents in mouse VSNs (Amjad et al., 2015; Dibattista et al., 2012; Kim et al., 2011; Yang and Delay, 2010). Yang and Delay (2010) measured calcium-activated chloride currents in dissociated VSNs during the response to urine stimulation and proposed that these currents have a role of amplifying the signal transduction (Yang and Delay, 2010). Kim et al. (2011) proposed that calcium-activated chloride currents can also work as an independent signaling pathway, where calcium-activated chloride currents are necessary and sufficient to activate the VSNs. Dibattista et al. (2012) showed that calcium-activated chloride channels are present in the apical portion of VSNs by using local photorelease of calcium from caged-calcium. Indeed, a localized, rapid, and reproducible increase in calcium concentration in the microvilli of VSNs developed a large chloride current that was blocked by the chloride channel blockers niflumic acid (NFA) and 4,4'-diisothiocyanatostilbene-2,2'-disulfonic acid (DIDS) (Dibattista et al., 2012).

TMEM16A and TMEM16B, two proteins forming calcium-activated chloride channels (Caputo et al., 2008; Pifferi et al., 2009; Schroeder et al., 2008; Stephan et al., 2009; Stöhr et al., 2009; Yang et al., 2008) have been shown to be expressed in the microvilli layer of the VNO (Amjad et al., 2015; Billig et al., 2011; Dauner et al., 2012; Dibattista et al., 2012; Rasche et al., 2010). Moreover, immunocytochemistry on isolated VSNs showed that TMEM16A and TMEM16B co-express in the neuronal microvilli (Dibattista et al., 2012). Although both channels are co-expressed in VSNs, Billig et al. (2011) reported that calcium-activated chloride currents were eliminated in the TMEM16B KO mouse (Billig et al., 2011). However, it is important to notice that Billig et al. compared a very small number of cells (WT n=7, TMEM16B KO n=5) and they reported that a residual current was still present in some neurons.

Amjad et al. (2015) provided the functional characterization of calcium-activated chloride currents in mouse VSNs (Amjad et al., 2015). Calcium sensitivity, voltage dependence, ion selectivity, kinetics, and

pharmacology of the calcium-activated chloride currents in isolated VSNs were measured using whole-cell and inside-out recordings and it was shown that the biophysical properties of VSN currents are more similar to those of TMEM16A than of TMEM16B channel (Amjad et al., 2015). Furthermore, calcium-activated chloride currents were abolished in VSNs of conditional knockout (cKO) mice for TMEM16A, demonstrating that TMEM16A is a necessary component of calcium-activated chloride channels in mouse VSNs (Amjad et al., 2015).

As calcium-activated chloride currents in VSNs of TMEM16A cKO mice are completely abolished, these mice are a very good model to study the physiological role of calcium-activated chloride currents in VSNs. The aim of this study was to investigate the physiological role of calcium-activated chloride currents in mouse VSNs. We compared spontaneous and evoked activity in VSNs of wild-type (WT) and TMEM16A cKO mice using the loose-patch technique. Although the mean frequency of spontaneous activity was not affected in TMEM16A cKO VSNs, we found that the firing pattern was different, with TMEM16A cKO VSNs showing a reduced burst activity, indicating that TMEM16A plays a role in defining the firing pattern. Urine stimulation generated an increase of firing activity both in VSNs from WT and TMEM16A cKO, showing that VSNs retain their ability to respond to urine stimulation also in the absence of calcium-activated chloride currents. However, although the mean frequency of evoked activity was not significantly different in WT and TMEM16A cKO VSNs, we found that the firing pattern was altered: TMEM16A cKO VSNs showed higher instantaneous firing frequency and shorter duration in response to urine stimulation. Our results demonstrate that TMEM16A regulates the firing pattern during spontaneous and evoked activity in mouse VSNs.

Materials and Methods

Animals

Mice were handled in accordance with the guidelines of the Italian Animal Welfare Act and European Union guidelines on animal research, under a protocol approved by the ethic committee of SISSA. TMEM16A conditional knockout mice (TMEM16A cKO), whose generation has been described in detail (Amjad et al., 2015), were homozygous for the floxed TMEM16A alleles and heterozygous for Cre and OMP. TMEM16A$^{fl/fl}$ mice were used as controls. In the following, WT mice correspond to TMEM16A$^{fl/fl}$ mice. 2–3-months-old mice were anaesthetized by CO_2 inhalation and decapitated before VNO removal.

Preparation of acute slices of mouse VNO

Acute slices of mouse VNO were prepared as described previously (Shimazaki et al., 2006). In brief, the VNO was removed and transferred to ice-cold artificial cerebrospinal fluid (ACSF). The capsule and all cartilaginous tissues were carefully removed and the two halves of the VNO were isolated from the vomer bone. Each half of the VNO was then separately treated. The VNO was embedded in 3% low-grade agar (A7002 Sigma) prepared in ACSF once the agar had cooled to 38°C. Upon solidification, the agar block was fixed in a glass Petri dish and sliced with a vibratome (Vibratome 1000 Plus Sectioning System) at 200-250 µm in oxygenated ACSF solution. Slices were then left to recover for >30 min on chilled and oxygenated ACSF before electrophysiological experiments were initiated.

Slices were viewed with an upright microscope (Olympus BX51WI) by infrared differential contrast optics with water immersion 20X or 60X objectives. The slice preparation maintained the VNO cross-sectional structure and many individual VSNs could be clearly distinguished by their morphology. Patch pipettes, pulled from borosilicate capillaries (WPI) with a PC-10 puller (Narishige), had a resistance of 3–

6 MΩ for whole-cell and loose-patch recordings. Currents were recorded with a Multiclamp 700B amplifier controlled by Clampex 10 via a Digidata 1440 (Molecular Devices). Data were low-pass filtered at 2 kHz and sampled at 10 kHz. Experiments were performed at room temperature (20–25°C). The recording chamber was continuously perfused with oxygenated (95% O_2, and 5% CO_2) ACSF by gravity flow. ACSF contained (mM): 120 NaCl, 20 $NaHCO_3$, 3 KCl, 2 $CaCl_2$, 1 $MgSO_4$, 10 HEPES, 10 glucose, pH 7.4. The slice was anchored to the base of the recording chamber using a home-made U-shaped silver wire, holding down the agar support without touching the slice itself.

Whole-cell recording in VSNs from acute slices

For whole-cell recordings, the intracellular solution filling the patch pipette contained (mM): 110 K-Gluconate, 30 KCl, 10 NaCl, 1 $MgCl_2$, 0.023 $CaCl_2$, 10 HEPES, and 10 EGTA, adjusted to pH 7.2 with KOH. The cell was kept at a holding potential of -70 mV from where 10 mV steps were applied from -100 mV to +40 mV. To test the membrane resistance, a -10 mV step was applied from the holding potential and the steady-state current was measured to calculate the membrane resistance. Series resistance was not compensated. Resting membrane potential was measured in current-clamp mode under I=0 configuration, shortly after obtaining the whole-cell configuration.

Loose-patch extracellular recording in VSNs from acute slices

Extracellular recordings from the soma of VSNs were obtained in the loose-patch configuration with seal resistances of 40-100 MΩ. Pipette solution was ACSF, as the bath solution, and the recordings were made in voltage-clamp mode with a holding potential of 0 mV. Data were low-pass filtered at 2 kHz and sampled at 10 kHz. Stimuli were focally delivered through a gravity-fed multi-valve perfusion system (ALA-VM8, ALA Scientific Instruments). The tip of the perfusion head had a diameter of 360 µm and was placed ~500 µm away from the slice. We estimated the time necessary for the stimulus to reach the cell by using a high-potassium solution as a stimulus and by placing the tip of a patch pipette at a distance of about 500 µm from the tip of the perfusion head. Recordings in voltage-clamp at 0 mV showed that the time necessary for the high-potassium solution to reach the tip of the patch pipette was about 300 ms from the opening of the valve. To avoid mechanical artifacts, the slice was constantly perfused with ACSF and the flow out of the pipette was switched between ACSF and stimulus solutions, resulting in a constant flow across the epithelium and sharp concentration transients, undiluted by the bath ACSF. Recordings were usually from single VSNs, although in a limited number of cases it was possible to record from two cells at the same time from a single electrode, but single action potentials of the two different cells were clearly distinguished by differences in size and shape.

Urine collection and solutions.

Urine was collected from both sexes of C57BL/6 mice, filtered with a 0.2-µm filter, and frozen at -80°C. Before use, male and female urines were mixed in 1:1 ratio and the mixture was diluted to 1:50 in ACSF (pH 7.4). Mouse urine contains urea and potassium ions, which could potentially cause neurons to fire by direct membrane depolarization. As a negative control, we used artificial urine diluted 1:50 (Holy et al., 2000), artificial urine contained (mM): 100 NaCl; 40 KCl; 20 NH_4OH; 4 $CaCl_2$; 2.5 $MgCl_2$; 15 NaH_2PO_4; 20 $NaHSO_4$; 333 urea; pH 7.4 adjusted with NaOH. As a positive control we used high-potassium solutions (25 mM KCl) by substituting equimolar quantities of KCl for NaCl. Urine and artificial urine were applied in 10 s pulses, and the inter-stimulus interval was at least 4 minutes to avoid desensitization or adaptation processes (Spehr et al., 2009). High-potassium solution was applied in 3 or 5 s pulses.

Chemicals

All compounds and chemicals were obtained from Sigma-Aldrich, unless otherwise stated.

Analysis of electrophysiological data

IgorPro software (WaveMetrics) and Clampfit (Molecular Devices) were used for data analysis and figure preparation. Data are presented as mean ± SEM. Because most of the data were not normally distributed (Shapiro–Wilk test), statistical significance was determined using Wilcoxon-Mann Whitney test or Kolmogorov-Smirnov test. p-values of <0.01 were considered statistically significant. For data normally distributed t-test was used (Fig 1D).

For spike detection, recordings were filtered offline with a high-pass filter at 2 Hz to eliminate slow changes in the baseline. Individual action potentials were identified by an event detection using an arbitrary threshold, and each event was confirmed by shape inspection. The start time of each event was taken as the time for that individual action potential. Mean spontaneous firing frequency was calculated as the number of spikes divided by the duration of the recording. Inter-spike interval (ISI) was calculated measuring the time between consecutive spikes (second to first, third to second, and so forth). To construct the ISI distribution during spontaneous activity we calculated the ISI for all spikes in 158 recordings of 90 s each from 20 WT VSNs, and 161 recordings of 90 s each from 22 TMEM16A cKO VSNs. Then we grouped the ISIs in 5 ms bins and divided the value of each bin by the total number of calculated ISIs for each group. The y-axes values in Fig 2C represents the percentage of spikes in each bin, the area under the curve is 100 %. ISI distribution during evoked activity was calculated from the spikes during the 10 s stimulus presentation and calculating the ISI as described for spontaneous activity but with 10 ms bins (Fig 4D). Average firing rate (Fig 3 bottom) was calculated dividing each recording (Fig 3 Middle) in 1 s bins and counting the number of spikes per bin. The histogram represents the mean ± SEM of all repeats for one single VSN.

As VSNs usually shows spontaneous activity in bursts (Arnson and Holy, 2011), it was difficult to identify a urine response from a single recording. To avoid false positives we applied at least 4 repetitive stimulations. Each recording was 90 s long divided in: 40 s of pre-stimulus, 10 s of stimulus, and 40 s of post-stimulus. To analyze the response to urine for a single cell we took basal period (40 s pre-stimulation) and stimulus period (10 s of stimulation), and we calculated the basal and stimulation frequency for each trace. We defined a threshold level as: $BF + 2*\sigma^2$; where BF is the average of basal frequency for all the traces of a given cell and σ^2 is the standard deviation of the basal frequency. A cell was considered responsive to urine if: 1) the average of spike frequency during the stimulations (SF) was higher than the threshold and 2) there was not response in artificial urine.

Results

Membrane properties and voltage-gated currents of VSNs from TMEM16A cKO mice are not altered.

To test if deleting TMEM16A protein has any effect on membrane properties and voltage-gated inward and outward currents of VSNs, we performed whole-cell recordings from WT and TMEM16A cKO VSNs in acute slices of VNO. In voltage-clamp mode, we applied voltage steps from -100 mV to +40 mV with 10 mV increment steps from a holding potential of -70 mV. We first evaluated the presence of the characteristic voltage-activated inward and outward currents (Liman and Corey, 1996; Shimazaki et al., 2006; Ukhanov et al., 2007) (Fig 1A), and plotted their I-V relation (Fig 1B). For the inward current, we plotted the minimum value during the first 20 ms after the voltage pulse (circles in Fig 1A-B), while for the outward current we took the current value at the end of the voltage pulses (triangles in Fig 1A-B). Figure 1B shows that I-V relations of voltage-gated currents were similar in VSNs from WT and TMEM16A cKO mice.

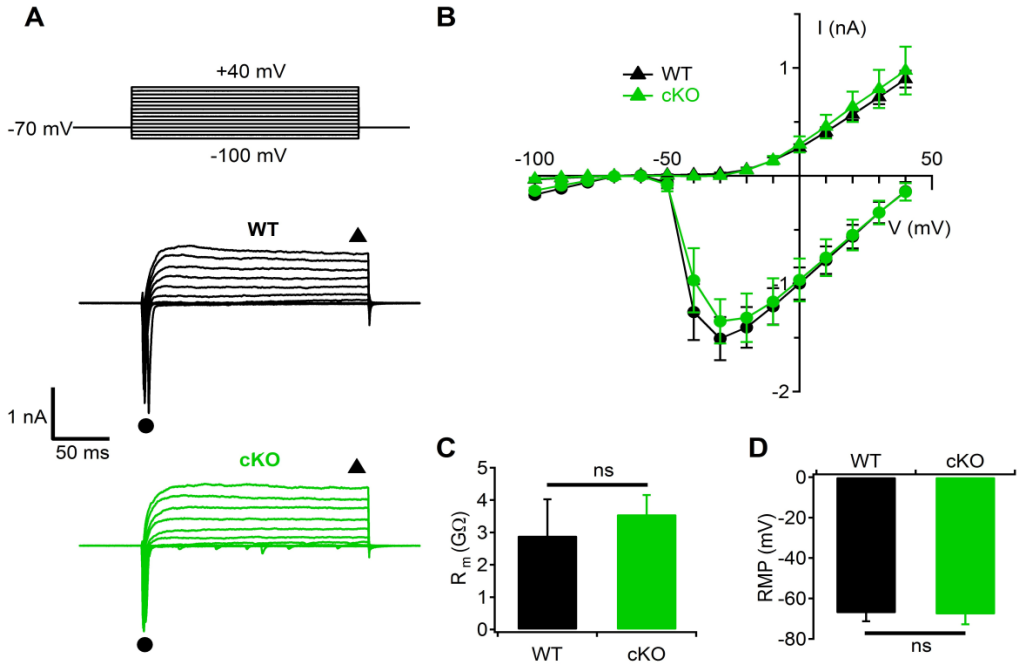

Figure 1. Membrane properties and voltage-gated currents of VSNs ***(A)*** *Representative whole-cell recordings of VSNs obtained from WT (black traces) and TMEM16A cKO (green traces) mice. The holding potential was -70 mV and voltage steps from -100 to +40 mV with 10 mV increment were applied.* ***(B)*** *Average of the IV relationships of inward currents (circles) and steady-state outward currents (triangles) from WT (black; n=11) and TMEM16A cKO (green; n=4) VSNs. Values were taken at the negative peak and at the end of voltage step as indicated by the symbols in A.* ***(C)*** *Average of membrane resistance (Rm) recorded in voltage-clamp mode. Membrane resistance was not statistically different between both groups (U-test: p=0.14). Average values were 2.9 ± 1.1 GΩ for WT (black bar; n=11) and 3.6 ± 0.6 GΩ for TMEM16A cKO (green bar; n=4) VSNs.* ***(D)*** *Average of resting membrane potential (RMP) recorded in current clamp mode. The values were -67 ± 4 mV for WT (black bar; n=9) and -68 ± 3 mV for TMEM16A cKO VSNs (green bar; n=5), no significant difference was found (t-test: p=0.93) in the RMP from both groups. Error bars: SEM.*

Membrane input resistance of each VSNs was evaluated in voltage-clamp mode with a negative pulse of 10 mV from a holding potential of -70 mV, as in these conditions we did not activate any voltage-gated current (Dibattista et al., 2008). The average membrane input resistances of VSNs from WT and TMEM16A cKO mice were 2.9 ± 1.1 GΩ and 3.6 ± 0.6 GΩ, respectively (Fig 1C). These values were not statistically different indicating that membrane resistance was not altered by the lack of TMEM16A protein. The resting membrane potential was measured in I=0 current-clamp mode. The average resting membrane potentials did not show any statistical difference between TMEM16A cKO and WT VSNs (Fig 1D) with values of -67 ± 4 mV for WT and -68 ± 3 mV for TMEM16A cKO VSNs. These results indicate that TMEM16A does not contribute to the resting membrane properties of mouse VSNs and does not alter voltage-gated inward and outward currents.

Spontaneous firing pattern is altered in VSNs from TMEM16A cKO.

To test whether the lack of TMEM16A produces an alteration in the spontaneous firing activity, we performed extracellular recordings in loose-patch configuration of individual neurons from acute VNO slices. Fig 2A shows representative recordings from WT and TMEM16A cKO VSNs (black and green traces respectively). The average spontaneous firing frequency for each neuron varied from 0.02 to 2.9 Hz in WT and from 0.02 to 1.9 Hz in TMEM16A cKO, with average values of 0.26 ± 0.15 Hz and 0.24 ± 0.08 Hz, respectively (Fig 2B).

To evaluate the pattern of firing activity, we measured the interspike interval (ISI) for 20 WT and 22 TMEM16A cKO VSNs taking at least 6 minutes of recording per cell. Figure 2C shows the ISI distribution of WT and TMEM16A cKO VSNs. To allow a clear comparison between the two groups, data were normalized to the area under the curve, ISIs were grouped in 5 ms bins and the distribution was plotted against the percentage of spikes by 5 ms bin. We found that the ISI distribution of spontaneous firing is statistically different ($p<0.01$) between WT and TMEM16A cKO VSNs. Indeed, as previously reported, WT VSNs tend to fire in bursts (Arnson and Holy, 2011) and show an ISI distribution with near the 80% of activity between 50 and 200 ms of ISI (Fig 2C-D black traces). In contrast, the ISI distribution of TMEM16A cKO is more wide-ranging with just 50% of activity in the 50-200 ms ISI range (Fig2 C-D green traces). These results indicate that the absence of the TMEM16A channel does not affect the average firing frequency but it alters the firing pattern by reducing the burst activity and increasing the random firing.

Response to urine from single VSNs from acute slices

To check if deleting the TMEM16A channel has any effect on the response to natural stimulation in VSNs, we first tested the possibility to record repetitive and stereotyped responses in single cells from acute slices. To stimulate VSNs we used diluted mouse urine which is a natural source of pheromones and it has been shown to activate VSNs (Celsi et al., 2012; Chamero et al., 2007; He et al., 2008; Holy et al., 2000; Inamura and Kashiwayanagi, 2000; Kim et al., 2011; Leinders-Zufall et al., 2004, 2014; Leypold et al., 2002; Spehr et al., 2009, 2002; Stowers et al., 2002; Yang and Delay, 2010; Zufall and Leinders-Zufall, 2000). We performed extracellular recordings in loose patch configuration from individual VSNs. Recording length was 90 s with 10 s urine stimulation. As VSNs usually show spontaneous activity coded in burst (Arnson and Holy, 2011), it was difficult to identify a urine response from a single recording and therefore, to avoid false positives, we applied at least 4 repetitive urine stimulations with inter-stimulus intervals of about 4 minutes to avoid possible adaptation.

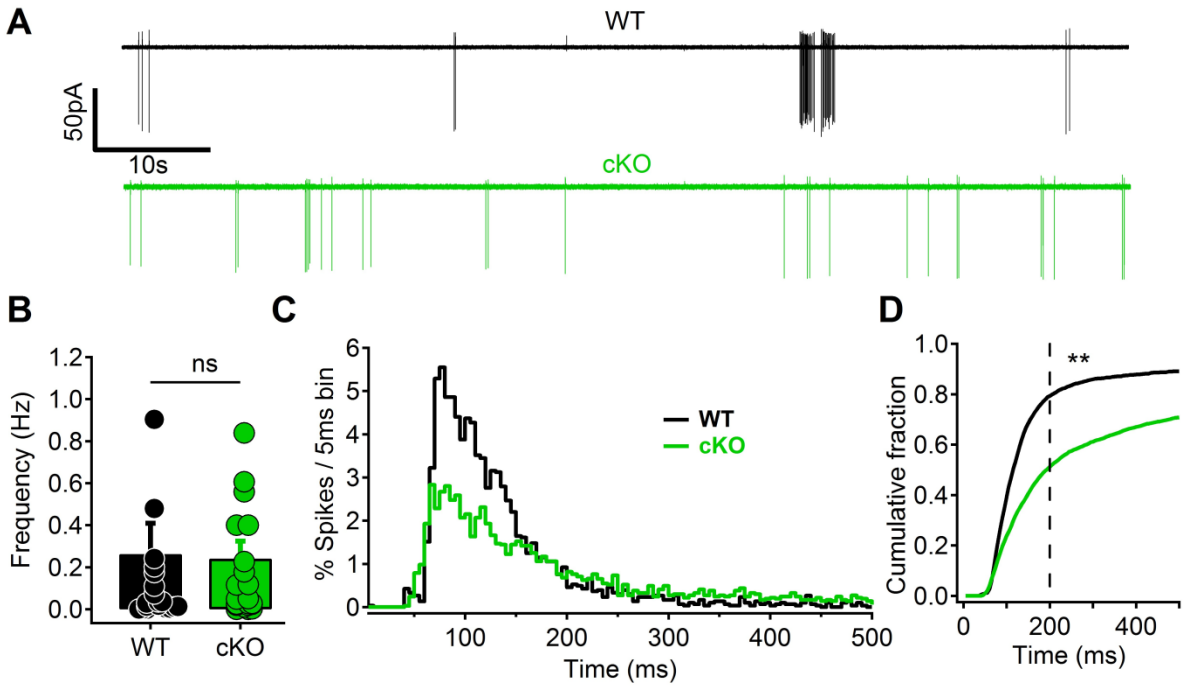

Figure 2. Spontaneous firing activity in WT and cKO TMEM16A VSNs. ***(A)*** *Representative loose-patch recordings of the spontaneous activity of VSNs from acute slices of VNO from WT and TMEM16A cKO mice.* ***(B)*** *Scatter dot plot and bar plot showing individual and average frequency of the spontaneous activity from WT (black; n=20) and TMEM16A cKO (green; n=22) VSNs. Each point represents the mean frequency of the spontaneous activity for one individual cell recorded for at least 6 minutes. Average frequency is not statistically different between both groups (U-test: p=0.43).* ***(C)*** *Interspike interval (ISI) distribution of the spontaneous activity of VSNs from WT (black trace) and TMEM16A cKO (green trace). Values were normalized to the area under the curve, y axis values represent the percentage of spikes by 5 ms bin.* ***(D)*** *Cumulative fraction of ISI distribution. Curves are statistically different (p-value < 0.0001) Dashed line indicates the point where the curve crosses ISI = 200 ms. Statistics: (B) Wilcoxon-Mann-Whitney unpaired test; (D) Kolmogorov-Smirnov test. Error bars: SEM.*

Figure 3 shows one VSN responding to dilute urine (1:50). The top traces are single recordings in the loose-patch configuration in response to urine (Fig 3A), artificial urine (Fig 3B), and ACSF with 25 mM KCl (Fig 3C). The decrease of spike amplitude during urine stimulation, an indication of the adaptation process, was shown in this and some other VSNs from WT mice. Middle panels represent the raster plots for different repetitions for the same cell and lower traces show the average of firing activity calculated in 1 s bins. We found consistent increase of firing activity during urine stimulation and positive control (25mM KCl) and no increase in firing activity during artificial urine stimulation.

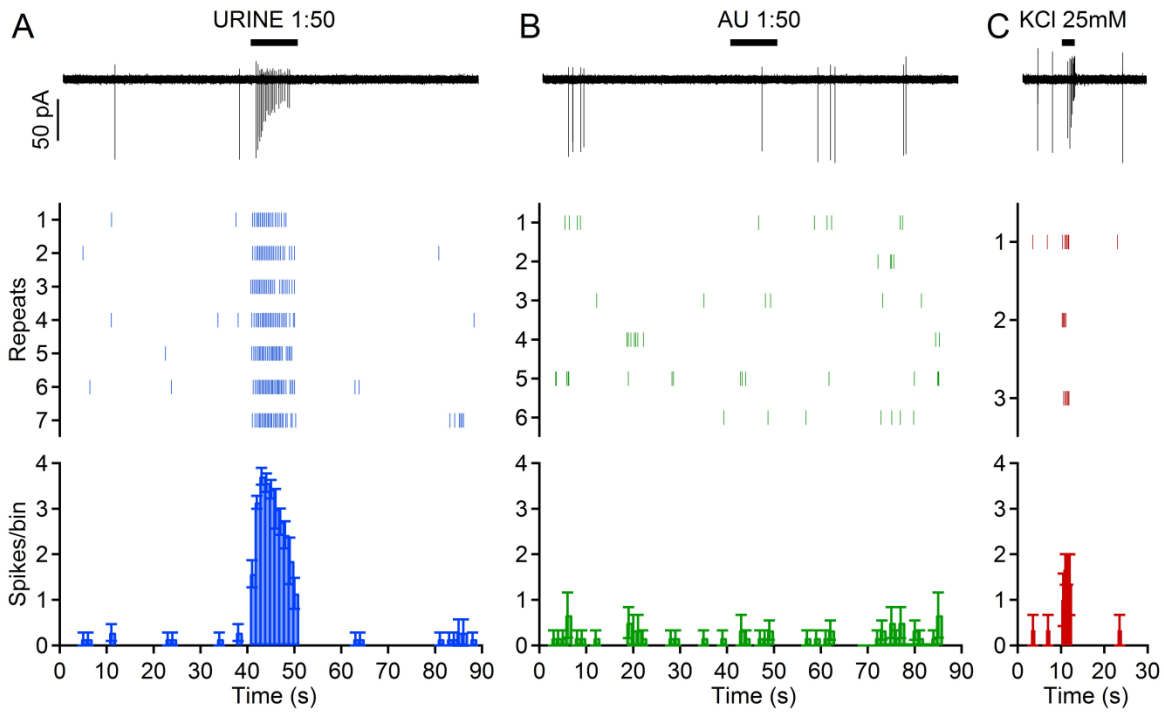

Figure 3. Evoked firing activity in a WT VSN. *Top trace; recordings in loose patch configuration from a WT VSN showing the firing activity in response to urine diluted 1:50 (A), artificial urine 1:50 (B) and high K^+ solution (C). Time of stimulus applications is indicated by the top bars. Middle; raster plot showing individual action potentials in several stimulus presentations in the same cell with inter-stimulus interval of at least 4 minutes. Bottom, average firing rate of the cell in bins of 1 s indicating the increase of firing in the presence of urine (A), or high K^+ solution as a positive control (C), but not in the presence of artificial urine as negative control (C). Traces for A, B and C were taken from the same cell. Error bars: SEM.*

Firing frequency is not altered while firing pattern is affected by deletion of TMEM16A in VSNs.

In loose-patch experiments, we measured responses to urine stimulation in 13 out of 20 WT VSNs, and in 8 out of 22 TMEM16A cKO VSNs. Figure 4 A-B shows representative loose-patch recordings from 4 different WT (A) and 4 TMEM16A cKO VSNs (B) responding to dilute urine stimulation (top bars). We compared the average firing frequency during urine response in both groups and we did not find any significant statistical difference (Fig 4C) indicating that VSNs from TMEM16A cKO have the same capability to increase spiking frequency in response to urine than VSNs from WT mice. Although VSNs from WT and TMEM16A cKO mice increased the firing frequency upon urine stimulation, individual neurons show differences in firing pattern (Fig. 4 A-B). To compare the firing patterns, we calculated the ISI in the stimulation period in each cell responding to urine and plotted the ISI distribution (Figure 4D-E). The evoked activity showed a significant reduction of ISI in TMEM16A cKO compared to WT neurons. Indeed, about 70% ISIs were shorter than 300 ms in TMEM16A cKO, while longer ISIs were measured in WT mice, with about 80% of activity comprised between 200 and 800 ms.

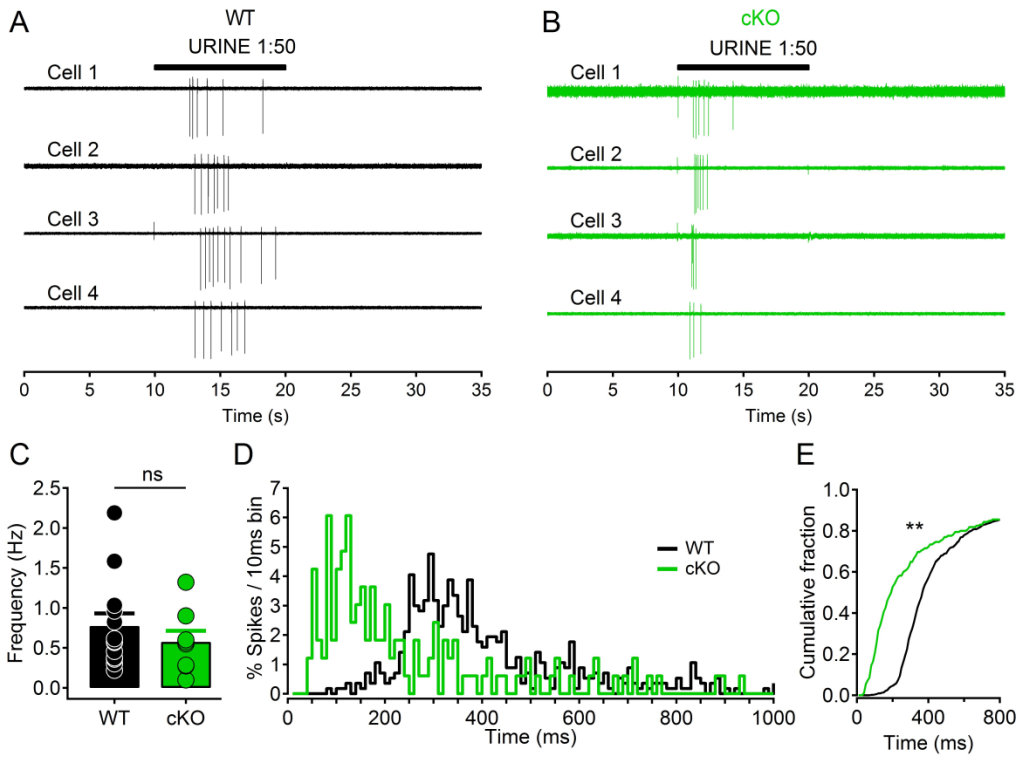

Figure 4. Evoked firing activity in WT and TMEM16A cKO VSNs. ***(A-B)*** *Representative loose-patch recordings of 4 different VSNs responding to urine 1:50 from WT (A) and TMEM16A cKO (B) mice. Time of stimulus applications is indicated by the top bars.* ***(C)*** *Scatter dot plot and bar plot of the mean frequency of evoked activity from WT VSNs (black; n=13) and TMEM16A cKO VSNs (green; n=8). Each dot represents the mean frequency of an individual cell calculated from a minimum of 4 stimulations. Bars represent the average frequency of all neurons for each group. Average frequency in evoked activity is not statistically different between WT and cKO (U-test: p=0.41, Wilcoxon-Mann-Whitney unpaired test).* ***(D)*** *ISI distribution of firing activity in response to urine. VSNs from TMEM16A cKO shows a left shifted firing pattern with respect to WT, with shorter ISIs, i.e. higher instantaneous frequency (Notice also traces shown in A and B).* ***(E)*** *Cumulative fraction of the ISI distribution shown in D. The two curves are statistically different (p-value<0.0001, Kolmogorov-Smirnov test). Error bars: SEM.*

We also analyzed the temporal development of responses. Figure 5A shows the average firing rate of individual cells (light traces) and the average of all cells responding to urine (dark traces) plotted versus time in WT (top) and TMEM16A cKO VSNs (bottom). The peak of response after the stimulus onset was reached in about 4 s in WT VSNs, while only about 1 s was sufficient to reach the peak of the response in TMEM16A cKO VSNs. Also the decay kinetics was different, as WT VSNs showed a more prolonged response compared to TMEM16A cKO VSNs (Fig 5B). To exclude that the delay in urine response and longer time course in WT was caused by a defect in the perfusion system, we evaluated the firing frequency in response to high KCl solution. Figure 5C shows that the peak frequency occurred almost at the same time in both groups, indicating that the change seen in Figure 5B is not due to problems in the perfusion system. However, the decay kinetics was still longer in WT than in KO VSNs, reflecting the ability of WT VSNs to generate spikes for a longer period also under stimulation with high KCl.

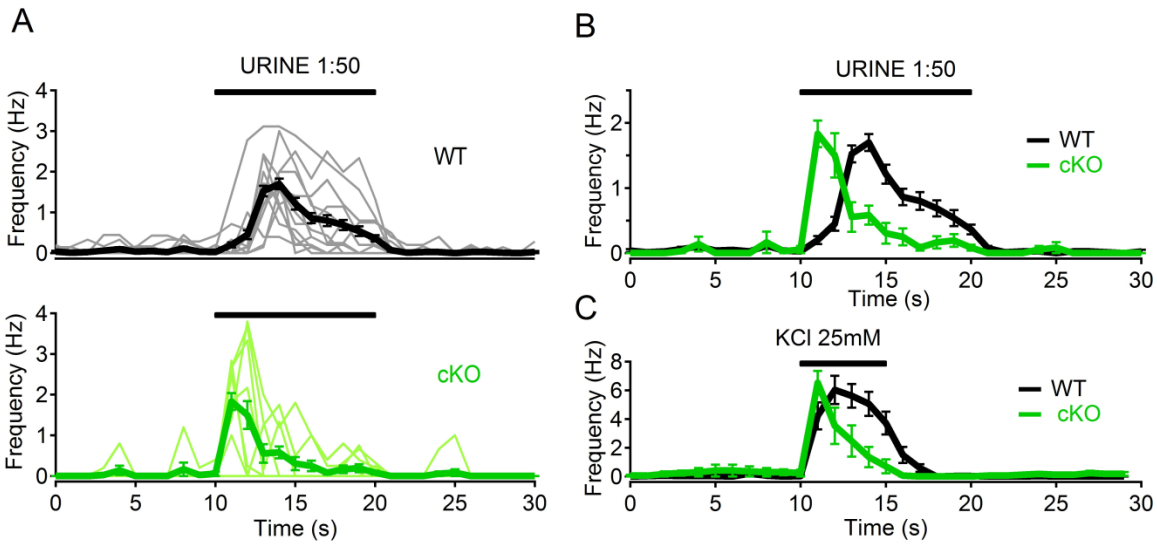

Figure 5. Time course of the urine response in VSNs. ***(A)*** *Average firing rate of WT (top) and TMEM16A cKO (bottom) VSNs in response to urine 1:50, light traces represent individual cells (WT, n=13; TMEM16A cKO, n=8) and dark traces represent the average of all cells.* ***(B)*** *Comparison of the time course of the average firing rate in WT and TMEM16A cKO in response to urine. Average firing rate in TMEM16A cKO VSNs rises and decays faster than the average firing rate in WT.* ***(C)*** *Kinetics of firing rate in response to high K^+ solution. Notice that the rising phase is similar in both groups, while the decay phase is slower in the WT group, indicating that an intrinsic mechanism is regulating the firing response duration. Time of stimulus applications is indicated by the top bars. Error bars: SEM.*

Discussion

We have previosuly shown that calcium-activated chloride currents are abolished in VSNs from the TMEM16A cKO mouse (Amjad et al., 2015), therefore, this mouse line is a good model to study the role of calcium-activated chloride currents in vomeronasal physiology.

TMEM16A regulates the spontaneous firing pattern in VSNs.

After establishing that the resting membrane potential, input membrane resistance and basic voltage-gated currents were similar in WT and TMEM16A cKO VSNs, we compared firing activity using loose-patch recordings, a technique that does not alter the cytosolic ionic conditions. We found that VSNs from acute slices have highly variable spontaneous activity in the range from 0.02 Hz to 2.9 Hz and similar mean frequencies of 0.26 ± 0.15 Hz in WT and 0.24 ± 0.08 Hz in TMEM16A cKO. These values are lower than the mean frequency of 0.7 Hz previously reported by Arnson and Holy (Arnson and Holy, 2011). The difference in mean frequency between our study and those reported by Holy's group could be due to different factors: preparation type (whole epithelium vs acute slices), recording configuration (multi electrode array vs loose-patch), temperature (37°C vs room temperature), ionic conditions, differences in the cell population recorded, or data analysis. However, our study shows that the lack of the TMEM16A channel does not change the mean frequency of spontaneous activity.

We also analyzed the pattern of spontaneous firing by plotting the ISI distribution and found that 80% of ISIs were between 50 and 200 ms with a peak at about 80 ms, values very similar to those previously reported in VSNs and defined as burst activity (Arnson and Holy, 2011), indicating that VSNs recorded in acute slices also showed a spontaneous activity coded in bursts. The ISI distribution from TMEM16A cKO

VSNs showed a reduced accumulation of activity in the range between 50 and 200 ms with respect to WT VSNs, indicating that TMEM16A plays a role in defining burst activity.

Arnson and Holy (Arnson and Holy, 2011) have shown that bursts in spontaneous activity are shaped by components of the signal transduction cascade. Indeed, as transduction in VSNs is PLC dependent (Dey et al., 2015; Holy et al., 2000; Krieger et al., 1999; Kroner et al., 1996; Sasaki et al., 1999; Spehr, 2016; Spehr et al., 2002; Thompson et al., 2004) they blocked the signaling pathway with the PLC inhibitor U-73122 and found that spontaneous activity was reduced and burst activity was altered. Our results indicate that TMEM16A calcium-activated chloride channels are active during spontaneous firing activity and that they contribute to regulating the burst structure in VSNs.

Olfactory sensory neurons (OSNs) also express a calcium-activated chloride channel from the TMEM16 family, TMEM16B. Recently, it was found that TMEM16B channel contributes to regulate spontaneous activity in OSNs (Dibattista et al., 2017; Pietra et al., 2016). Indeed, OSNs lacking the TMEM16B channel showed a reduction in the instantaneous frequency (inverse of ISI) of spontaneous activity but mean frequency was not altered. When the same parameters were evaluated in a population of OSNs expressing a defined olfactory receptor (I7 OR), that exhibits high spontaneous activity (Reisert, 2010), Pietra et al. (Pietra et al., 2016) found a lower instantaneous frequency and lower mean frequency in OSNs lacking TMEM16B channel. This suggests a common role of calcium-activated chloride currents in different olfactory subsystems.

TMEM16A regulates firing pattern during evoked activity in VSNs

Activation of signal transduction in VSNs produces a membrane depolarization and the generation of action potentials (Holy et al., 2000; Inamura and Kashiwayanagi, 2000; Kim et al., 2011; Leinders-Zufall et al., 2014; Spehr et al., 2009; Stowers et al., 2002; Yang and Delay, 2010; Zhang et al., 2010; Zufall and Leinders-Zufall, 2000). Here we showed that urine at 1:50 dilution can generate an increase in firing activity in some cells that was reproducible after sequential applications of the stimulus (Fig 3); those responses were due to signal transduction activation rather than to an indirect effect of the high concentration of ions in urine, as the same cells did not respond to artificial urine. We found urine responses in both WT and TMEM16A VSNs, indicating that VSNs lacking calcium-activated chloride currents were still able to activate signal transduction after stimulus presentation, producing an increase in firing activity. Two different roles have been proposed for calcium-activated chloride currents in vomeronasal signaling transduction; 1) Amplification of the transduction current in response to urine (Yang and Delay, 2010) or 2) activation of a TRPC2-independent signaling pathway, where calcium-activated chloride channels are necessary and sufficient to activate the VSNs (Kim et al., 2011). Here we found that, although the firing frequency during evoked activity was not altered in VSNs from TMEM16A cKO (Fig 4C), the firing pattern during the response was strongly affected (Fig 4D). ISI distribution of evoked activity showed that VSNs from WT tended to fire with longer ISIs, while VSNs from TMEM16A cKO fired with a shorter ISIs, i.e. higher instantaneous frequency.

Our results cannot support any of the two proposed roles for calcium-activated chloride currents in VSNs. First, with extracellular recordings is not possible to check if calcium-activated chloride currents amplify the signal transduction in VSNs, as proposed by Yang and Delay (2010). And second, our data contradict the hypothesis that calcium-activated chloride currents are sufficient and necessary to activate VSNs in a TRPC2-independent signaling pathway, as reported by Kim and coworkers, who showed that responses to urine were abolished by the addition of niflumic acid, a blocker of calcium-activated chloride channels (Kim et al., 2011). In TMEM16A cKO we measured evoked activity in 8 of 22

cells, showing that some VSNs were able to respond to urine (Fig 4B). As deletion of TMEM16A in VSNs did not produce a complete lack of responses to urine, but caused a modification in the characteristics of the firing pattern, we can conclude that calcium-activated chloride currents play a role in signal transduction modulation.

Arnson and Holy (2011) reported the identification of two types of VSNs based on the spontaneous firing patterns. One type of cells fired with tonic activity and a second one fired in bursts. The tonic cells did not respond to urine, whereas the cells firing in bursts responded to urine increasing the numbers of bursts, without changing the characteristics of individual burst (Arnson and Holy, 2011). Similarly to Arnson and Holy (2011) data, we also identified cells with activity coded by bursts and cells with tonic activity, but differently from them, we measured responses to urine in both types of cells. Interestingly, we also found that in cells firing in bursts, the characteristics of the single burst in spontaneous activity showed differences in the ISI distribution with respect to bursts from evoked activity (notice the shift of the ISI distribution between Fig 2C and Fig 4D; black traces-WT). Finally, we showed that cells firing in tonic mode (e.g. cell in Fig 3), responded to urine with an increase in the mean frequency. That indicates that chemosensory coding in VSNs is very complex, with cells presenting spontaneous firing in burst coding responses also in bursts, as reported by Arnson and Holy (2011), and cells with tonic spontaneous activity coding responses with the increase of mean firing frequency.

OSNs from TMEM16B KO mice showed a longer response to odor stimulation compared with WT, indicating that calcium-activated chloride channels help to depolarize the membrane potential and contribute to shorten the evoked activity (Dibattista et al., 2017; Pietra et al., 2016). Surprisingly, our results showed that eliminating calcium-activated chloride currents in VSNs produced shorter and faster evoked activity in response to urine. These contrasting effects could reflect the fact that both systems work in a different way and it is not easy to interpolate results from one to the other, with calcium activated-chloride currents playing opposite roles in OSNs and VSNs.

Another characteristic that was affected by the deletion of TMEM16A channels in VSNs was the time course of the response to urine. WT neurons showed a longer time course of the response than TMEM16A cKO neurons, indicating that calcium-activated chloride currents are responsible to prolong the time of spiking during the response to urine. Surprisingly TMEM16A cKO neurons showed a shorter delay in the starting of the response after stimulus onset compared to WT neurons (Fig 5B). A comparison of whole-cell recordings in TMEM16A cKO and WT VSNs may help to better define the role of calcium-activated chloride currents in the time course of the response to urine.

This study constitutes the first approach to clarify the physiological role of calcium-activated chloride currents in VSNs and gives some clues about the role that TMEM16A is playing in the modulation of the system. For a better understanding of the role of TMEM16A currents in VSNs, it will be important to reduce the internal variability of the system evaluating the role of TMEM16A cKO in a specific population of cells with more stereotyped behavior. A key factor to understand the physiological role of calcium-activated chloride currents is the knowledge of internal and external chloride concentrations. The internal chloride concentration has been estimated to be near 85 mM or 42 mM (Kim et al., 2015; Untiet et al., 2016), but it is still necessary to know the chloride concentration in the mucus outside the neurons to replicate the physiological conditions during experiments.

Bibliography

Amjad, A., Hernandez-Clavijo, A., Pifferi, S., Maurya, D.K., Boccaccio, A., Franzot, J., Rock, J., and Menini, A. (2015). Conditional knockout of TMEM16A/anoctamin1 abolishes the calcium-activated chloride current in mouse vomeronasal sensory neurons. J Gen Physiol *145*.

Arnson, H.A., and Holy, T.E. (2011). Chemosensory burst coding by mouse vomeronasal sensory neurons. J. Neurophysiol.

Billig, G.M., Pal, B., Fidzinski, P., and Jentsch, T.J. (2011). Ca2+-activated Cl- currents are dispensable for olfaction. Nat Neurosci *14*, 763–769.

Caputo, A., Caci, E., Ferrera, L., Pedemonte, N., Barsanti, C., Sondo, E., Pfeffer, U., Ravazzolo, R., Zegarra-Moran, O., and Galietta, L.J.V. (2008). TMEM16A, A Membrane Protein Associated with Calcium-Dependent Chloride Channel Activity. Science *322*, 590.

Celsi, F., D'Errico, A., and Menini, A. (2012). Responses to Sulfated Steroids of Female Mouse Vomeronasal Sensory Neurons. Chem. Senses *37*, 849–858.

Chamero, P., Marton, T.F., Logan, D.W., Flanagan, K., Cruz, J.R., Saghatelian, A., Cravatt, B.F., and Stowers, L. (2007). Identification of protein pheromones that promote aggressive behaviour. Nature *450*, 899–902.

Dauner, K., Lißmann, J., Jeridi, S., Frings, S., and Möhrlen, F. (2012). Expression patterns of anoctamin 1 and anoctamin 2 chloride channels in the mammalian nose. Cell Tissue Res. *347*, 327–341.

Dey, S., Chamero, P., Pru, J.K., Chien, M.-S., Ibarra-Soria, X., Spencer, K.R., Logan, D.W., Matsunami, H., Peluso, J.J., and Stowers, L. (2015). Cyclic Regulation of Sensory Perception by a Female Hormone Alters Behavior. Cell *161*, 1334–1344.

Dibattista, M., Mazzatenta, A., Grassi, F., Tirindelli, R., and Menini, A. (2008). Hyperpolarization-Activated Cyclic Nucleotide-Gated Channels in Mouse Vomeronasal Sensory Neurons. J. Neurophysiol. *100*, 576.

Dibattista, M., Amjad, A., Maurya, D.K., Sagheddu, C., Montani, G., Tirindelli, R., and Menini, A. (2012). Calcium-activated chloride channels in the apical region of mouse vomeronasal sensory neurons. J Gen Physiol *140*.

Dibattista, M., Pifferi, S., Boccaccio, A., Menini, A., and Reisert, J. (2017). The long tale of the calcium activated Cl− channels in olfactory transduction. Channels 1–16.

He, J., Ma, L., Kim, S., Nakai, J., and Yu, C.R. (2008). Encoding gender and individual information in the mouse vomeronasal organ. Science *320*.

Holy, T.E., Dulac, C., and Meister, M. (2000). Responses of vomeronasal neurons to natural stimuli. Science *289*.

Inamura, K., and Kashiwayanagi, M. (2000). Inward current responses to urinary substances in rat vomeronasal sensory neurons. Eur. J. Neurosci. *12*, 3529–3536.

Inamura, K., Kashiwayanagi, M., and Kurihara, K. (1997). Inositol-1,4,5-trisphosphate Induces Responses in Receptor Neurons in Rat Vomeronasal Sensory Slices. Chem. Senses *22*, 93–103.

Kim, S., Ma, L., and Yu, C.R. (2011). Requirement of calcium-activated chloride channels in the activation of mouse vomeronasal neurons. Nat Commun *2*.

Kim, S., Ma, L., Unruh, J., McKinney, S., and Yu, C.R. (2015). Intracellular chloride concentration of the mouse vomeronasal neuron. BMC Neurosci. *16*, 90.

Krieger, J., Schmitt, A., Löbel, D., Gudermann, T., Schultz, G., Breer, H., and Boekhoff, I. (1999). Selective Activation of G Protein Subtypes in the Vomeronasal Organ upon Stimulation with Urine-derived Compounds. J. Biol. Chem. *274*, 4655–4662.

Kroner, C., Breer, H., Singer, A.G., and O'Connell, R.J. (1996). Pheromone-induced second messenger signaling in the hamster vomeronasal organ. NeuroReport *7*.

Leinders-Zufall, T., Brennan, P., Widmayer, P., S., P.C., Maul-Pavicic, A., Jäger, M., Li, X.-H., Breer, H., Zufall, F., and Boehm, T. (2004). MHC Class I Peptides as Chemosensory Signals in the Vomeronasal Organ. Science *306*, 1033.

Leinders-Zufall, T., Ishii, T., Chamero, P., Hendrix, P., Oboti, L., Schmid, A., Kircher, S., Pyrski, M., Akiyoshi, S., Khan, M., et al. (2014). A Family of Nonclassical Class I MHC Genes Contributes to Ultrasensitive Chemodetection by Mouse Vomeronasal Sensory Neurons. J. Neurosci. *34*, 5121.

Leypold, B.G., Yu, C.R., Leinders-Zufall, T., Kim, M.M., Zufall, F., and Axel, R. (2002). Altered sexual and social behaviors in trp2 mutant mice. Proc. Natl. Acad. Sci. *99*, 6376–6381.

Liman, E.R., and Corey, D.P. (1996). Electrophysiological Characterization of Chemosensory Neurons from the Mouse Vomeronasal Organ. J. Neurosci. *16*, 4625.

Liman, E.R., Corey, D.P., and Dulac, C. (1999). TRP2: A candidate transduction channel for mammalian pheromone sensory signaling. Proc. Natl. Acad. Sci. *96*, 5791–5796.

Munger, S.D., Lane, A.P., Zhong, H., Leinders-Zufall, T., Yau, K.-W., Zufall, F., and Reed, R.R. (2001). Central Role of the CNGA4 Channel Subunit in Ca^{2+}-Calmodulin-Dependent Odor Adaptation. Science *294*, 2172.

Pietra, G., Dibattista, M., Menini, A., Reisert, J., and Boccaccio, A. (2016). The Ca^{2+}-activated Cl^- channel TMEM16B regulates action potential firing and axonal targeting in olfactory sensory neurons. J. Gen. Physiol. *148*, 293.

Pifferi, S., Dibattista, M., and Menini, A. (2009). TMEM16B induces chloride currents activated by calcium in mammalian cells. Pflüg. Arch. - Eur. J. Physiol. *458*, 1023–1038.

Rasche, S., Toetter, B., Adler, J., Tschapek, A., Doerner, J.F., Kurtenbach, S., Hatt, H., Meyer, H., Warscheid, B., and Neuhaus, E.M. (2010). Tmem16b is Specifically Expressed in the Cilia of Olfactory Sensory Neurons. Chem. Senses *35*, 239–245.

Reisert, J. (2010). Origin of basal activity in mammalian olfactory receptor neurons. J. Gen. Physiol. *136*, 529–540.

Riviere, S., Challet, L., Fluegge, D., Spehr, M., and Rodriguez, I. (2009). Formyl peptide receptor-like proteins are a novel family of vomeronasal chemosensors. Nature *459*, 574–577.

Sasaki, K., Okamoto, K., Inamura, K., Tokumitsu, Y., and Kashiwayanagi, M. (1999). Inositol-1,4,5-trisphosphate accumulation induced by urinary pheromones in female rat vomeronasal epithelium. Brain Res. *823*, 161–168.

Schroeder, B.C., Cheng, T., Jan, Y.N., and Jan, L.Y. (2008). Expression Cloning of TMEM16A as a Calcium-Activated Chloride Channel Subunit. Cell *134*, 1019–1029.

Shimazaki, R., Boccaccio, A., Mazzatenta, A., Pinato, G., Migliore, M., and Menini, A. (2006). Electrophysiological Properties and Modeling of Murine Vomeronasal Sensory Neurons in Acute Slice Preparations. Chem. Senses *31*, 425–435.

Spehr, M. (2016). Chapter 11 - Vomeronasal Transduction and Cell Signaling A2 - Zufall, Frank. In Chemosensory Transduction, S.D. Munger, ed. (Academic Press), pp. 191–206.

Spehr, J., Hagendorf, S., Weiss, J., Spehr, M., Leinders-Zufall, T., and Zufall, F. (2009). Ca^{2+}–Calmodulin Feedback Mediates Sensory Adaptation and Inhibits Pheromone-Sensitive Ion Channels in the Vomeronasal Organ. J. Neurosci. *29*, 2125.

Spehr, M., Hatt, H., and Wetzel, C.H. (2002). Arachidonic Acid Plays a Role in Rat Vomeronasal Signal Transduction. J. Neurosci. *22*, 8429.

Stephan, A.B., Shum, E.Y., Hirsh, S., Cygnar, K.D., Reisert, J., and Zhao, H. (2009). ANO2 is the cilial calcium-activated chloride channel that may mediate olfactory amplification. Proc Natl Acad Sci USA *106*.

Stöhr, H., Heisig, J.B., Benz, P.M., Schöberl, S., Milenkovic, V.M., Strauss, O., Aartsen, W.M., Wijnholds, J., Weber, B.H.F., and Schulz, H.L. (2009). TMEM16B, A Novel Protein with Calcium-Dependent Chloride Channel Activity, Associates with a Presynaptic Protein Complex in Photoreceptor Terminals. J. Neurosci. *29*, 6809.

Stowers, L., Holy, T.E., Meister, M., Dulac, C., and Koentges, G. (2002). Loss of Sex Discrimination and Male-Male Aggression in Mice Deficient for TRP2. Science *295*, 1493.

Thompson, R.N., Robertson, B.K., Napier, A., and Wekesa, K.S. (2004). Sex-specific Responses to Urinary Chemicals by the Mouse Vomeronasal Organ. Chem. Senses *29*, 749–754.

Tirindelli, R., Dibattista, M., Pifferi, S., and Menini, A. (2009). From Pheromones to Behavior. Physiol. Rev. *89*, 921.

Trotier, D., and Døving, K.B. (1998). 'Anatomical Description of a New Organ in the Nose of Domesticated Animals' by Ludvig Jacobson (1813). Chem. Senses *23*, 743–754.

Ukhanov, K., Leinders-Zufall, T., and Zufall, F. (2007). Patch-Clamp Analysis of Gene-Targeted Vomeronasal Neurons Expressing a Defined V1r or V2r Receptor: Ionic Mechanisms Underlying Persistent Firing. J. Neurophysiol. *98*, 2357.

Untiet, V., Moeller, L.M., Ibarra-Soria, X., Sánchez-Andrade, G., Stricker, M., Neuhaus, E.M., Logan, D.W., Gensch, T., and Spehr, M. (2016). Elevated Cytosolic Cl − Concentrations in Dendritic Knobs of Mouse Vomeronasal Sensory Neurons. Chem. Senses *41*, 669–676.

Yang, C., and Delay, R.J. (2010). Calcium-activated chloride current amplifies the response to urine in mouse vomeronasal sensory neurons. J Gen Physiol *135*.

Yang, Y.D., Cho, H., Koo, J.Y., Tak, M.H., Cho, Y., Shim, W.-S., Park, S.P., Lee, J., Lee, B., Kim, B.-M., et al. (2008). TMEM16A confers receptor-activated calcium-dependent chloride conductance. Nature *455*, 1210–1215.

Zhang, P., Yang, C., and Delay, R.J. (2010). Odors activate dual pathways, a TRPC2 and a AA-dependent pathway, in mouse vomeronasal neurons. Am. J. Physiol. - Cell Physiol. *298*, C1253.

Zufall, F., and Leinders-Zufall, T. (2000). The Cellular and Molecular Basis of Odor Adaptation. Chem. Senses *25*, 473–481.

1. DISCUSSION

Calcium-activated chloride currents in VSNs have been described by several groups (Dibattista et al., 2012; Kim et al., 2011; Yang and Delay, 2010) and at least two possible physiological roles were proposed: amplification of signal transduction (Yang and Delay, 2010) or main current for a TRPC2-independent signaling pathway (Kim et al., 2011). To clearly decipher the physiological role of calcium-activated chloride currents in VSNs, it would be necessary to know the molecular identity of the channel and its functional characterization. In this thesis, we made the functional characterization of calcium-activated chloride currents in VSNs. We created a conditional knockout mice line for TMEM16A channel and evaluated the role of TMEM16A on calcium-activated chloride currents in VSNs. Furthermore, through extracellular loose-patch recordings, we studied the role of calcium-activated chloride currents in spontaneous and evoked activity in VSNs.

1.1 Calcium-activated chloride currents in isolated VSNs

In whole-cell recording from the soma and inside-out recordings from the knob/microvilli of isolated VSNs, we measured calcium-activated currents using different intracellular free calcium concentrations, ranging from 0.5 µM to 2 mM. Although calcium-activated non-selective cation currents have been reported in VSNs (Liman, 2003; Spehr et al., 2009), ionic substitution experiments revealed only anionic calcium-activated current in VSNs, even at intracellular free calcium concentration reaching 2 mM.

1.2 Conditional knockout of TMEM16A abolishes the calcium-activated chloride current in mouse VSNs

TMEM16A and TMEM16B calcium-activated chloride channels have been reported to be expressed in the knob/microvilli of isolated VSNs (Dibattista et al., 2012). The electrophysiological properties of calcium-activated chloride currents recorded from isolated VSNs in whole-cell and inside-out configuration were more similar to those of heterologous TMEM16A than TMEM16B currents. We investigated the contribution of TMEM16A channels to calcium-activated chloride currents in VSNs. As constitutive knockout mouse for TMEM16A protein do not live more than one week, we crossed floxed TMEM16A$^{fl/fl}$ mice (Faria et al., 2014; Schreiber et al., 2015) with OMP-Cre mice (Li et al., 2004) to obtain a conditional knockout (cKO) mice for TMEM16A protein in VSNs. Surprisingly, when we performed whole-cell recording in VSNs from TMEM16A cKO, we found that calcium-activated currents were abolished, although, immunohistochemistry experiments showed the presence of TMEM16B at the apical surface of the vomeronasal epithelium in TMEM16A cKO mice. These results reveal that TMEM16A is an essential component of calcium-activated chloride currents in mouse VSN.

Billig et al., (Billig et al., 2011) reported that calcium-activated chloride currents were absent in VSNs from TMEM16B KO mice recorded at 1.5 µM calcium, suggesting a prominent role of TMEM16B in calcium-activated chloride currents in VSNs. If deleting TMEM16A or TMEM16B protein from VSNs abolished the calcium-activated chloride currents, we could suggest that only heteromeric channels composed by TMEM16A and TMEM16B are functional in VSNs. However, the report of a reminiscent current in some neurons and the small number of neurons evaluated in the work from Billig et al., (Billig et al., 2011), necessitates a more detailed study of the effect of deleting the TMEM16B protein in VSNs. At present, we do not know which TMEM16A and TMEM16B splice variants are expressed in VSNs, but it could be possible that VSNs express the TMEM16B isoforms lacking the exon 4 sequence, which do not form functional channels by themselves in the MOE (Ponissery Saidu et al., 2014).

1.3 TMEM16A regulates the spontaneous and evoked firing pattern in VSNs

As TMEM16A cKO mice lack calcium-activated chloride currents, they are a good model to study the role of calcium-activated chloride currents in vomeronasal physiology. We performed whole-cell recordings and found that lack of TMEM16A does not alter the resting membrane properties and voltage-gated currents in VSNs. To check if TMEM16A is involved in firing activity, we recorded spontaneous or evoked activity in loose-patch configuration. We found that VSNs from acute slices have spontaneous activity with similar mean frequencies in WT and TMEM16A cKO. When we analyzed the pattern of spontaneous firing, we found that in both WT and TMEM16A cKO VSNs, spontaneous activity was coded mainly by bursts, in accordance with previous reports from VSNs (Arnson and Holy, 2011; Holy et al., 2000). However, our experiments showed that TMEM16A cKO VSNs have a reduced burst activity with respect to WT VSNs. These results indicate that TMEM16A calcium-activated chloride channels are active during spontaneous firing activity and that they contribute to regulate the burst structure in VSNs.

To study the possible role of calcium-activated chloride currents during signal transduction, we stimulated VSNs from acute slices with diluted urine and we found urine responses in both WT and TMEM16A VSNs, showing that VSNs lacking calcium-activated chloride currents were still able to activate signal transduction after stimulus presentation, producing an increase in firing activity. Here we found that, although the mean firing frequency during evoked activity was not altered in VSNs from TMEM16A cKO, the firing pattern during the response was strongly affected, showing VSNs from TMEM16A cKO fired with a higher instantaneous frequency than VSNs from WT. As deletion of TMEM16A in VSNs did not produce a complete lack of responses to urine, but caused a modification in the characteristics of the firing pattern, we can conclude that calcium-activated chloride currents play a role in signal transduction modulation.

In this thesis we have provided the first functional characterization of calcium-activated chloride currents in isolated VSNs and we have shown that TMEM16A channels are a necessary component of calcium-activated chloride currents in VSNs. Furthermore, we have made the first approach to clarify the physiological role of calcium-activated chloride currents in VSNs, giving some clues about the role that TMEM16A is playing in the modulation of the system. For a better understanding of the role of calcium-activated chloride currents in VSNs, it will be important to know some characteristics of the system

that we currently ignore: the external chloride concentration in the mucus of the VNO and the dynamic of chloride currents during signal transduction in VSNs. It is also necessary to reduce the internal variability of the system evaluating the effect of TMEM16A cKO in a specific population of cells with more stereotyped behavior and evaluate the role of calcium-activated chloride currents with different stimulus concentrations.

2. REFERENCES

Arnson, H.A., and Holy, T.E. (2011). Chemosensory burst coding by mouse vomeronasal sensory neurons. J. Neurophysiol.

Baxi, K.N., Dorries, K.M., and Eisthen, H.L. (2006). Is the vomeronasal system really specialized for detecting pheromones? Trends Neurosci. *29*, 1–7.

Belluscio, L., Koentges, G., Axel, R., and Dulac, C. (1999). A Map of Pheromone Receptor Activation in the Mammalian Brain. Cell *97*, 209–220.

Benarroch, E.E. (2017). Anoctamins (TMEM16 proteins): Functions and involvement in neurologic disease. Neurology.

Berghard, A., and Buck, L. (1996). Sensory transduction in vomeronasal neurons: evidence for G alpha o, G alpha i2, and adenylyl cyclase II as major components of a pheromone signaling cascade. J. Neurosci. *16*, 909.

Beynon, R.J., and Hurst, J.L. (2004). Urinary proteins and the modulation of chemical scents in mice and rats. M Altstein *25*, 1553–1563.

Billig, G.M., Pal, B., Fidzinski, P., and Jentsch, T.J. (2011). Ca2+-activated Cl- currents are dispensable for olfaction. Nat Neurosci *14*, 763–769.

Brechbühl, J., Klaey, M., and Broillet, M.-C. (2008). Grueneberg Ganglion Cells Mediate Alarm Pheromone Detection in Mice. Science *321*, 1092.

Brechbühl, J., Moine, F., Klaey, M., Nenniger-Tosato, M., Hurni, N., Sporkert, F., Giroud, C., and Broillet, M.-C. (2013). Mouse alarm pheromone shares structural similarity with predator scents. Proc. Natl. Acad. Sci. *110*, 4762–4767.

Brechbühl, J., Klaey, M., Moine, F., Bovay, E., Hurni, N., Nenniger-Tosato, M., and Broillet, M.-C. (2014). Morphological and physiological species-dependent characteristics of the rodent Grueneberg ganglion. Front. Neuroanat. *8*, 87.

Brignall, A.C., and Cloutier, J.-F. (2015). Neural map formation and sensory coding in the vomeronasal system. Cell. Mol. Life Sci. *72*, 4697–4709.

Bruce, H.M. (1959). An Exteroceptive Block to Pregnancy in the Mouse. Nature *184*, 105–105.

Brunner, J.D., Lim, N.K., Schenck, S., Duerst, A., and Dutzler, R. (2014). X-ray structure of a calcium-activated TMEM16 lipid scramblase. Nature *516*, 207–212.

Buck, L., and Axel, R. (1991). A novel multigene family may encode odorant receptors: A molecular basis for odor recognition. Cell *65*, 175–187.

Bumbalo, R., Lieber, M., Schroeder, L., Polat, Y., Breer, H., and Fleischer, J. (2017). Grueneberg Glomeruli in the Olfactory Bulb are Activated by Odorants and Cool Temperature. Cell. Mol. Neurobiol. *37*, 729–742.

Caputo, A., Caci, E., Ferrera, L., Pedemonte, N., Barsanti, C., Sondo, E., Pfeffer, U., Ravazzolo, R., Zegarra-Moran, O., and Galietta, L.J.V. (2008). TMEM16A, A Membrane Protein Associated with Calcium-Dependent Chloride Channel Activity. Science *322*, 590.

Cavaggioni, A., and Mucignat-Caretta, C. (2000). Major urinary proteins, α2U-globulins and aphrodisin. Biochim. Biophys. Acta BBA - Protein Struct. Mol. Enzymol. *1482*, 218–228.

Celsi, F., D'Errico, A., and Menini, A. (2012). Responses to Sulfated Steroids of Female Mouse Vomeronasal Sensory Neurons. Chem. Senses *37*, 849–858.

Chamero, P., Marton, T.F., Logan, D.W., Flanagan, K., Cruz, J.R., Saghatelian, A., Cravatt, B.F., and Stowers, L. (2007). Identification of protein pheromones that promote aggressive behaviour. Nature *450*, 899–902.

Chamero, P., Weiss, J., Alonso, M.T., Rodríguez-Prados, M., Hisatsune, C., Mikoshiba, K., Leinders-Zufall, T., and Zufall, F. (2017). Type 3 inositol 1,4,5-trisphosphate receptor is dispensable for sensory activation of the mammalian vomeronasal organ. Sci. Rep. *7*, 10260.

Cichy, A., Ackels, T., Tsitoura, C., Kahan, A., Gronloh, N., Söchtig, M., Engelhardt, C.H., Ben-Shaul, Y., Müller, F., Spehr, J., et al. (2015). Extracellular pH Regulates Excitability of Vomeronasal Sensory Neurons. J. Neurosci. *35*, 4025.

Cloutier, J.-F., Giger, R.J., Koentges, G., Dulac, C., Kolodkin, A.L., and Ginty, D.D. (2002). Neuropilin-2 Mediates Axonal Fasciculation, Zonal Segregation, but Not Axonal Convergence, of Primary Accessory Olfactory Neurons. Neuron *33*, 877–892.

Dauner, K., Lißmann, J., Jeridi, S., Frings, S., and Möhrlen, F. (2012). Expression patterns of anoctamin 1 and anoctamin 2 chloride channels in the mammalian nose. Cell Tissue Res. *347*, 327–341.

Dean, D.M., Mazzatenta, A., and Menini, A. (2004). Voltage-activated current properties of male and female mouse vomeronasal sensory neurons: sexually dichotomous? J. Comp. Physiol. A *190*, 491–499.

Del Punta, K., Leinders-Zufall, T., Rodriguez, I., Jukam, D., Wysocki, C.J., Ogawa, S., Zufall, F., and Mombaerts, P. (2002a). Deficient pheromone responses in mice lacking a cluster of vomeronasal receptor genes. Nature *419*, 70–74.

Del Punta, K., Puche, A., Adams, N.C., Rodriguez, I., and Mombaerts, P. (2002b). A Divergent Pattern of Sensory Axonal Projections Is Rendered Convergent by Second-Order Neurons in the Accessory Olfactory Bulb. Neuron *35*, 1057–1066.

Dey, S., Chamero, P., Pru, J.K., Chien, M.-S., Ibarra-Soria, X., Spencer, K.R., Logan, D.W., Matsunami, H., Peluso, J.J., and Stowers, L. (2015). Cyclic Regulation of Sensory Perception by a Female Hormone Alters Behavior. Cell *161*, 1334–1344.

Dibattista, M., Mazzatenta, A., Grassi, F., Tirindelli, R., and Menini, A. (2008). Hyperpolarization-Activated Cyclic Nucleotide-Gated Channels in Mouse Vomeronasal Sensory Neurons. J. Neurophysiol. *100*, 576.

Dibattista, M., Amjad, A., Maurya, D.K., Sagheddu, C., Montani, G., Tirindelli, R., and Menini, A. (2012). Calcium-activated chloride channels in the apical region of mouse vomeronasal sensory neurons. J Gen Physiol *140*.

Dibattista, M., Pifferi, S., Boccaccio, A., Menini, A., and Reisert, J. (2017). The long tale of the calcium activated Cl− channels in olfactory transduction. Channels 1–16.

Dulac, C., and Axel, R. (1995). A novel family of genes encoding putative pheromone receptors in mammals. Cell *83*, 195–206.

Dulac, C., and Axel, R. (1998). Expression of Candidate Pheromone Receptor Genes in Vomeronasal Neurons. Chem. Senses *23*, 467–475.

Duran, C., Thompson, C.H., Xiao, Q., and Hartzell, H.C. (2010). Chloride Channels: Often Enigmatic, Rarely Predictable. Annu. Rev. Physiol. *72*, 95–121.

Faria, D., Rock, J.R., Romao, A.M., Schweda, F., Bandulik, S., Witzgall, R., Schlatter, E., Heitzmann, D., Pavenstädt, H., Herrmann, E., et al. (2014). The calcium-activated chloride channel Anoctamin 1 contributes to the regulation of renal function. Kidney Int. *85*, 1369–1381.

Ferrero, D.M., Moeller, L.M., Osakada, T., Horio, N., Li, Q., and Roy, D.S. (2013). A juvenile mouse pheromone inhibits sexual behaviour through the vomeronasal system. Nature. *502*.

Firestein, S. (2001). How the olfactory system makes sense of scents. Nature *413*, 211–218.

Fleischer, J., Schwarzenbacher, K., Besser, S., Hass, N., and Breer, H. (2006). Olfactory receptors and signalling elements in the Grueneberg ganglion. J. Neurochem. *98*, 543–554.

Francia, S., Silvotti, L., Ghirardi, F., Catzeflis, F., Percudani, R., and Tirindelli, R. (2015). Evolution of Spatially Coexpressed Families of Type-2 Vomeronasal Receptors in Rodents. Genome Biol. Evol. *7*, 272–285.

Fuss, S.H., Omura, M., and Mombaerts, P. (2005). The Grueneberg ganglion of the mouse projects axons to glomeruli in the olfactory bulb. Eur. J. Neurosci. *22*, 2649–2654.

Ghiaroni, V., Fieni, F., Tirindelli, R., Pietra, P., and Bigiani, A. (2003). Ion conductances in supporting cells isolated from the mouse vomeronasal organ. J Neurophysiol *89*.

Giannetti, N., Saucier, D., and Astic, L. (1992). Organization of the septal organ projection to the main olfactory bulb in adult and newborn rats. J. Comp. Neurol. *323*, 288–298.

Grüneberg, H. (1973). A ganglion probably belonging to the N. terminalis system in the nasal mucosa of the mouse. Z. Für Anat. Entwicklungsgeschichte *140*, 39–52.

Haga, S., Hattori, T., Sato, T., Sato, K., Matsuda, S., Kobayakawa, R., Sakano, H., Yoshihara, Y., Kikusui, T., and Touhara, K. (2010). The male mouse pheromone ESP1 enhances female sexual receptive behaviour through a specific vomeronasal receptor. Nature *466*, 118–122.

Halpern, M. (1987). The Organization and Function of the Vomeronasal System. Annu. Rev. Neurosci. *10*, 325.

Hartzell, C., Putzier, I., and Arreola, J. (2004). Calcium-activated chloride channels. Annu. Rev. Physiol. *67*, 719–758.

Hattori, T., Osakada, T., Masaoka, T., Ooyama, R., Horio, N., Mogi, K., Nagasawa, M., Haga-Yamanaka, S., Touhara, K., and Kikusui, T. (2017). Exocrine Gland-Secreting Peptide 1 Is a Key Chemosensory Signal Responsible for the Bruce Effect in Mice. Curr. Biol. *27*, 3197–3201.e3.

Hengl, T., Kaneko, H., Dauner, K., Vocke, K., Frings, S., and Möhrlen, F. (2010). Molecular components of signal amplification in olfactory sensory cilia. Proc. Natl. Acad. Sci. *107*, 6052–6057.

Herrada, G., and Dulac, C. (1997). A Novel Family of Putative Pheromone Receptors in Mammals with a Topographically Organized and Sexually Dimorphic Distribution. Cell *90*, 763–773.

Holy, T.E., Dulac, C., and Meister, M. (2000). Responses of vomeronasal neurons to natural stimuli. Science *289*.

Huang, F., Wong, X., and Jan, L.Y. (2012). International Union of Basic and Clinical Pharmacology. LXXXV: Calcium-Activated Chloride Channels. Pharmacol. Rev. *64*, 1–15.

Inamura, K., Kashiwayanagi, M., and Kurihara, K. (1997). Inositol-1,4,5-trisphosphate Induces Responses in Receptor Neurons in Rat Vomeronasal Sensory Slices. Chem. Senses *22*, 93–103.

Ishii, T., and Mombaerts, P. (2008). Expression of Nonclassical Class I Major Histocompatibility Genes Defines a Tripartite Organization of the Mouse Vomeronasal System. J. Neurosci. *28*, 2332.

Ishii, T., and Mombaerts, P. (2011). Coordinated coexpression of two vomeronasal receptor V2R genes per neuron in the mouse. Mol. Cell. Neurosci. *46*, 397–408.

Isogai, Y., Si, S., Pont-Lezica, L., Tan, T., Kapoor, V., Murthy, V.N., and Dulac, C. (2011). Molecular organization of vomeronasal chemoreception. Nature *478*, 241–245.

Jemiolo, B., Andreolini, F., Xie, T.-M., Wiesler, D., and Novotny, M. (1989). Puberty-affecting synthetic analogs of urinary chemosignals in the house mouse, Mus domesticus. Physiol. Behav. *46*, 293–298.

Johnston, R.E. (1992). Vomeronasal and/or olfactory mediation of ultrasonic calling and scent marking by female golden hamsters. Physiol. Behav. *51*, 437–448.

Kaneko, H., Putzier, I., Frings, S., Kaupp, U.B., and Gensch, T. (2004). Chloride accumulation in mammalian olfactory sensory neurons. J Neurosci *24*.

Kang, N., Janes, A., Baum, M.J., and Cherry, J.A. (2006). Sex difference in Fos induced by male urine in medial amygdala-projecting accessory olfactory bulb mitral cells of mice. Neurosci. Lett. *398*, 59–62.

Karlson, P., and Luscher, M. (1959). Pheromones': a new term for a class of biologically active substances. Nature *183*, 55–56.

Kaur, A.W., Ackels, T., Kuo, T.-H., Cichy, A., Dey, S., Hays, C., Kateri, M., Logan, D.W., Marton, T.F., Spehr, M., et al. (2014). Murine Pheromone Proteins Constitute a Context-Dependent Combinatorial Code Governing Multiple Social Behaviors. Cell *157*, 676–688.

Kelliher, K.R., Spehr, M., Li, X.-H., Zufall, F., and Leinders-Zufall, T. (2006). Pheromonal recognition memory induced by TRPC2-independent vomeronasal sensing. Eur. J. Neurosci. *23*, 3385–3390.

Kim, S., Ma, L., and Yu, C.R. (2011). Requirement of calcium-activated chloride channels in the activation of mouse vomeronasal neurons. Nat Commun *2*.

Kim, S., Ma, L., Jensen, K.L., Kim, M.M., Bond, C.T., Adelman, J.P., and Yu, C.R. (2012). Paradoxical contribution of SK3 and GIRK channels to the activation of mouse vomeronasal organ. Nat Neurosci *15*, 1236–1244.

Kim, S., Ma, L., Unruh, J., McKinney, S., and Yu, C.R. (2015). Intracellular chloride concentration of the mouse vomeronasal neuron. BMC Neurosci. *16*, 90.

Kimoto, H., Haga, S., Sato, K., and Touhara, K. (2005). Sex-specific peptides from exocrine glands stimulate mouse vomeronasal sensory neurons. Nature *437*, 898–901.

Kimoto, H., Sato, K., Nodari, F., Haga, S., Holy, T.E., and Touhara, K. (2007). Sex- and Strain-Specific Expression and Vomeronasal Activity of Mouse ESP Family Peptides. Curr. Biol. *17*, 1879–1884.

Kleene, S.J. (2008). The Electrochemical Basis of Odor Transduction in Vertebrate Olfactory Cilia. Chem. Senses *33*, 839–859.

Kleene, S.J., and Gesteland, R.C. (1991). Calcium-activated chloride conductance in frog olfactory cilia. J Neurosci *11*.

Knoll, B., Zarbalis, K., Wurst, W., and Drescher, U. (2001). A role for the EphA family in the topographic targeting of vomeronasal axons. Development *128*, 895.

Knöll, B., Schmidt, H., Andrews, W., Guthrie, S., Pini, A., Sundaresan, V., and Drescher, U. (2003). On the topographic targeting of basal vomeronasal axons through Slit-mediated chemorepulsion. Development *130*, 5073.

Koos, D.S., and Fraser, S.E. (2005). The Grueneberg ganglion projects to the olfactory bulb. NeuroReport *16*.

Krieger, J., Schmitt, A., Löbel, D., Gudermann, T., Schultz, G., Breer, H., and Boekhoff, I. (1999). Selective Activation of G Protein Subtypes in the Vomeronasal Organ upon Stimulation with Urine-derived Compounds. J. Biol. Chem. *274*, 4655–4662.

Kroner, C., Breer, H., Singer, A.G., and O'Connell, R.J. (1996). Pheromone-induced second messenger signaling in the hamster vomeronasal organ. NeuroReport *7*.

Larriva-Sahd, J. (2008). The accessory olfactory bulb in the adult rat: A cytological study of its cell types, neuropil, neuronal modules, and interactions with the main olfactory system. J. Comp. Neurol. *510*, 309–350.

Leinders-Zufall, T., Brennan, P., Widmayer, P., S., P.C., Maul-Pavicic, A., Jäger, M., Li, X.-H., Breer, H., Zufall, F., and Boehm, T. (2004). MHC Class I Peptides as Chemosensory Signals in the Vomeronasal Organ. Science *306*, 1033.

Leinders-Zufall, T., Ishii, T., Mombaerts, P., Zufall, F., and Boehm, T. (2009). Structural requirements for the activation of vomeronasal sensory neurons by MHC peptides. Nat Neurosci *12*, 1551–1558.

Leinders-Zufall, T., Ishii, T., Chamero, P., Hendrix, P., Oboti, L., Schmid, A., Kircher, S., Pyrski, M., Akiyoshi, S., Khan, M., et al. (2014). A Family of Nonclassical Class I MHC Genes Contributes to Ultrasensitive Chemodetection by Mouse Vomeronasal Sensory Neurons. J. Neurosci. *34*, 5121.

Li, J., Ishii, T., Feinstein, P., and Mombaerts, P. (2004). Odorant receptor gene choice is reset by nuclear transfer from mouse olfactory sensory neurons. Nature *428*, 393–399.

Liberles, S.D. (2014). Mammalian Pheromones. Annu. Rev. Physiol. *76*, 151–175.

Liberles, S.D., Horowitz, L.F., Kuang, D., Contos, J.J., Wilson, K.L., Siltberg-Liberles, J., Liberles, D.A., and Buck, L.B. (2009). Formyl peptide receptors are candidate chemosensory receptors in the vomeronasal organ. Proc. Natl. Acad. Sci. *106*, 9842–9847.

Liman, E.R. (2003). Regulation by voltage and adenine nucleotides of a Ca2+-activated cation channel from hamster vomeronasal sensory neurons. J Physiol *548*.

Liman, E.R., and Corey, D.P. (1996). Electrophysiological Characterization of Chemosensory Neurons from the Mouse Vomeronasal Organ. J. Neurosci. *16*, 4625.

Liman, E.R., Corey, D.P., and Dulac, C. (1999). TRP2: A candidate transduction channel for mammalian pheromone sensory signaling. Proc. Natl. Acad. Sci. *96*, 5791–5796.

Lucas, P., Ukhanov, K., Leinders-Zufall, T., and Zufall, F. (2003). A Diacylglycerol-Gated Cation Channel in Vomeronasal Neuron Dendrites Is Impaired in TRPC2 Mutant Mice. Neuron *40*, 551–561.

Luo, Y., Lu, S., Chen, P., Wang, D., and Halpern, M. (1994). Identification of chemoattractant receptors and G-proteins in the vomeronasal system of garter snakes. J. Biol. Chem. *269*, 16867–16877.

Ma, M. (2007). Encoding Olfactory Signals via Multiple Chemosensory Systems. Crit. Rev. Biochem. Mol. Biol. *42*, 463–480.

Ma, M., Grosmaitre, X., Iwema, C.L., Baker, H., Greer, C.A., and Shepherd, G.M. (2003). Olfactory Signal Transduction in the Mouse Septal Organ. J. Neurosci. Off. J. Soc. Neurosci. *23*, 317–324.

Mamasuew, K., Breer, H., and Fleischer, J. (2008). Grueneberg ganglion neurons respond to cool ambient temperatures. Eur. J. Neurosci. *28*, 1775–1785.

Martínez-Marcos, A., and Halpern, M. (1999). Differential projections from the anterior and posterior divisions of the accessory olfactory bulb to the medial amygdala in the opossum, Monodelphis domestica. Eur. J. Neurosci. *11*, 3789–3799.

Martini, S., Silvotti, L., Shirazi, A., Ryba, N.J.P., and Tirindelli, R. (2001). Co-Expression of Putative Pheromone Receptors in the Sensory Neurons of the Vomeronasal Organ. J. Neurosci. *21*, 843.

Matsunami, H., and Buck, L.B. (1997). A Multigene Family Encoding a Diverse Array of Putative Pheromone Receptors in Mammals. Cell *90*, 775–784.

Meisami, E., and Bhatnagar, K.P. (1998). Structure and diversity in mammalian accessory olfactory bulb. Microsc. Res. Tech. *43*, 476–499.

Mohedano-Moriano, A., Pro-Sistiaga, P., Ubeda-Bañon, I., de la Rosa-Prieto, C., Saiz-Sanchez, D., and Martinez-Marcos, A. (2008). V1R and V2R segregated vomeronasal pathways to the hypothalamus. NeuroReport *19*.

Mombaerts, P., Wang, F., Dulac, C., Chao, S.K., Nemes, A., Mendelsohn, M., Edmondson, J., and Axel, R. (1996). Visualizing an Olfactory Sensory Map. Cell *87*, 675–686.

Montani, G., Tonelli, S., Sanghez, V., Ferrari, P.F., Palanza, P., Zimmer, A., and Tirindelli, R. (2013). Aggressive behaviour and physiological responses to pheromones are strongly impaired in mice deficient for the olfactory G-protein γ-subunit Gγ8. J. Physiol. *591*, 3949–3962.

Mucignat-Caretta, C. (2014). Neurobiology of Chemical Communication (CRC Press).

Munger, S.D., Lane, A.P., Zhong, H., Leinders-Zufall, T., Yau, K.-W., Zufall, F., and Reed, R.R. (2001). Central Role of the CNGA4 Channel Subunit in Ca^{2+}-Calmodulin-Dependent Odor Adaptation. Science *294*, 2172.

Nakahara, T.S., Cardozo, L.M., Ibarra-Soria, X., Bard, A.D., Carvalho, V.M.A., Trintinalia, G.Z., Logan, D.W., and Papes, F. (2016). Detection of pup odors by non-canonical adult vomeronasal neurons expressing an odorant receptor gene is influenced by sex and parenting status. BMC Biol. *14*, 12.

Newman, R., and Winans, S.S. (1980). An experimental study of the ventral striatum of the golden hamster. II. Neuronal connections of the olfactory tubercle. J. Comp. Neurol. *191*, 193–212.

Niimura, Y., Matsui, A., and Touhara, K. (2014). Extreme expansion of the olfactory receptor gene repertoire in African elephants and evolutionary dynamics of orthologous gene groups in 13 placental mammals. Genome Res. *24*, 1485–1496.

Norlin, E.M., Gussing, F., and Berghard, A. (2003). Vomeronasal Phenotype and Behavioral Alterations in Gαi2 Mutant Mice. Curr. Biol. *13*, 1214–1219.

Novotny, M., Jorgenson, J.W., Carmack, M., Wilson, S.R., Boyse, E.A., Yamazaki, K., Wilson, M., Beamer, W., and Whitten, W.K. (1980). Chemical Studies of the Primer Mouse Pheromones. In Chemical Signals: Vertebrates and Aquatic Invertebrates, D. Müller-Schwarze, and R.M. Silverstein, eds. (Boston, MA: Springer US), pp. 377–390.

Novotny, M., Schwende, F.J., Wiesler, D., Jorgenson, J.W., and Carmack, M. (1984). Identification of a testosterone-dependent unique volatile constituent of male mouse urine: 7-exo-ethyl-5-methyl-6,8-dioxabicyclo[3.2.1]-3-octene. Experientia *40*, 217–219.

Novotny, M., Jemiolo, B., Harvey, S., Wiesler, D., and Marchlewska-Koj, A. (1986). Adrenal-mediated endogenous metabolites inhibit puberty in female mice. Science *231*, 722.

Novotny, M.V., Ma, W., Wiesler, D., and Zídek, L. (1999). Positive identification of the puberty-accelerating pheromone of the house mouse: the volatile ligands associating with the major urinary protein. Proc. R. Soc. B Biol. Sci. *266*, 2017–2022.

Oboti, L., Pérez-Gómez, A., Keller, M., Jacobi, E., Birnbaumer, L., Leinders-Zufall, T., Zufall, F., and Chamero, P. (2014). A wide range of pheromone-stimulated sexual and reproductive behaviors in female mice depend on G protein Gαo. BMC Biol. *12*, 31–31.

Omura, M., and Mombaerts, P. (2014). Trpc2-Expressing Sensory Neurons in the Main Olfactory Epithelium of the Mouse. Cell Rep. *8*, 583–595.

Patton, C., Thompson, S., and Epel, D. (2004). Some precautions in using chelators to buffer metals in biological solutions. Cell Calcium *35*, 427–431.

Pietra, G., Dibattista, M., Menini, A., Reisert, J., and Boccaccio, A. (2016). The Ca^{2+}-activated Cl^- channel TMEM16B regulates action potential firing and axonal targeting in olfactory sensory neurons. J. Gen. Physiol. *148*, 293.

Pifferi, S., Pascarella, G., Boccaccio, A., Mazzatenta, A., Gustincich, S., Menini, A., and Zucchelli, S. (2006). Bestrophin-2 is a candidate calcium-activated chloride channel involved in olfactory transduction. Proc. Natl. Acad. Sci. *103*, 12929–12934.

Pifferi, S., Dibattista, M., Sagheddu, C., Boccaccio, A., Al Qteishat, A., Ghirardi, F., Tirindelli, R., and Menini, A. (2009a). Calcium-activated chloride currents in olfactory sensory neurons from mice lacking bestrophin-2. J. Physiol. *587*, 4265–4279.

Pifferi, S., Dibattista, M., and Menini, A. (2009b). TMEM16B induces chloride currents activated by calcium in mammalian cells. Pflüg. Arch. - Eur. J. Physiol. *458*, 1023–1038.

Ponissery Saidu, S., Stephan, A.B., Talaga, A.K., Zhao, H., and Reisert, J. (2014). Channel properties of the splicing isoforms of the olfactory calcium-activated chloride channel Anoctamin 2. J. Gen. Physiol. *144*, 203–203.

Prince, J.E.A., Cho, J.H., Dumontier, E., Andrews, W., Cutforth, T., Tessier-Lavigne, M., Parnavelas, J., and Cloutier, J.-F. (2009). Robo-2 Controls the Segregation of a Portion of Basal Vomeronasal Sensory Neuron Axons to the Posterior Region of the Accessory Olfactory Bulb. J. Neurosci. *29*, 14211.

Rasche, S., Toetter, B., Adler, J., Tschapek, A., Doerner, J.F., Kurtenbach, S., Hatt, H., Meyer, H., Warscheid, B., and Neuhaus, E.M. (2010). Tmem16b is Specifically Expressed in the Cilia of Olfactory Sensory Neurons. Chem. Senses *35*, 239–245.

Reisert, J., Lai, J., Yau, K.-W., and Bradley, J. (2005). Mechanism of the Excitatory Cl(−) Response in Mouse Olfactory Receptor Neurons. Neuron *45*, 553–561.

Ressler, K.J., Sullivan, S.L., and Buck, L.B. (1993). A zonal organization of odorant receptor gene expression in the olfactory epithelium. Cell *73*, 597–609.

Reuter, D., Zierold, K., Schroder, W.H., and Frings, S. (1998). A depolarizing chloride current contributes to chemoelectrical transduction in olfactory sensory neurons in situ. J Neurosci *18*.

Riviere, S., Challet, L., Fluegge, D., Spehr, M., and Rodriguez, I. (2009). Formyl peptide receptor-like proteins are a novel family of vomeronasal chemosensors. Nature *459*, 574–577.

Roberts, S.A., Simpson, D.M., Armstrong, S.D., Davidson, A.J., Robertson, D.H., and McLean, L. (2010). Darcin: a male pheromone that stimulates female memory and sexual attraction to an individual male's odour. BMC Biol *8*.

Rodriguez, I. (2016). Chapter 10 - Vomeronasal Receptors: V1Rs, V2Rs, and FPRs A2 - Zufall, Frank. In Chemosensory Transduction, S.D. Munger, ed. (Academic Press), pp. 175–190.

Rodriguez, I., Feinstein, P., and Mombaerts, P. (1999). Variable Patterns of Axonal Projections of Sensory Neurons in the Mouse Vomeronasal System. Cell *97*, 199–208.

Rodriguez, I., Del Punta, K., Rothman, A., Ishii, T., and Mombaerts, P. (2002). Multiple new and isolated families within the mouse superfamily of V1r vomeronasal receptors. Nat Neurosci *5*, 134–140.

Rössler, P., Kroner, C., Krieger, J., Löbel, D., Breer, H., and Boekhoff, I. (2000). Cyclic Adenosine Monophosphate Signaling in the Rat Vomeronasal Organ: Role of an Adenylyl Cyclase Type VI. Chem. Senses *25*, 313–322.

Rünnenburger, K., Breer, H., and Boekhoff, I. (2002). Selective G protein βγ-subunit compositions mediate phospholipase C activation in the vomeronasal organ. Eur. J. Cell Biol. *81*, 539–547.

Ryba, N.J.., and Tirindelli, R. (1997). A New Multigene Family of Putative Pheromone Receptors. Neuron *19*, 371–379.

Sagheddu, C., Boccaccio, A., Dibattista, M., Montani, G., Tirindelli, R., and Menini, A. (2010). Calcium concentration jumps reveal dynamic ion selectivity of calcium-activated chloride currents in mouse olfactory sensory neurons and TMEM16b-transfected HEK 293T cells. J. Physiol. *588*, 4189–4204.

Salazar, I., and Brennan, P.A. (2001). Retrograde labelling of mitral/tufted cells in the mouse accessory olfactory bulb following local injections of the lipophillic tracer DiI into the vomeronasal amygdala. Brain Res. *896*, 198–203.

Sam, M., Vora, S., Malnic, B., Ma, W., Novotny, M.V., and Buck, L.B. (2001). Neuropharmacology: Odorants may arouse instinctive behaviours. Nature *412*, 142–142.

Sasaki, K., Okamoto, K., Inamura, K., Tokumitsu, Y., and Kashiwayanagi, M. (1999). Inositol-1,4,5-trisphosphate accumulation induced by urinary pheromones in female rat vomeronasal epithelium. Brain Res. *823*, 161–168.

Scalia, F., and Winans, S.S. (1975). The differential projections of the olfactory bulb and accessory olfactory bulb in mammals. J. Comp. Neurol. *161*, 31–55.

Schild, D., and Restrepo, D. (1998). Transduction mechanisms in vertebrate olfactory receptor cells. Physiol. Rev. *78*, 429–466.

Schreiber, R., Faria, D., Skryabin, B.V., Wanitchakool, P., Rock, J.R., and Kunzelmann, K. (2015). Anoctamins support calcium-dependent chloride secretion by facilitating calcium signaling in adult mouse intestine. Pflüg. Arch. - Eur. J. Physiol. *467*, 1203–1213.

Schroeder, B.C., Cheng, T., Jan, Y.N., and Jan, L.Y. (2008). Expression Cloning of TMEM16A as a Calcium-Activated Chloride Channel Subunit. Cell *134*, 1019–1029.

Shimazaki, R., Boccaccio, A., Mazzatenta, A., Pinato, G., Migliore, M., and Menini, A. (2006). Electrophysiological Properties and Modeling of Murine Vomeronasal Sensory Neurons in Acute Slice Preparations. Chem. Senses *31*, 425–435.

Silvotti, L., Moiani, A., Gatti, R., and Tirindelli, R. (2007). Combinatorial co-expression of pheromone receptors, V2Rs. J. Neurochem. *103*, 1753–1763.

Silvotti, L., Cavalca, E., Gatti, R., Percudani, R., and Tirindelli, R. (2011). A Recent Class of Chemosensory Neurons Developed in Mouse and Rat. PLOS ONE *6*, e24462.

Singh, P.B., Brown, R.E., and Roser, B. (1987). MHC antigens in urine as olfactory recognition cues. Nature *327*, 161–164.

Spehr, M. (2016). Chapter 11 - Vomeronasal Transduction and Cell Signaling A2 - Zufall, Frank. In Chemosensory Transduction, S.D. Munger, ed. (Academic Press), pp. 191–206.

Spehr, J., Hagendorf, S., Weiss, J., Spehr, M., Leinders-Zufall, T., and Zufall, F. (2009). Ca^{2+}–Calmodulin Feedback Mediates Sensory Adaptation and Inhibits Pheromone-Sensitive Ion Channels in the Vomeronasal Organ. J. Neurosci. *29*, 2125.

Spehr, M., Hatt, H., and Wetzel, C.H. (2002). Arachidonic Acid Plays a Role in Rat Vomeronasal Signal Transduction. J. Neurosci. *22*, 8429.

Stephan, A.B., Shum, E.Y., Hirsh, S., Cygnar, K.D., Reisert, J., and Zhao, H. (2009). ANO2 is the cilial calcium-activated chloride channel that may mediate olfactory amplification. Proc Natl Acad Sci USA *106*.

Stöhr, H., Heisig, J.B., Benz, P.M., Schöberl, S., Milenkovic, V.M., Strauss, O., Aartsen, W.M., Wijnholds, J., Weber, B.H.F., and Schulz, H.L. (2009). TMEM16B, A Novel Protein with Calcium-Dependent Chloride Channel Activity, Associates with a Presynaptic Protein Complex in Photoreceptor Terminals. J. Neurosci. *29*, 6809.

Stowers, L., Holy, T.E., Meister, M., Dulac, C., and Koentges, G. (2002). Loss of Sex Discrimination and Male-Male Aggression in Mice Deficient for TRP2. Science *295*, 1493.

Suzuki, J., Umeda, M., Sims, P.J., and Nagata, S. (2010). Calcium-dependent phospholipid scrambling by TMEM16F. Nature *468*, 834–838.

Tachibana, T., Fujiwara, N., and Nawa, T. (1990). The Ultrastructure of the Ganglionated Nerve Plexus in the Nasal Vestibular Mucosa of the Musk Shrew (*Suncus murinus*, Insectivora). Arch. Histol. Cytol. *53*, 147–156.

Thompson, R.N., Robertson, B.K., Napier, A., and Wekesa, K.S. (2004). Sex-specific Responses to Urinary Chemicals by the Mouse Vomeronasal Organ. Chem. Senses *29*, 749–754.

Tian, H., and Ma, M. (2004). Molecular Organization of the Olfactory Septal Organ. J. Neurosci. *24*, 8383.

Tirindelli, R., and Ryba, N.J.P. (1996). The G-protein γ-subunit Gy8 is Expressed in the Developing Axons of Olfactory and Vomeronasal Neurons. Eur. J. Neurosci. *8*, 2388–2398.

Tirindelli, R., Dibattista, M., Pifferi, S., and Menini, A. (2009). From Pheromones to Behavior. Physiol. Rev. *89*, 921.

Touhara, K., Niimura, Y., and Ihara, S. (2016). Chapter 3 - Vertebrate Odorant Receptors A2 - Zufall, Frank. In Chemosensory Transduction, S.D. Munger, ed. (Academic Press), pp. 49–66.

Trotier, D., and Døving, K.B. (1998). 'Anatomical Description of a New Organ in the Nose of Domesticated Animals' by Ludvig Jacobson (1813). Chem. Senses *23*, 743–754.

Ukhanov, K., Leinders-Zufall, T., and Zufall, F. (2007). Patch-Clamp Analysis of Gene-Targeted Vomeronasal Neurons Expressing a Defined V1r or V2r Receptor: Ionic Mechanisms Underlying Persistent Firing. J. Neurophysiol. *98*, 2357.

Untiet, V., Moeller, L.M., Ibarra-Soria, X., Sánchez-Andrade, G., Stricker, M., Neuhaus, E.M., Logan, D.W., Gensch, T., and Spehr, M. (2016). Elevated Cytosolic Cl − Concentrations in Dendritic Knobs of Mouse Vomeronasal Sensory Neurons. Chem. Senses *41*, 669–676.

Van der Lee, S., and Boot, L. (1955). Spontaneous pseudopregnancy in mice. Acta Physiol. Pharmacol. Neerl. *4*, 442.

Vandenbergh, J.G., Whitsett, J.M., and Lombardi, J.R. (1975). Partial isolation of a pheromone accelerating puberty in female mice. J. Reprod. Fertil. *43*, 515–523.

Vassar, R., Ngai, J., and Axel, R. (1993). Spatial segregation of odorant receptor expression in the mammalian olfactory epithelium. Cell *74*, 309–318.

Von Campenhausen, H., and Mori, K. (2000). Convergence of segregated pheromonal pathways from the accessory olfactory bulb to the cortex in the mouse. Eur. J. Neurosci. *12*, 33–46.

Wagner, S., Gresser, A.L., Torello, A.T., and Dulac, C. (2006). A Multireceptor Genetic Approach Uncovers an Ordered Integration of VNO Sensory Inputs in the Accessory Olfactory Bulb. Neuron *50*, 697–709.

Whitlock, J.M., and Hartzell, H.C. (2017). Anoctamins/TMEM16 Proteins: Chloride Channels Flirting with Lipids and Extracellular Vesicles. Annu. Rev. Physiol. *79*, 119–143.

Whitten, W.K. (1959). Occurrence of anoestrus in mice caged in groups. J. Endocrinol. *18*, 102–107.

Winans, S.S., and Scalia, F. (1970). Amygdaloid Nucleus: New Afferent Input from the Vomeronasal Organ. Science *170*, 330–332.

Wyatt, T.D. (2003). Pheromones and animal behaviour: communication by smell and taste (Cambridge university press).

Wysocki, C.J., Wellington, J.L., and Beauchamp, G.K. (1980). Access of Urinary Nonvolatiles to the Mammalian Vomeronasal Organ. Science *207*, 781–783.

Yang, C., and Delay, R.J. (2010). Calcium-activated chloride current amplifies the response to urine in mouse vomeronasal sensory neurons. J Gen Physiol *135*.

Yang, H., Shi, P., Zhang, Y., and Zhang, J. (2005). Composition and evolution of the V2r vomeronasal receptor gene repertoire in mice and rats. Genomics *86*, 306–315.

Yang, Y.D., Cho, H., Koo, J.Y., Tak, M.H., Cho, Y., Shim, W.-S., Park, S.P., Lee, J., Lee, B., Kim, B.-M., et al. (2008). TMEM16A confers receptor-activated calcium-dependent chloride conductance. Nature *455*, 1210–1215.

Yildirim, E., Dietrich, A., and Birnbaumer, L. (2003). The mouse C-type transient receptor potential 2 (TRPC2) channel: Alternative splicing and calmodulin binding to its N terminus. Proc. Natl. Acad. Sci. *100*, 2220–2225.

Yonekura, J., and Yokoi, M. (2008). Conditional genetic labeling of mitral cells of the mouse accessory olfactory bulb to visualize the organization of their apical dendritic tufts. Mol. Cell. Neurosci. *37*, 708–718.

Yoshikawa, K., Nakagawa, H., Mori, N., Watanabe, H., and Touhara, K. (2013). An unsaturated aliphatic alcohol as a natural ligand for a mouse odorant receptor. *9*, 160.

Zapiec, B., and Mombaerts, P. (2015). Multiplex assessment of the positions of odorant receptor-specific glomeruli in the mouse olfactory bulb by serial two-photon tomography. Proc. Natl. Acad. Sci. *112*, E5873–E5882.

Zhang, P., Yang, C., and Delay, R.J. (2008). Urine Stimulation Activates BK Channels in Mouse Vomeronasal Neurons. J. Neurophysiol. *100*, 1824.

Zhang, P., Yang, C., and Delay, R.J. (2010). Odors activate dual pathways, a TRPC2 and a AA-dependent pathway, in mouse vomeronasal neurons. Am. J. Physiol. - Cell Physiol. *298*, C1253.

Zhao, H., Ivic, L., Otaki, J.M., Hashimoto, M., Mikoshiba, K., and Firestein, S. (1998). Functional Expression of a Mammalian Odorant Receptor. Science *279*, 237.

Zhou, Y., and Rui, L. (2010). Major Urinary Protein Regulation of Chemical Communication and Nutrient Metabolism. Pheromones *83*, 151–163.

Zufall, F., and Leinders-Zufall, T. (2000). The Cellular and Molecular Basis of Odor Adaptation. Chem. Senses *25*, 473–481.